


2017

Thermally stable encapsulated intermetallic and bimetallic nanoparticles for heterogeneous catalysis

Raghu Maligal Ganesh
Iowa State University

Follow this and additional works at: <https://lib.dr.iastate.edu/etd>

 Part of the [Inorganic Chemistry Commons](#), and the [Nanoscience and Nanotechnology Commons](#)

Recommended Citation

Maligal Ganesh, Raghu, "Thermally stable encapsulated intermetallic and bimetallic nanoparticles for heterogeneous catalysis" (2017). *Graduate Theses and Dissertations*. 16286.
<https://lib.dr.iastate.edu/etd/16286>

This Dissertation is brought to you for free and open access by the Iowa State University Capstones, Theses and Dissertations at Iowa State University Digital Repository. It has been accepted for inclusion in Graduate Theses and Dissertations by an authorized administrator of Iowa State University Digital Repository. For more information, please contact digirep@iastate.edu.

Thermally stable encapsulated intermetallic and bimetallic nanoparticles for heterogeneous catalysis

by

Raghu Maligal Ganesh

A dissertation submitted to the graduate faculty

in partial fulfillment of the requirements for the degree of

DOCTOR OF PHILOSOPHY

Major: Chemistry

Program of Study Committee:

Wenyu Huang, Adviser

Patricia Thiel

Gordon Miller

Igor Slowing

Aaron Sadow

The student author, whose presentation of the scholarship herein was approved by the program of study committee, is solely responsible for the content of this dissertation. The Graduate College will ensure this dissertation is globally accessible and will not permit alterations after a degree is conferred.

Iowa State University

Ames, Iowa

2017

Copyright © Raghu Maligal Ganesh, 2017. All rights reserved.

TABLE OF CONTENTS

	Page
ACKNOWLEDGEMENTS.....	iii
ABSTRACT.....	iv
CHAPTER 1. GENERAL INTRODUCTION	1
CHAPTER 2. A SHIP-IN-A-BOTTLE STRATEGY TO SYNTHESIZE ENCAPSULATED INTERMETALLIC NANOPARTICLE CATALYSTS: EXEMPLIFIED FOR FURFURAL HYDROGENATION.....	21
Abstract.....	21
Introduction.....	22
Results and Discussion	25
Conclusions.....	53
Experimental Section.....	53
References.....	58
CHAPTER 3. ENHANCED CHEMOSELECTIVITY IN BIMETALLIC NANOPARTICLES IN THE ABSENCE OF SURFACE MODIFYING LIGANDS.....	63
Abstract.....	63
Introduction.....	64
Results and Discussion	66
Conclusions.....	79
Experimental Section.....	79
References.....	85
CHAPTER 4. SELECTIVE HYDROGENATION OF ACETYLENE OVER SUB-5 NM INTERMETALLIC NANOPARTICLES IN MESOPOROUS SILICA WELLS	88
Abstract.....	88
Introduction.....	89
Results and Discussion	90
Conclusions.....	103
Experimental Section.....	103
References.....	108
CHAPTER 5. CONCLUSIONS	113

ACKNOWLEDGMENTS

My acceptance into Iowa State University towards earning a doctorate in Chemistry has indeed been an extraordinary learning opportunity. For starters, I'm extremely grateful to Dr. Wenyu Huang for accepting me into his group in Fall 2011 and spending inordinate amounts of time guiding me on the nuances of academic research. There has always been an opportunity to carry out innovative research in the Huang group.

Dr. Chaoxian Xiao joined our group in 2012 and has been one of the most resourceful scientists I have had the good fortune to work with and be inspired by. His extraordinary work ethic has thankfully rubbed off on all of us in some fashion or the other and is a model to truly replicate if we seek to do meaningful science that benefits the world at large. I am extremely grateful for all the projects I got to work with him on and in the process, learn from.

I'd like to thank all the members of my group, both past, and present, as we have consistently worked as a team to help each other realize our goals as graduate students. Working in the lab and carrying out rational research wouldn't have been possible without the constant consultation with Huang group members. I'd like to thank all my committee members, Dr. Patricia Thiel, Dr. Gordon Miller, Dr. Aaron Sadow and Dr. Igor Slowing for helping me along the way. I'd also like to thank Dr. Aaron Rossini for giving us the opportunity to collaborate with him and for agreeing to be on my committee for the final defense at such short notice. I'd also like to thank Dr. Javier Vela for his advice as a former committee member. Finally, I'd like to thank our collaborators with whom we have had the opportunity to carry out some very exciting work – Adding meaning to the whole grind that was graduate school.

ABSTRACT

Intermetallic compounds have shown promise as efficient heterogeneous catalysts, displaying improved performance over their monometallic parent metals for chemical transformations. Furthermore, colloidal intermetallic nanoparticles (iNPs) afford additional improvements via increased catalyst surface area and enhanced catalytic performance. However, these iNPs are not efficiently protected against sintering during thermal treatment procedures such as catalyst regeneration, resulting in a loss of their active surface area. Herein, we have successfully developed porous encapsulation strategies using inert silica that afford monodisperse iNPs that address this concern. These iNPs are highly stable thermally and the inert silica-based mesoporous encapsulation doesn't present mass transfer obstacles during catalysis. Their efficiency as heterogeneous catalysts is also extensively explored.

CHAPTER 1. GENERAL INTRODUCTION

This thesis is composed of 5 chapters. Chapter 1 is an introduction to the burgeoning field of intermetallic compounds, specifically nanoscale intermetallic compounds, for extensive applications in heterogeneous catalysis. It traces the history of the use of catalysts both heterogeneous and homogeneous while providing grounds for the necessity to use bimetallic and intermetallic-based heterogeneous catalysts for a wide range of catalytic applications. The significance of intermetallic nanoparticles (iNPs) via the change in the physicochemical properties when transitioning from disordered alloys to ordered alloys with specific compositions is a central focus of both this general introduction and the thesis at large. In addition to these aspects, the introduction also gives an overview of advances made in nanoparticle encapsulation strategies to prevent agglomeration, with a specific focus on iNPs.

Chapter 2 focuses on the seed-mediated synthesis of encapsulated iNPs. Drawing upon a wealth of knowledge on the use of porous supports to procure sinter-resistant nanoparticles (NPs), we synthesized these materials that are thermally stable and have important applications in catalysis. Chapter 3 focuses on furthering the usefulness of the encapsulation strategy for bimetallic/intermetallic NPs. Various reports exist to show the role of surface modifying organic ligands in catalysis carried out by both monometallic and bimetallic NPs. Functioning as protecting agents against nanoparticle aggregation, many of these ligand systems have also shown an ability to improve selectivity in important chemical processes via the influence they wield on the adsorption geometries of substrates on the catalyst surface. In certain bimetallic systems, although the role of the ligand and the noble metal of catalytic interest is clarified, literature is ambiguous on the role of the additional metals in the nanoparticle. Independently

verifying the role played by both the ligand systems that modify the surface and the additional metal is a challenge. Our inorganic encapsulation strategy shows a way forward with the porous encapsulation making the role of Fe in Pt-Fe compounds evident in the hydrogenation of α , β -unsaturated aldehydes selectively to the unsaturated alcohols. Additionally, the ligands of interest can be adsorbed post-synthesis on the surface of metal NPs to study the effect of the ligands on their catalytic properties independently.

Chapters 2 and 3 used an encapsulation strategy that involved relatively larger NPs (>14 nm). Although the promise exhibited by these encapsulated bimetallic iNPs is undeniable, the potential to have large active metal surface areas (larger surface to volume ratio) available to substrates is diminished. Hence, Chapter 4 focuses on an alternative encapsulation-based bimetallic/intermetallic NP synthesis strategy that could synthesize small active metal NPs for catalysis. Smaller Pt NPs (~2.9 nm) were synthesized in advance using solution chemistry techniques. A previously reported core-shell nanostructure was then used to sandwich these small NPs prior to intermetallic synthesis to procure iNPs of Pt and Sn. The semi-hydrogenation of acetylene is an important industrial process that was used as a model reaction for these materials. Adding larger quantities of Sn to Pt played an important role in improving selectivity during the conversion of acetylene to ethylene. Using these smaller sized iNPs at around 6-7 nm high activity and selectivity were obtained in contrast to a typical control catalyst. The mesoporous silica (mSiO₂) shells around these smaller iNPs also lent them the added benefit of high thermal stability and easy regeneration for the recycling of catalysts.

Chapter 5 is a general conclusion of all the themes explored in the thesis. Additional light will be thrown on how Chapter 2 is being extended to other catalytically active iNPs of

Au and Pd encapsulated within mesoporous silica. Finally, the chapter will propose strategies to explore encapsulated iNPs for more economical metals such as Fe, Co, and Ni.

Introduction

Catalysis holds sway over modern society as we know it.¹ With population surges in the recent past, our reliance on catalytic technologies to meet global demands in terms of our food, energy and general material needs has only continued to increase.² Additionally, faced with the twin challenges of climate change and environmental degradation, catalytic transformations have also been at the forefront of the growing global clean energy drive.³

Two prominent classes of catalytic transformations are homogeneous and heterogeneous catalysis. Homogeneous catalytic reactions are typically carried out by catalysts that exist in the same phase as the reactants in a solution.⁴ Most homogenous catalytic systems utilize transition metal complex catalysts that are unmatched in terms of the control they exert for activity and selectivity in innumerable organic reactions. And yet recyclability of the active catalysts used in homogeneous catalysis is a significant challenge owing to the difficulty in their separation from the reaction medium. Immobilizing these homogeneous catalysts on inert supports has led to a certain degree of recyclability.⁵ However, even such immobilization cannot prevent leaching of the active metal ions from the catalytic complex.⁶

Heterogeneous catalysts, on the other hand, being solid catalysts, can conveniently be separated from the reaction medium which could be either gas phase or liquid phase reaction mediums. Besides the ease of their separability, they also foster economical utilization of reactants and ensure less waste is generated. Diverse chemical industries and businesses rely on heterogeneous catalysts to furnish the many amenities that mankind uses daily. An important class of heterogeneous catalysts that have helped mitigate some of the drawbacks of

homogeneous catalysts are metal nanoparticle-based systems.⁷ Nanocrystals with and without the use of supports/stabilizers can conveniently be separated, recycled and leave more room to contain leaching-related issues.⁸⁻¹⁰ Although there has been limited success in replicating the activity and selectivity of homogeneous catalysts using NPs, advances in the resources and methodologies available today are gradually bridging that gap.¹¹⁻¹³

Enhanced heterogeneous catalysis via size, morphology and support effects

Colloidally prepared metal NPs have witnessed a surge in their exploration as heterogeneous catalysts over the last two decades.¹⁴⁻¹⁵ Furthermore, enabling the synthesis of these materials with reasonable control over their size, shape and support-based interactions has further added to their allure over homogeneous catalysts.¹⁶⁻¹⁹ The synthesis of these NPs primarily utilizes the aid of organic ligands that are capable of both protecting the NPs during their synthesis and aiding in their morphological evolution.

One of the chief advantages of nanoparticle synthesis is an ability to control their size to influence their catalytic properties. For instance, dendrimer encapsulated palladium NPs varying in size from 1.3-1.9 nm, show a rapid change in both their electronic and geometric properties, resulting in higher TOF values for the 1.9 nm Pd NPs for the hydrogenation of allyl alcohol.²⁰ Alternatively, Tsunoyama et al. demonstrated that smaller gold NPs with sizes of 1.3 nm exhibited higher catalytic activity in the aerobic oxidation of benzylic alcohols to their aldehydes and acids, when compared to their larger counterparts at 9.5 nm.²¹ Hence size effects play significant roles for different metal NPs and can be influential in deciding the best performance for a given reaction.

Morphological effects also play an important role in the catalysis carried out by NPs. Work carried out by Tsung et al. demonstrated that for the hydrogenation of pyrrole, platinum

nanocubes enhanced ring-opening to ensure higher selectivity to the desired n-butylamine while the nanopolyhedra furnished both pyrrolidine and n-butylamine.²² Wang et al. synthesized spinous gold NPs which were used to catalyze the hydrogenation of 4-nitrobenzenethiol (4-NTP) selectively to 4-aminobenzenethiol (4-ATP).²³ In contrast, spherical gold NPs that were essentially produced by a lack of the spinous surface favored the intramolecular conversion of the 4-NTP to 4,4'-dimercaptoazobenzene (4,4'-DMAB). This selectivity was primarily due to the presence of low coordinate steps on the spinous gold NPs, which do not favor the co-adsorption of the intermediate nitroso and hydroxylamine derivatives of nitrobenzene that are essential for the intramolecular generation of 4, 4'-DMAB.

Additionally, the presence of a support and any subsequent interactions with these NPs affords further interesting possibilities. Gold nanoclusters supported on TiO_2 and Al_2O_3 showed support and size-dependent catalytic activity for the water gas shift reaction.²⁴ Turnover rates for the TiO_2 support were almost 10 times that of the Al_2O_3 support. Moreover, smaller nanoclusters on TiO_2 were more active for the reaction, due to a higher number of surface undercoordinated Au atoms. Studies on charge transfer interactions of small gold clusters with their metal oxide supports and the presence of oxygen vacancies in these systems provide further insight into the forces at play in these heterogeneous catalytic systems.²⁵⁻²⁶ Zhou et al. demonstrated a strong morphology and support dependence in the catalytic oxidation of CO by gold nanoclusters supported on CeO_2 .²⁷ Preparing and testing these various types of nanoclusters supported on CeO_2 nanocubes, from single atoms through sub 5 nm nanoclusters, it was shown that at least two layers of the gold clusters were necessary to express the best CO oxidation activity.

Furthermore, support interactions can extend to other implications for the NPs when it comes to catalysis. One such pertinent implication is the formation of alloys at the interphases of supports that are catalytically active. Work by Kamiuchi et al. indicated strong chemical interactions between Pt NPs supported on tin oxide leading to the reversible formation of their intermetallic compounds depending on oxidation and reduction treatments.²⁸ Structural changes in the Pt/SnO₂ interphase resulted in an unusual CO adsorption ability by the composite. In work carried out by the Bokhoven group, palladium supported on zinc oxide (4.3 wt% Pd/ZnO) led to the formation of surface PdZn alloys supported on zinc oxide that exhibited improved activity and selectivity in the semi-hydrogenation of 1-pentyne to 1-pentene.²⁹ Vajda et al. demonstrated that in the oxidative dehydrogenation of propane to propene subnanometer platinum clusters supported on ALD (Atomic Layer Deposition) coated Al₂O₃ exhibited improved selectivity to propene in the presence of an additional overcoat of SnO.³⁰

However, there are drawbacks in each of the above approaches towards heterogeneous catalysis. For example, size and morphologically controlled NPs enlist organic stabilizers to prevent their aggregation during synthesis. These stabilizers, however, are strongly adsorbed on the surface of these NPs hindering their catalytic activity and requiring complicated treatments to remove them.³¹⁻³³ Moving on to the use of conventional supports, these are limited by the low loadings of the metal NPs, the inability to control particle size distribution and the possibility of the NPs aggregating under harsh pretreatment and reaction conditions.³⁴⁻

Encapsulated nanocrystals for improved stability under reaction conditions

Given the disadvantages of using organic protecting agents and conventional supports for the synthesis of metal NPs, a prominent direction has been the use of encapsulated core-shell or yolk-shell architectures. A popular example is the design of silica and carbon-based encapsulation, to obtain single or multi-core encapsulation of metal NPs.³⁸⁻⁴¹ These designed supports, besides being thermally stable at high temperatures, also allow for the tuning of their properties such as functionalization of the porous environment and tuning porosity,⁴²⁻⁴³ providing added facets to these encapsulated nanostructures.

As mentioned in the previous section metal NPs on conventional supports are prone to aggregation at reaction conditions. Hence the design of these porous encapsulated architectures is guided by the desire to stem aggregation without affecting the catalytic activity of the metal NPs. Early indications of the value of these materials was evident in the preparation of a yolk-shell “Au, @ZrO₂” (the space indicates the porous nature of the zirconia shell) nanocomposite by the Schuth group.⁴⁴ Individual Au NPs could be contained within a single zirconia shell, which was stable at a calcination temperature as high as 800 °C, ahead of their application in CO oxidation. In a similar fashion Ikeda et al. prepared ligand-free 2.2 nm Pt NPs in hollow porous carbon shells, using silica coated Pt NPs as the sacrificial template for the final Pt@hmC (hmC = hollow porous carbon) composites.⁴⁵ The encapsulated Pt NPs were much more active in hydrogenation reactions than PVP-protected 2.2 nm Pt particles or Pt supported on Active carbon. Additionally, both these systems could easily be recycled due to the sinter-proof nature of their encapsulating layers.

Adding to the ease of the coating of silica on most NPs, more diverse composites with added functionalities can be envisioned. Yin et al. synthesized a core-satellite nanocomposite

protected by a porous silica shell, $\text{Fe}_3\text{O}_4/\text{SiO}_2/\text{Au}/\text{por-SiO}_2$, that added the attractive feature of magnetic recyclability via the magnetite core.⁴⁶ In the catalytic reduction of 4-nitrophenol to 4-aminophenol, the catalyst could be conveniently recycled at least 6 times without any loss in activity. Yolk-shell $\text{Au}@\text{TiO}_2$ structures have been shown to enhance the photocatalytic ability of TiO_2 , with the localized surface plasmon resonance ability of gold functioning as an impetus for the TiO_2 to overcome its UV-only irradiation limitation.⁴⁷ Potential future applications of such heterostructures could lead to more efficient water-splitting catalysts.⁴⁸

Another significant development of such porous encapsulation has been the ability to use templated synthesis for their preparation. Joo et al. used a surfactant-based strategy to obtain $\text{Pt}@\text{mSiO}_2$ NPs, wherein individual Pt NPs were thermally stable within their mesoporous encapsulation at calcination temperatures as high as 750 °C.³⁸ Compared to the Pt NPs supported on a pre-synthesized silica support, the templated $\text{Pt}@\text{mSiO}_2$ catalysts were much more efficient catalysts for ethylene hydrogenation and high-temperature CO oxidation. Chen et al. synthesized hollow $\text{Pd}@\text{mSiO}_2$ nanoreactors with a carbon nanosphere template and demonstrated their superior activity in Suzuki coupling reactions.⁹ Ultrafine metal NPs supported on graphene oxide (M-rGO) were afforded further stability against aggregation by a surfactant-assisted mSiO_2 encapsulation of the M-rGO composite.⁴⁹ The catalytic activity of $\text{Pt-rGO}@\text{mSiO}_2$ for CO oxidation showed enhanced activity compared to the non-encapsulated version.

In progressing from ligand-stabilized metal NPs and those supported on conventional supports to these porous inorganic capping platforms, additional enhancements were made to the catalytically active nanocrystals. Besides being able to encapsulate these morphology- and size-controlled monometallic NPs, they have also enabled the preparation of bimetallic and

intermetallic compounds that show more promise as catalysts for selective chemical transformations in comparison to their monometallic precursors.⁵⁰⁻⁵²

Bimetallic NPs for improvements in heterogeneous catalysis

While size- and morphology-controlled NPs have shown promise as catalysts, they are still limited by issues of selectivity. The adsorption of substrate molecules varies on different facets of monometallic NPs, which can lead to diverse products even in the case of designed particles. Additionally, the modification of monometallic NPs to ensure improved selectivity is a laborious process that requires specific surface directing agents or synthesis conditions which are not feasible when preparing catalysts for industrial scale processes. To overcome these drawbacks, bimetallic NPs have emerged as a more straightforward solution to improve aspects of selectivity in various chemical transformations.⁵³ The properties of these bimetallic NPs are noticeably different from their constituent monometallic counterparts, due to the operation of unique geometric or electronic effects when differing metal atoms are arranged on the surface.⁵⁴

Common strategies for the synthesis of these bimetallic NPs include co-reduction, seeded growth, thermal decomposition and galvanic replacement.⁵⁵ Effectively using these liquid phase synthetic strategies can furnish various types of bimetallic nanocrystals, ranging from core-shell, metal/metal oxide heterostructures to alloys and intermetallic compounds.⁵⁶⁻⁵⁷ Furthermore, bimetallic NPs can be used as a platform to transition from disordered alloys to ordered intermetallic compounds, either through morphology changes or via overgrowth on the disordered alloys.⁵⁸⁻⁵⁹ Hence bimetallic NPs open up even more catalytic possibilities, given their architectural flexibility.

Regarding their catalytic activity, bimetallic catalysts offer multiple advantages. PtCo (3.6 ± 0.7 nm) bimetallic NPs synthesized in hollow carbon spheres (PtCo@HCS) were highly selective catalysts for the conversion of 5-hydroxymethylfurfural to 2,5-dimethylfuran.⁴¹ Additionally, the PtCo@HCS iteration also exhibited complete conversion of the substrate in comparison to the monometallic Pt@HCS material (24% conversion for the same quantity of Pt). Monodisperse bimetallic Pt-Fe catalysts in the presence of surface modifying ligands, whose specific adsorption is facilitated by surface iron, show enhanced activity and selectivity in the selective hydrogenation of cinnamaldehyde to cinnamyl alcohol.⁶⁰ With greater catalytic efficiencies and reduced precious metal usage, bimetallic catalysts are thus an important advancement in the preparation of more viable catalysts.

The composition of these bimetallic NPs can also be conveniently tuned via their solution phase synthesis, resulting in composition-dependent catalytic activity. In the synthesis of compositionally different but constant size (~9 nm) PtRh NPs, a twenty-fold increase in activity was observed for CO oxidation activity, going from pure Pt to pure Rh.⁶¹ However the catalytic activity was non-linear with the changing Rh/Pt composition, attesting to the surface segregation of Pt at the surface. The Strasser group demonstrated exceptional oxygen reduction activity (ORR) on octahedral PtNi nanoparticle catalysts whose surface composition could be controlled via the duration of their synthesis.⁶² In their utilization for ORR, the octahedral PtNi NPs exhibited significant enhancements in both surface-area specific and Pt-mass based activity.

Although bimetallic catalysts have clear advantages over their monometallic counterparts and offer a wider scope than support-based nanoparticle interactions, there is still room for improvement in their catalytic activity. Due to the random arrangement of alloy NPs

surface composition is subject to changes induced by the reaction environment.⁵⁴ Hence in alloy NPs, a complete picture of the surface structure-catalytic property relationship is difficult to obtain with respect to the active site in operation.

Intermetallic compounds for heterogeneous catalysis

Multimetallic alloys lack the requisite structural control that in turn affect their surface geometric and electronic properties. In recent years there has thus been growing focus on an important iteration of multimetallic compounds (Figure 1), their ordered iteration known more commonly as intermetallic compounds.⁶³ To define them broadly, intermetallic compounds are alloys that are formed at discrete compositions and possess specific crystal structures.⁶⁴ Owing to their well-defined crystal structures their electronic and geometric properties are relatively easier to pin down.⁶⁵

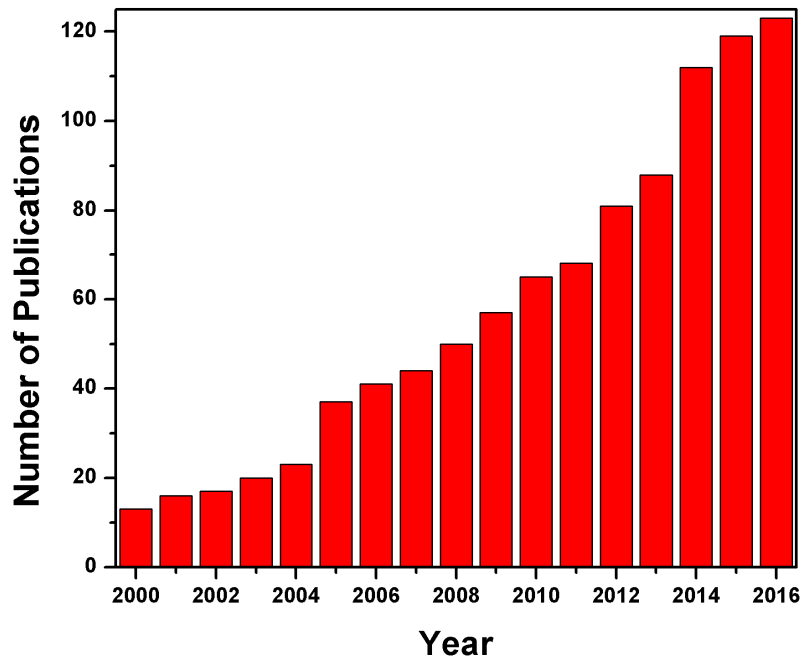


Figure 1. Number of publications on the use of intermetallic compounds as catalysts using Web of Science.

In the important industrial polymerization of polyethylene trace amounts of acetylene can poison the polymerizing catalyst.⁶⁶ Hence, Pd supported on Al_2O_3 is used as a catalyst to remove acetylene molecules by hydrogenating them to ethylene or ethane. However, the catalyst decays over time due to carbon deposition and tends to hydrogenate feed ethylene to ethane, which decreases the atomic efficiency.⁶⁶ As an alternative, Pd-Ag alloys have been shown to be an improvement for this process, showing selectivity to the semi-hydrogenation of acetylene to ethylene.⁶⁷ Armbruster et al. made a significant stride in the use of intermetallic Pd-Ga compounds to demonstrate drastically improved selectivity over the alloy catalyst, in addition to being stable for longer durations.⁶⁸⁻⁶⁹ They also demonstrated intermetallic $\text{Al}_{13}\text{Fe}_4$ as an efficient low-cost alternative to the Pd-based systems.⁷⁰ A unique aspect of these intermetallic compounds is the site isolation of the catalytically active metal atoms. In $\text{Al}_{13}\text{Fe}_4$ isolated iron atoms in cages of aluminum atoms are chiefly responsible for the improved selectivity (almost 84 % acetylene is converted to ethylene). Hence these structural provisions uniquely differentiate the intermetallic compounds from random alloys and are the central explanation for their enhanced chemoselectivity.⁶⁵

To further increase the surface area of these intermetallic compounds, solution chemistry methods have been used for iNP synthesis. Nanoparticle iterations of the Pd-Ga intermetallic compounds, synthesized again by Armbruster et al., were demonstrated to be even more active (while retaining selectivity) for the semi-hydrogenation of acetylene, compared to their bulk versions.⁷¹ Schaak et al. have reported the synthesis of various polyol-mediated intermetallic compounds that could potentially find applications across the board, including catalysis.⁷²⁻⁷⁵ Furthermore, they also prepared a seed-mediated synthesis of these iNPs on various supports, showing that the nanoscale intermetallic compounds were less prone to

aggregation during synthesis in the presence of supports.⁷⁶ The use of supports also enables the formation of intermetallic compounds from their alloys. Murray et al. synthesized intermetallic Pt-Zn alloy NPs and obtained Pt₃Zn intermetallic nanocrystals upon annealing the alloy supported on Vulcan XC72R.⁷⁷ Intermetallic Pt₃Zn displayed improved catalytic activity in the methanol oxidation reaction, while also being less prone to poisoning by CO compared to the standard Pt catalyst and Pt-Zn alloy nanocrystals. However, in all the above cases there were still examples of aggregation that were inevitable because of the use of capping agents and conventional supports.

Encapsulation strategies for iNPs

To avoid the pitfalls of the conventional supports that were used for the synthesis of iNPs, porous coatings or embedded support strategies are required to prevent any agglomeration of the NPs. Work done by Li et al. used a Layered Double Hydroxide (LDH) strategy to prepare ternary Ni_xM_yIn_z LDHs (where M = Mg, Al), which on reduction afforded size-controlled synthesis of Ni-In NPs supported on MgO or Al₂O₃.⁷⁸ The oxide support prevented aggregation and the intermetallic NPs were shown to be superior catalysts to the unsupported variants for the selective hydrogenation of α,β -unsaturated aldehydes. Hyeon et al. employed thin polydopamine shells to coat PtFe alloy NPs dispersed on carbon supports. The coating helped anneal the NPs at the requisite temperature of 700 °C to form the intermetallic compound while preventing their aggregation.⁷⁹ Additionally, the 1-3.5 nm coatings were transformed to porous N-doped carbon shells that did not pose mass transfer hindrances and helped the PtFe iNPs exhibit enhanced ORR activity.

Surface modification of common supports to graft metal ions ahead of their reduction can also furnish monodisperse iNPs with tunable sizes. Using a wetness impregnation method,

Pt-based intermetallic compounds could be synthesized in sulfur-modified ordered mesoporous carbon.⁸⁰ These size controlled iNPs were shown to be excellent catalysts for the electrocatalytic oxidation of formic acid. Using a precipitation deposition method, our group supported Pt ions on multi-walled carbon nanotubes.⁸¹ Using the protection of a mesoporous silica shell reduced Pt NPs could then be used to prepare monodisperse intermetallic PtZn/MWNT@mSiO₂. After the etching of the silica shell, the PtZn/MWNT material proved to be an efficient catalyst for the methanol oxidation reaction.

In work covered in this thesis modified porous shell encapsulation strategies were consistently used in various capacities to synthesize both intermetallic and bimetallic platinum-containing NPs.^{38,51} These thermally stable catalysts displayed enhanced selectivity for the desired products in the hydrogenation of furfural and cinnamaldehyde. They also demonstrated enhanced selectivity in the semi-hydrogenation of acetylene to ethylene. Easy recycling of the catalysts and enhanced performance with reduced noble metal usage were added bonuses. Additionally, in chapter 3 the mesoporous shell also allows the adsorption of surface modifying ligands on the core intermetallic NPs, adding another facet to these materials.

References

- (1) Oyama, S. T.; Somorjai, G. A., *J. Chem Educ.* **1988**, *65*, 765.
- (2) Catlow, C. R.; Davidson, M.; Hardacre, C.; Hutchings, G. J., *Phil. Trans. R. Soc. A*, **2016**, *374*.
- (3) Lanzafame, P.; Perathoner, S.; Centi, G.; Gross, S.; Hensen, E. J. M., *Catal. Sci. Tech.* **2017**.
- (4) Cornils, B.; Herrmann, W. A., *J. Catal.* **2003**, *216*, 23-31.
- (5) Corma, A., *Cat. Rev. - Sci. Eng.* **2004**, *46*, 369-417.

- (6) Gladysz, J. A., *Chem. Rev.* **2002**, *102*, 3215-3216.
- (7) Astruc, D.; Lu, F.; Aranzaes, J. R., *Angew. Chem. Int. Ed.* **2005**, *44*, 7852-7872.
- (8) Pachón, L. D.; Rothenberg, G., *Appl. Organomet. Chem.* **2008**, *22*, 288-299.
- (9) Chen, Z.; Cui, Z.-M.; Niu, F.; Jiang, L.; Song, W.-G., *Chem. Comm.* **2010**, *46*, 6524-6526.
- (10) Balanta, A.; Godard, C.; Claver, C., *NPsChem. Soc. Rev.* **2011**, *40*, 4973-4985.
- (11) Rothenberg, G., *Nat. Chem.* **2010**, *2*, 9-10.
- (12) Thomas, J. M., *Proc. Royal Soc. A* **2012**, *468*, 1884-1903.
- (13) Ball, P., *Natl. Sci. Rev.* **2015**, *2*, 202-204.
- (14) Campelo, J. M.; Luna, D.; Luque, R.; Marinas, J. M.; Romero, A. A., *ChemSusChem* **2009**, *2*, 18-45.
- (15) Narayanan, R.; El-Sayed, M. A., *J. Phys. Chem. B.* **2005**, *109*, 12663-126.
- (16) Li, Y.; Boone, E.; El-Sayed, M. A., *Langmuir* **2002**, *18*, 4921-4925.
- (17) Joo, S. H.; Park, J. Y.; Renzas, J. R.; Butcher, D. R.; Huang, W.; Somorjai, G. A., *Nano Lett.* **2010**, *10*, 2709-2713.
- (18) Mostafa, S.; Behafarid, F.; Croy, J. R.; Ono, L. K.; Li, L.; Yang, J. C.; Frenkel, A. I.; Cuenya, B. R., *J. Am. Chem. Soc.* **2010**, *132*, 15714-15719.
- (19) Cuenya, B. R., *Thin Solid Films* **2010**, *518*, 3127-3150.
- (20) Wilson, O. M.; Knecht, M. R.; Garcia-Martinez, J. C.; Crooks, R. M., *J. Am. Chem. Soc.* **2006**, *128*, 4510-4511.
- (21) Tsunoyama, H.; Sakurai, H.; Negishi, Y.; Tsukuda, T., *J. Am. Chem. Soc.* **2005**, *127*, 9374-9375.

- (22) Tsung, C.-K.; Kuhn, J. N.; Huang, W.; Aliaga, C.; Hung, L.-I.; Somorjai, G. A.; Yang, P., *J. Am. Chem. Soc.* **2009**, *131*, 5816-5822.
- (23) Wang, D.; Sun, Y.; Sun, Y.; Huang, J.; Liang, Z.; Li, S.; Jiang, L., *Nanoscale* **2017**, *9*, 7727-7733.
- (24) Shekhar, M.; Wang, J.; Lee, W.-S.; Williams, W. D.; Kim, S. M.; Stach, E. A.; Miller, J. T.; Delgass, W. N.; Ribeiro, F. H., *J. Am. Chem. Soc.* **2012**, *134*, 4700-4708.
- (25) Häkkinen, H.; Abbet, S.; Sanchez, A.; Heiz, U.; Landman, U., *Angew. Chem. Int. Ed.* **2003**, *42*, 1297-1300.
- (26) Yan, Z.; Chinta, S.; Mohamed, A. A.; Fackler, J. P.; Goodman, D. W., *J. Am. Chem. Soc.* **2005**, *127*, 1604-1605.
- (27) Wang, J.; Tan, H.; Yu, S.; Zhou, K., *ACS Catal.* **2015**, *5*, 2873-2881.
- (28) Kamiuchi, N.; Matsui, T.; Kikuchi, R.; Eguchi, K., *J. Phys. Chem. C* **2007**, *111*, 16470-16476.
- (29) Tew, M. W.; Emerich, H.; van Bokhoven, J. A., *J. Phys. Chem. C* **2011**, *115*, 8457-8465.
- (30) Vajda, S.; Pellin, M. J.; Greeley, J. P.; Marshall, C. L.; Curtiss, L. A.; Ballentine, G. A.; Elam, J. W.; Catillon-Mucherie, S.; Redfern, P. C.; Mehmood, F.; Zapol, P., *Nat. Mater.* **2009**, *8*, 213-216.
- (31) Naresh, N.; Wasim, F. G. S.; Ladewig, B. P.; Neergat, M., *J. Mater. Chem. A* **2013**, *1*, 8553-8559.
- (32) Li, Y.; El-Sayed, M. A., *J. Phys. Chem. B* **2001**, *105*, 8938-8943.
- (33) Niu, Z.; Li, Y., *Chem. Mater.* **2014**, *26*, 72-83.
- (34) Harris, P. J. F., *J. Catal.* **1986**, *97*, 527-542.

- (35) Newton, M. A.; Belver-Coldeira, C.; Martinez-Arias, A.; Fernandez-Garcia, M., *Nat Mater* **2007**, *6*, 528-532.
- (36) Barau, A.; Budarin, V.; Caragheorghopol, A.; Luque, R.; Macquarrie, D. J.; Prella, A.; Teodorescu, V. S.; Zaharescu, M., *Catal. Lett.* **2008**, *124*, 204-214.
- (37) White, R. J.; Luque, R.; Budarin, V. L.; Clark, J. H.; Macquarrie, D. J., *Chem. Soc. Rev.* **2009**, *38*, 481-494.
- (38) Joo, S. H.; Park, J. Y.; Tsung, C.-K.; Yamada, Y.; Yang, P.; Somorjai, G. A., *Nat. Mater.* **2009**, *8*, 126-131.
- (39) Fang, X.; Liu, Z.; Hsieh, M.-F.; Chen, M.; Liu, P.; Chen, C.; Zheng, N., *ACS Nano* **2012**, *6*, 4434-4444.
- (40) Xiao, C.; Maligal-Ganesh, R. V.; Li, T.; Qi, Z.; Guo, Z.; Brashler, K. T.; Goes, S.; Li, X.; Goh, T. W.; Winans, R. E.; Huang, W., *ChemSusChem* **2013**, *6* (10), 1915-1922.
- (41) Wang, G.-H.; Hilgert, J.; Richter, F. H.; Wang, F.; Bongard, H.-J.; Spliethoff, B.; Weidenthaler, C.; Schüth, F., *Nat. Mater.* **2014**, *13*, 293-300.
- (43) Mizutani, M.; Yamada, Y.; Nakamura, T.; Yano, K., *Chem. Mater.* **2008**, *20*, 4777-4782.
- (44) Arnal, P. M.; Comotti, M.; Schüth, F., *Angew. Chem. Int. Ed.* **2006**, *118*, 8404-8407.
- (45) Ikeda, S.; Ishino, S.; Harada, T.; Okamoto, N.; Sakata, T.; Mori, H.; Kuwabata, S.; Torimoto, T.; Matsumura, M., *Angew. Chem. Int. Ed.* **2006**, *45*, 7063-7066.
- (46) Ge, J.; Zhang, Q.; Zhang, T.; Yin, Y., *Angew. Chem. Int. Ed.* **2008**, *47*, 8924-8928.
- (47) Sun, H.; He, Q.; Zeng, S.; She, P.; Zhang, X.; Li, J.; Liu, Z., *New J. Chem.* **2017**, *41*, 7244-7252.

- (48) Lee, I.; Albiter, M. A.; Zhang, Q.; Ge, J.; Yin, Y.; Zaera, F., *Phys. Chem. Chem. Phys.* **2011**, *13*, 2449-2456.
- (49) Shang, L.; Bian, T.; Zhang, B.; Zhang, D.; Wu, L.-Z.; Tung, C.-H.; Yin, Y.; Zhang, T., *Angew. Chem. Int. Ed.* **2014**, *53*, 250-254.
- (50) Lin, M.; Wang, Y.; Sun, X.; Wang, W.; Chen, L., *ACS Appl. Mater. Interfaces* **2015**, *7*, 7516-7525.
- (51) Pei, Y.; Maligal-Ganesh, R. V.; Xiao, C.; Goh, T.-W.; Brashler, K.; Gustafson, J. A.; Huang, W., *Nanoscale* **2015**.
- (52) Maligal-Ganesh, R. V.; Xiao, C.; Goh, T. W.; Wang, L.-L.; Gustafson, J.; Pei, Y.; Qi, Z.; Johnson, D. D.; Zhang, S.; Tao, F.; Huang, W., *ACS Catal.* **2016**, *6*, 1754-1763.
- (53) Singh, A. K.; Xu, Q., *ChemCatChem* **2013**, *5*, 652-676.
- (54) Tao, F.; Zhang, S.; Nguyen, L.; Zhang, X., *Chem. Soc. Rev.* **2012**, *41* (24), 7980-7993.
- (55) Wang, D.; Li, Y., *Adv. Mater.* **2011**, *23*, 1044-1060.
- (56) Wang, C.; Daimon, H.; Sun, S., *Nano Lett.* **2009**, *9* (4), 1493-1496.
- (57) Liu, Z.; Jackson, G. S.; Eichhorn, B. W., *Angew. Chem., Int. Ed.* **2010**, *49*, 3173-3176.
- (58) Wang, C.; Chen, D. P.; Sang, X.; Unocic, R. R.; Skrabalak, S. E., *SACS Nano* **2016**, *10*, 6345-6353.
- (59) Jana, S.; Chang, J. W.; Rioux, R. M., *Nano Lett.* **2013**, *13* (8), 3618-3625.
- (60) Vu, K. B.; Bukhryakov, K. V.; Anjum, D. H.; Rodionov, V. O., *ACS Catal.* **2015**, *5*, 2529-2533.
- (61) Park, J. Y.; Zhang, Y.; Grass, M.; Zhang, T.; Somorjai, G. A., *Nano Lett.* **2008**, *8*, 673-677.

- (62) Cui, C.; Gan, L.; Li, H.-H.; Yu, S.-H.; Heggen, M.; Strasser, P., *Nano Lett.* **2012**, *12* (11), 5885-5889.
- (63) Armbrüster, M., *Encyclopedia of Catalysis*, John Wiley & Sons, Inc.: **2002**.
- (64) Furukawa, S.; Komatsu, T., *ACS Catal.* **2017**, *7*, 735-765.
- (65) Kovnir, K.; Armbrüster, M.; Teschner, D.; Venkov, T. V.; Jentoft, F. C.; Knop-Gericke, A.; Grin, Y.; Schlögl, R., *Sci. Technol. Adv. Mater.* **2007**, *8*, 420-427.
- (66) McGown, W. T.; Kemball, C.; Whan, D. A.; Scurrrell, M. S., *J. Chem. Soc. Faraday Trans 1*, **1977**, *73*, 632-647.
- (67) Osswald, J.; Kovnir, K.; Armbrüster, M.; Giedigkeit, R.; Jentoft, R. E.; Wild, U.; Grin, Y.; Schlögl, R., *J. Catal.* **2008**, *258* (1), 219-227.
- (68) Shao, L.; Zhang, W.; Armbrüster, M.; Teschner, D.; Girgsdies, F.; Zhang, B.; Timpe, O.; Friedrich, M.; Schlögl, R.; Su, D. S., *Angew. Chem., Int. Ed.* **2011**, *50* (43), 10231-10235.
- (69) Armbrüster, M.; Kovnir, K.; Behrens, M.; Teschner, D.; Grin, Y.; Schlögl, R., *J. Am. Chem. Soc.* **2010**, *132*, 14745-14747.
- (70) Armbrüster, M.; Kovnir, K.; Friedrich, M.; Teschner, D.; Wowsnick, G.; Hahne, M.; Gille, P.; Szentmiklósi, L.; Feuerbacher, M.; Heggen, M.; Girgsdies, F.; Rosenthal, D.; Schlögl, R.; Grin, Y., *Nat. Mater.* **2012**, *11*, 690-693.
- (71) Armbrüster, M.; Wowsnick, G.; Friedrich, M.; Heggen, M.; Cardoso-Gil, R., *J. Am. Chem. Soc.* **2011**, *133*, 9112-9118.
- (72) Sra, A. K.; Schaak, R. E., *J Am Chem Soc* **2004**, *126*, 6667-72.
- (73) Cable, R. E.; Schaak, R. E., *Chem. Mater.* **2005**, *17*, 6835-6841.

- (74) Leonard, B. M.; Bhuvanesh, N. S.; Schaak, R. E., *J. Am. Chem. Soc.* **2005**, *127*, 7326-7.
- (75) Cable, R. E.; Schaak, R. E., *J. Am. Chem. Soc.* **2006**, *128*, 9588-9.
- (76) Bauer, J. C.; Chen, X.; Liu, Q.; Phan, T.-H.; Schaak, R. E., *J. Mater. Chem.* **2008**, *18*, 275-282.
- (77) Kang, Y.; Pyo, J. B.; Ye, X.; Gordon, T. R.; Murray, C. B., *ACS Nano* **2012**, *6*, 5642-5647.
- (78) Li, C.; Chen, Y.; Zhang, S.; Xu, S.; Zhou, J.; Wang, F.; Wei, M.; Evans, D. G.; Duan, X., *Chem. Mater.* **2013**, *25* (19), 3888-3896.
- (79) Chung, D. Y.; Jun, S. W.; Yoon, G.; Kwon, S. G.; Shin, D. Y.; Seo, P.; Yoo, J. M.; Shin, H.; Chung, Y.-H.; Kim, H.; Mun, B. S.; Lee, K.-S.; Lee, N.-S.; Yoo, S. J.; Lim, D.-H.; Kang, K.; Sung, Y.-E.; Hyeon, T., *J. Am. Chem. Soc.* **2015**, *137*, 15478-15485.
- (80) Ji, X.; Lee, K. T.; Holden, R.; Zhang, L.; Zhang, J.; Botton, G. A.; Couillard, M.; Nazar, L. F., *Nat. Chem.* **2010**, *2*, 286-293.
- (81) Qi, Z.; Xiao, C.; Liu, C.; Goh, T. W.; Zhou, L.; Maligal-Ganesh, R.; Pei, Y.; Li, X.; Curtiss, L. A.; Huang, W., *J. Am. Chem. Soc.* **2017**, *139*, 4762-4768.

**CHAPTER 2. A SHIP-IN-A-BOTTLE STRATEGY TO SYNTHESIZE
ENCAPSULATED INTERMETALLIC NANOPARTICLE CATALYSTS:
EXEMPLIFIED FOR FURFURAL HYDROGENATION**

ACS Catalysis, **2016**, 6, 1754-1763

Raghu V. Maligal-Ganesh, Chaoxian Xiao, Tian Wei Goh, Linlin Wang, Jeffrey Gustafson, Yuchen Pei, Zhiyuan Qi, Duane Johnson, Shiran Zhang, Franklin (Feng) Tao, and
Wenyu Huang

Abstract

Intermetallic compounds are garnering much attention for their prowess as efficient catalysts for improved selectivity in chemical processes. Herein, single phase platinum containing intermetallic NPs (iNPs) protected by a mesoporous silica (mSiO₂) shell were synthesized by the heterogeneous reduction and nucleation of Sn, Pb, or Zn on mSiO₂-encapsulated Pt NPs using a *ship-in-a-bottle* strategy. In the selective hydrogenation of furfural to furfuryl alcohol, a dramatic increase in activity and selectivity was observed when the intermetallic NPs were used as the catalyst in comparison to Pt@mSiO₂. Among the iNPs, PtSn@mSiO₂ exhibited the best performance, requiring only one-tenth of the quantity of Pt used in Pt@mSiO₂ for similar activity and close to 100% selectivity to furfuryl alcohol. Carbon deposition-induced catalyst deactivation could be conveniently reversed via a high-temperature oxidation-reduction treatment. X-ray photoelectron spectroscopy (XPS) measurements further shed light on the relevance of surface composition to the activity. Using density

functional theory (DFT) calculations, the enhanced selectivity to furfuryl alcohol on PtSn in comparison with Pt was attributed to the different adsorption configurations of furfural on these two surfaces.

Introduction

Intermetallic compounds have been the subject of significant scientific interest as efficient catalytic materials with vastly improved activity and selectivity compared to their monometallic counterparts.¹⁻⁴ The site isolation of the active metal in these ordered structures, as opposed to their random arrangement in alloys, affords geometric and electronic changes directed towards noticeable enhancement in activity, selectivity, and stability during catalysis.⁵ The synthesis of these intermetallic compounds, however, involves high temperatures and an inability to exert control over size or morphology, resulting in lower surface areas for catalysis.

Nanosizing intermetallic compounds to increase their specific surface areas is necessary to enhance their activity by several orders of magnitude.^{6,7} Schaak et al. reported the synthesis of a number of nanocrystalline intermetallic compounds using low-temperature solution chemistry methods.⁸⁻¹¹ The use of organic stabilizers in their synthetic protocol provides limited protection against aggregation of the iNPs.^{8,12} Furthermore, the use of popular supports (e.g., alumina and ceria) for the iNPs did not prevent aggregation completely.¹³ A layered double hydroxide (LDH) approach to obtain monodisperse nanoscale Ni-In intermetallic compounds for the enhanced chemoselective hydrogenation of α,β -unsaturated aldehydes has been reported.¹⁴ Without the incorporation of Al or Mg in the Ni-In LDHs, however, severe aggregation was observed in the intermetallics during their synthesis.

Here we report a unique and facile approach to synthesizing monodisperse nanoscale intermetallic compounds via seed NPs confined in a thermally robust inorganic capsule. Metal

NPs encapsulated by inorganic shells have demonstrated enhanced stability at high temperatures compared to those capped with organic agents.¹⁵⁻¹⁸ Pt NPs encapsulated in mesoporous silica shells (Pt@mSiO₂) demonstrated their stability against aggregation when annealed at 750 °C.¹⁹ Using the aforementioned Pt@mSiO₂ as the Pt seeds and the metal precursor of the additional metal (salts of Sn, Pb, Zn), we synthesized iNPs within the mSiO₂ shell. Low-temperature solution chemistry methods^{20,21} facilitated this *ship-in-a-bottle* conversion of Pt@mSiO₂ to the Pt-based iNPs as shown by the scheme in Figure 1. Intermetallic nanoparticles synthesized by this method were well confined within the mesoporous silica environment. Moreover, the mesoporous silica encapsulation did not pose any hindrance during catalytic reactions.

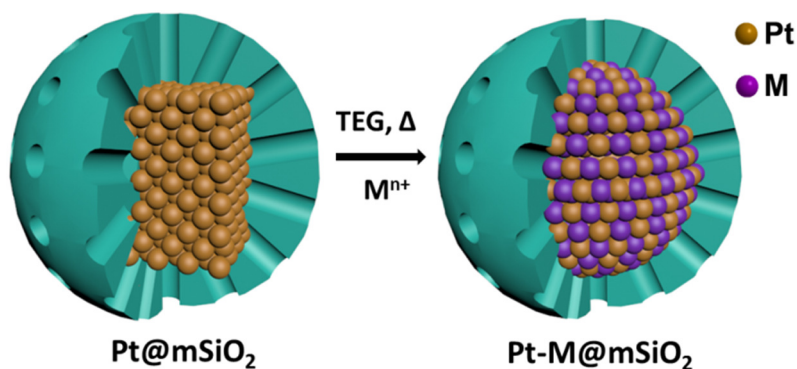


Figure 1. The ship-in-a-bottle synthesis of iNPs in a mesoporous silica-shell enclosure, a solvent-cum-reducing agent such as TEG (Tetraethylene glycol). M^{n+} = metal precursor e.g. using Sn^{2+} (as $SnCl_2 \cdot 2H_2O$)

We chose the hydrogenation of furfural to demonstrate the catalytic property of the Pt-based intermetallic compounds. Upon hydrogenation, furfural (2-furfuraldehyde), an important renewable chemical feedstock,²²⁻²⁴ produces furfuryl alcohol among other derivatives. Furfuryl alcohol features prominently as an important precursor in the synthesis

of a wide variety of chemicals.²⁵⁻²⁸ However, selectively hydrogenating furfural to furfuryl alcohol poses a considerable challenge.

Industrially, the toxic copper-chromite catalyst has been used to carry out vapor phase selective hydrogenation of furfural to furfuryl alcohol with moderate yields. However, significant deactivation of the catalyst occurs due to coking and the migration of chromium on the catalyst, effectively blocking the active sites on reduced copper NPs.²⁹ Additionally, the catalyst poses an environmental (toxic chromium) hazard and reinforces the need to find greener alternatives. Using noble metal nanoparticle catalysts, the selectivity to furfuryl alcohol is poor with the increased possibility of decarbonylation and ring hydrogenation, as opposed to the selective hydrogenation of the carbonyl bond to obtain furfuryl alcohol.³⁰ Variations in shape, size, the use of supports and surface modifiers have been reported for improved selectivity.³¹⁻³⁵ However, these still require delicate methodologies and careful design, narrowing the possibility to recycle the catalysts in their optimum state.

Using Pd NPs capped with self-assembled molecules, selectivity to furfuryl alcohol could be controlled by blocking active sites responsible for the undesired reactions.³¹ However, there is no enhancement in the activity of these catalysts to the desired product. On the contrary, for the intermetallic compounds synthesized using the shape-in-a-bottle approach, especially PtSn@mSiO₂, activity was enhanced ten-fold in comparison with Pt@mSiO₂ at nearly 100% selectivity to furfuryl alcohol. An additional advantage of the mSiO₂ protection is that a deactivated PtSn@mSiO₂ catalyst can be regenerated with a convenient oxidation/reduction treatment. We didn't observe any loss in activity and selectivity of the catalyst after six cycles of the regeneration treatment.

Results and Discussion

NiAs-type PtSn and PtPb iNPs were readily synthesized in tetraethylene glycol (TEG) and did not require further thermal treatment. The synthesis of PtSn@mSiO₂ was used as a comparison to determine the duration of the solution phase synthesis of all the other intermetallic compounds of Pt reported here. This was done regardless of further treatment beyond the solution phase or the use of different solvents (such as an oleyl amine/oleic acid mixture for the Pt-Zn systems). Samples were taken at various intervals of time from the reaction flask, centrifuged, washed, dried and characterized by Powder X-ray Diffraction (PXRD). The PXRD of these samples indicated the formation of the intermetallic phase after 2 hours at 280 °C (Figure 2).

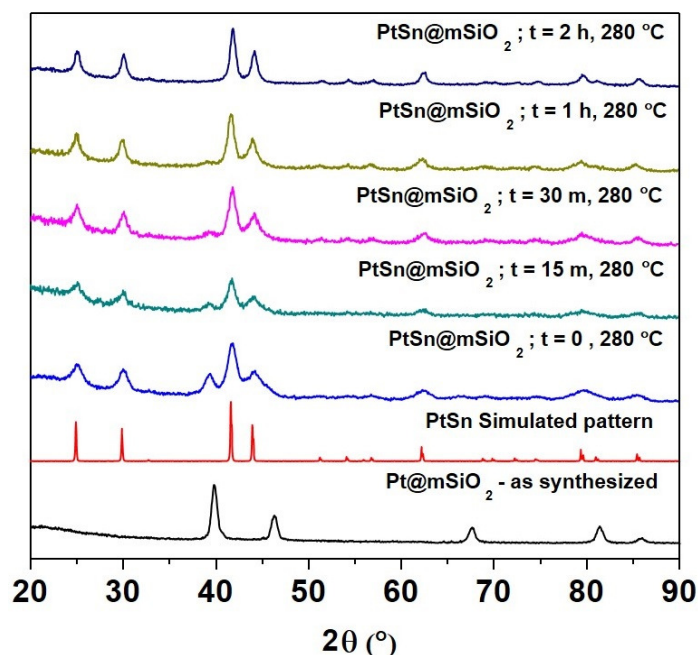


Figure 2. Time-dependent synthesis of PtSn@mSiO₂ indicating a minimum of 2 hours to completely form the intermetallic phase.

Cu₃Au-type Pt₃Sn NPs (Pt:Sn molar ratio = 3:1) were not formed in TEG, yielding alloy NPs instead even after 2 hours. However, further annealing the alloy NPs at 600 °C resulted in

the ordered intermetallic Pt₃Sn NPs (Figure 3). Similarly, Cu₃Au-type Pt₃Zn and CuAu-type PtZn (1:1 molar ratio) were not obtained after the 350 °C reaction in the mixture of oleyl amine and oleic acid until a further annealing treatment at 600 °C under 10% H₂ in Ar.

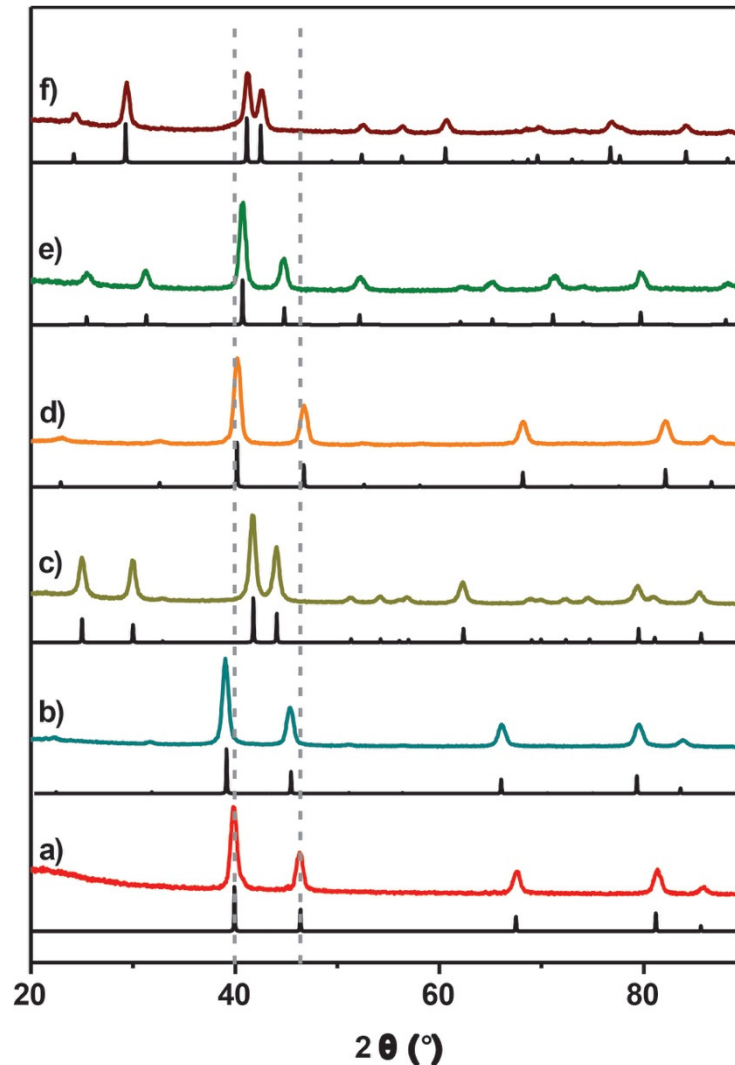


Figure 3. PXRD patterns for synthesized a) Pt@mSiO₂ and b-f) intermetallic Pt_xM@mSiO₂ NPs with Pt_xM being b) Pt₃Sn, c) PtSn, d) Pt₃Zn, e) PtZn, f) PtPb. For comparison, their simulated patterns (in black) obtained using available standard JCPDS data are also shown.

Transmission Electron Microscopy (TEM) images confirm that the intermetallic NPs are monodisperse and encapsulated within the mesoporous silica shell after the synthesis (Figure 3), which indicates the secondary metal deposits on the Pt core in Pt@mSiO₂.

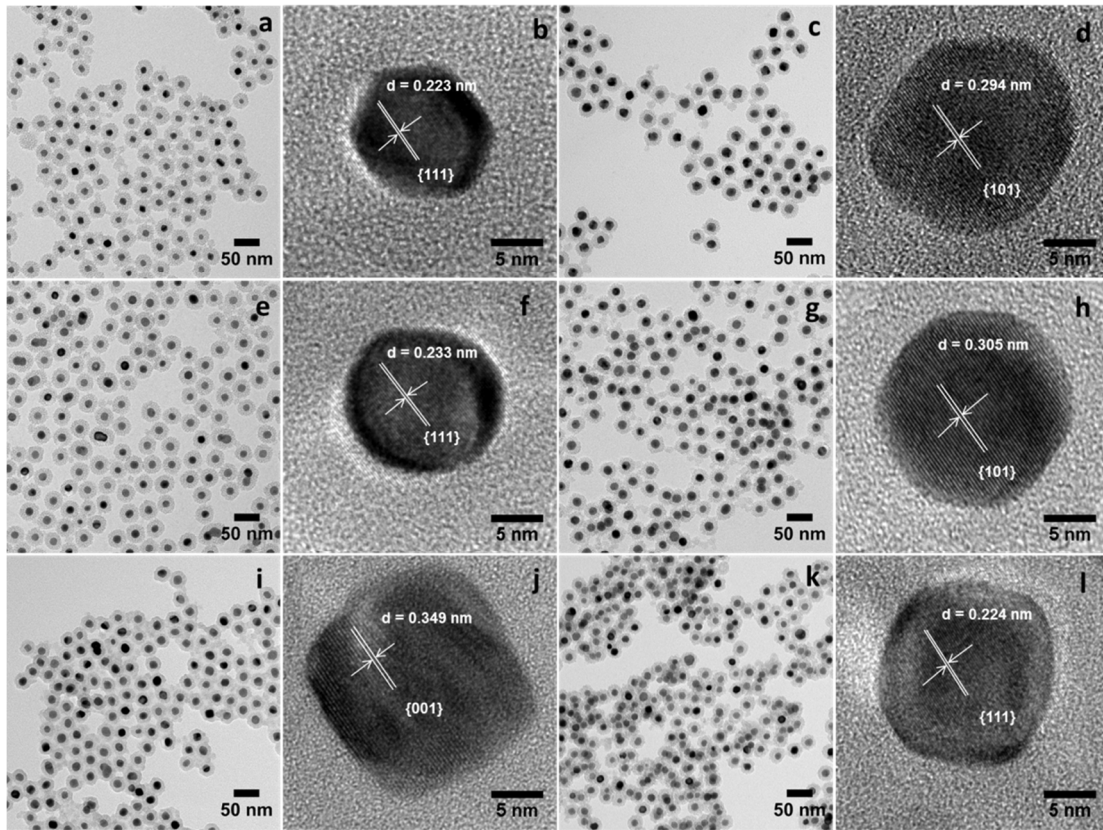


Figure 4. TEM and HRTEM images of a, b) Pt@mSiO₂ and c-l) intermetallic Pt_xM@mSiO₂ NPs with Pt_xM being c, d) PtSn; e, f) Pt₃Sn; g, h) PtPb; i, j) PtZn; and k, l) Pt₃Zn. Lattice spacings calculated from the HRTEM images are also indicated.

Comparing the overall size of the initial Pt@mSiO₂ NPs to those of the intermetallic compound NPs (Figure 5 and Table 1), the overall sizes of the particles (including the mSiO₂ shell) are almost unchanged. However, the sizes of the cores increase significantly, accompanied by a decrease in the thickness of the mesoporous silica shell. These size increases

in the cores observed from the TEM indicate the diffusion of the secondary metal precursors through the $m\text{SiO}_2$ shell and their reduction/deposition on the Pt core.

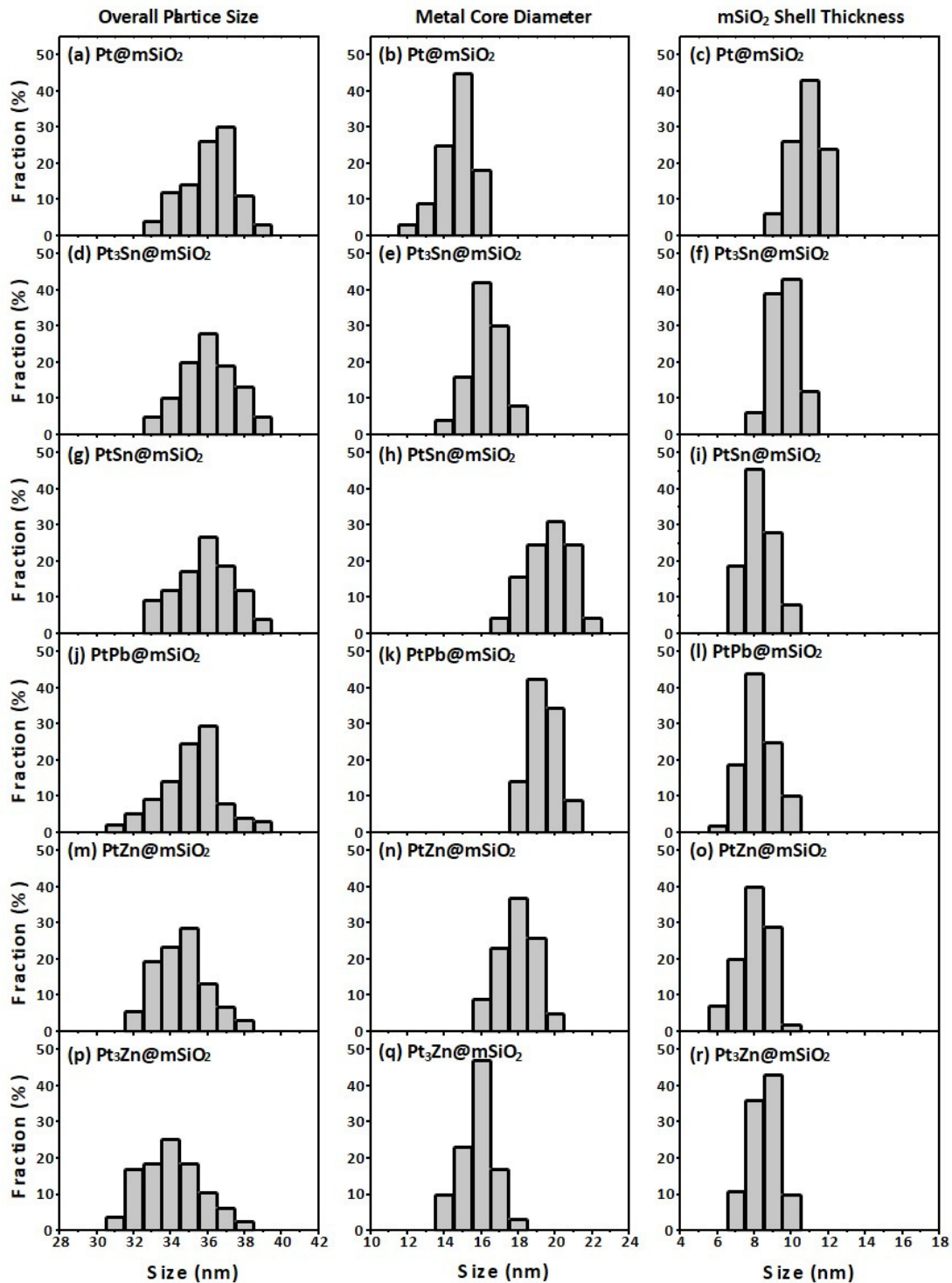


Figure 5. Size distributions of the whole particles, their cores, and the $m\text{SiO}_2$ shell.

Table 1. Size-related aspects of the metal NPs

Sample	Overall Particle Size (nm)	Metal core Diameter(nm)	Silica shell thickness (nm)
Pt@mSiO ₂	36.1 ± 1.5	14.3 ± 0.8	10.9 ± 0.8
Pt ₃ Sn@mSiO ₂	36.1 ± 1.6	16.6 ± 0.9	9.1 ± 0.8
PtSn@mSiO ₂	35.8 ± 1.7	20.6 ± 0.9	8.25 ± 0.8
PtPb@mSiO ₂	35.1 ± 1.8	19.4 ± 1.1	8.22 ± 0.9
PtZn@mSiO ₂	34.6 ± 1.3	18.1 ± 0.9	7.8 ± 0.9
Pt ₃ Zn@mSiO ₂	34.9 ± 1.6	15.8 ± 1.0	8.5 ± 0.8

For the histograms (whose data is summarized in this table) around 200 nanoparticle composites were counted before plotting the histograms to gain insight into the size of the core, the shell, and particles overall.

The decrease in mSiO₂ shell thickness could be due to etching of less cross-linked internal silica under synthesis conditions. Park et al. reported the internal hollowing of silica spheres in aqueous media suggesting the relatively less cross-linked, high surface-energy inner environs to be more reactive and susceptible to dissolution, especially in aqueous or basic media.³⁶ Other reports have also suggested a preferential internal etching of silica rather than at the periphery.^{37,38}

EDS line-scans carried out on single PtSn@mSiO₂ particles show that Pt and Sn were predominantly in the metallic core of the composite NPs (Figure 6).

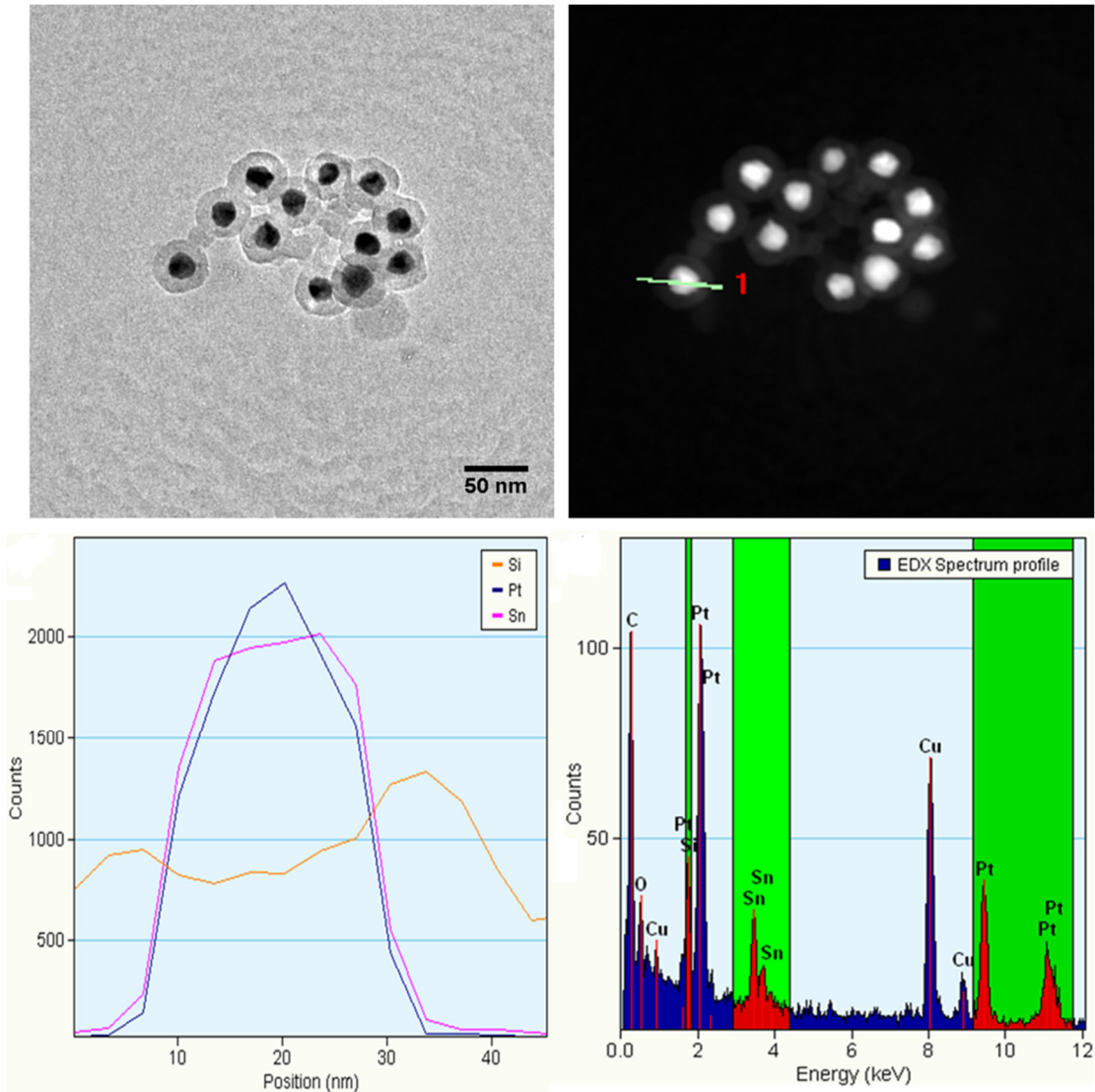


Figure 6. The EDX spectrum profile of a single PtSn@mSiO₂. The EDX line scans are an indication that both Pt and Sn are predominantly within the nanoparticle core with silica forming an encapsulation around it.

N₂ physisorption measurements carried out on a sample of Pt@mSiO₂ and PtSn@mSiO₂ show the BET surface area decreases from 570 to 474 m²/g after converting the core from Pt to PtSn, which agrees with the decrease in the mSiO₂ shell thickness (Figure 7

and Table 2). The pore size of the mesoporous SiO₂ shell increases slightly from 2.5 nm (Pt@mSiO₂) to 2.7 nm (PtSn@mSiO₂).

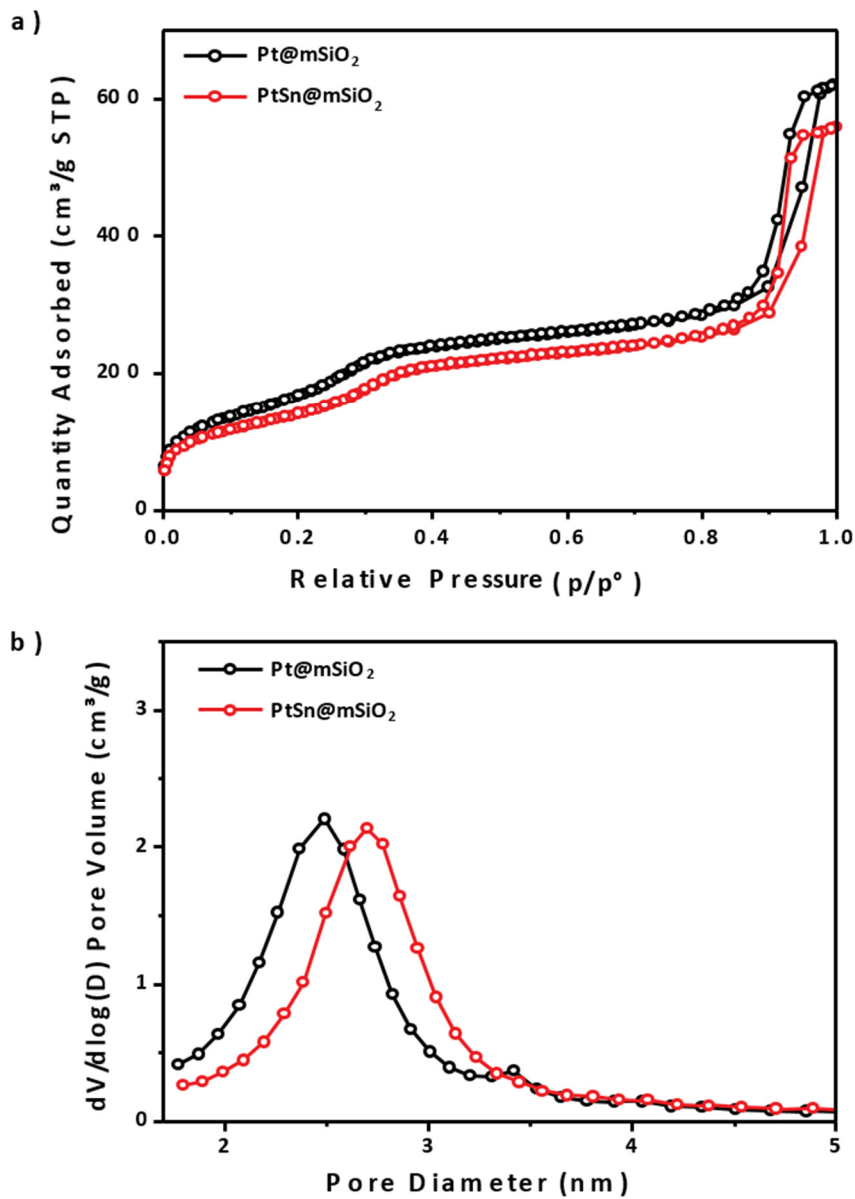


Figure 7. a) BET Surface Area measurements and b) BJH curves of Pt@mSiO₂ and PtSn@mSiO₂, respectively.

Incorporating Sn into Pt@mSiO₂ to obtain PtSn@mSiO₂ results in a significant decrease in the BET surface area. As discussed earlier, this was attributed to the loss of silica via etching of the same in the solution to accommodate the addition of Sn to the Pt NPs. Pore width didn't change significantly once intermetallic PtSn@mSiO₂ was formed.

Table 2. Summary of BET Measurements

Sample	BET Surface Area (m ² /g)	Pore Volume (cm ³ /g)	Pore Width (nm)
Pt@mSiO ₂	570.2 ± 6.3	0.58	2.5
PtSn@mSiO ₂	474.4 ± 8.2	0.48	2.7

Vapor-phase Furfural Hydrogenation

Furfural hydrogenation was carried out in a gas-phase plug-flow reactor equipped with an online gas chromatograph. Pt@mSiO₂ and PtSn@mSiO₂ were calcined at 500 °C for 4h in air to remove organic residues from synthesis followed by reduction at 300 °C for 4h under 10% H₂/He before catalysis studies. PtSn@mSiO₂ after this calcination and reduction treatment, as observed by TEM and measured by PXRD, is still well encapsulated within the silica shell and maintains its intermetallic phase (Figure 8). PtSn@mSiO₂, containing the same amount of Pt as in Pt@mSiO₂, results in conversion of 99% of the feed furfural, while it is only 24% for Pt@mSiO₂ (Figure 9a). In the case of PtSn@mSiO₂ high selectivity (97%) was also obtained towards furfuryl alcohol – the desired product.

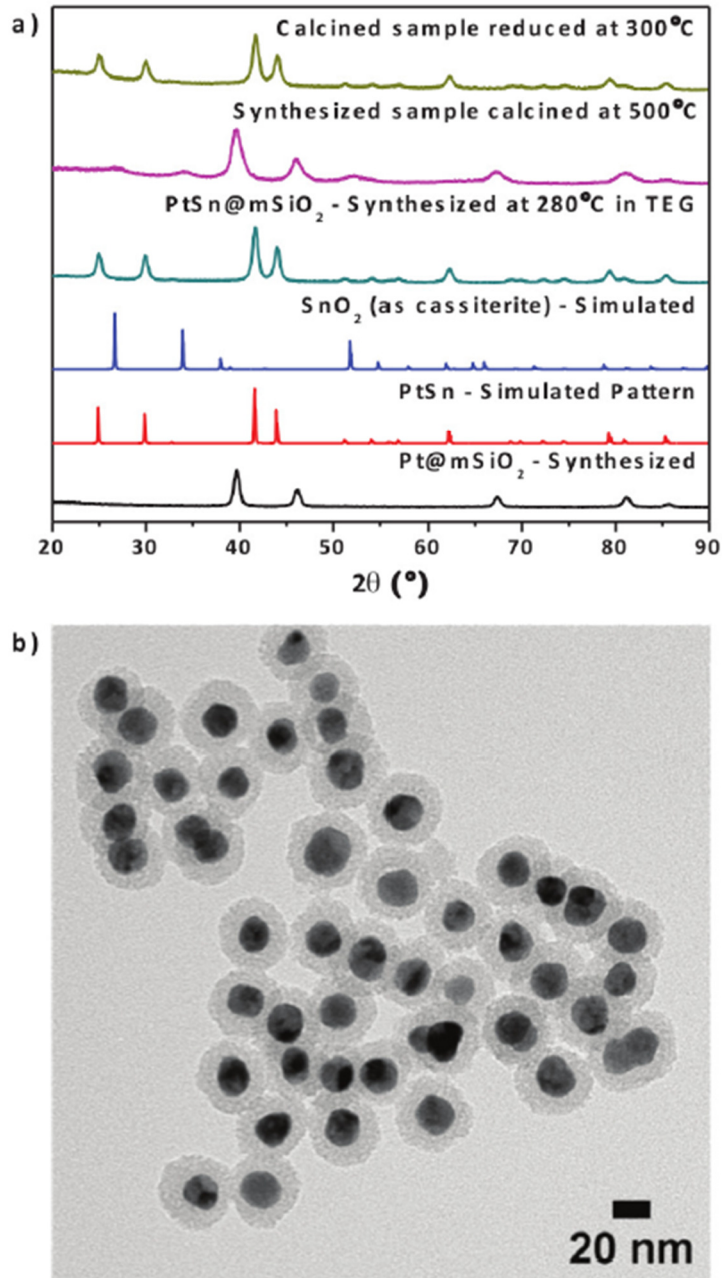


Figure 8. a) PXRD patterns for the calcination/reduction of PtSn@mSiO₂. b) TEM of the sample after calcination and reduction indicates that even after the high-temperature treatment the nanoparticle core is still well encapsulated in the mesoporous silica shell.

Along with the greatly enhanced furfuryl alcohol selectivity on PtSn@mSiO₂ compared to that on Pt@mSiO₂, the intermetallic catalyst is very stable, giving close to 100% conversion over a time on stream study for 40 hours.

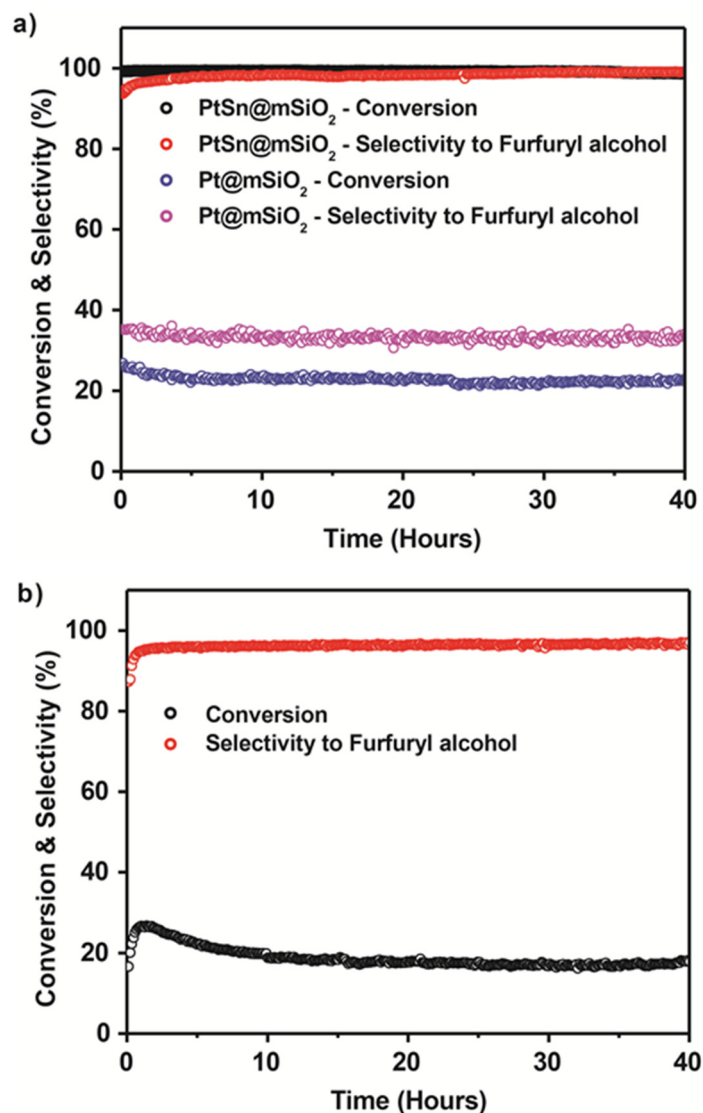


Figure 9. a) Catalytic performance of Pt@mSiO₂ versus PtSn@mSiO₂. b) Furfural hydrogenation by PtSn@mSiO₂ with a lower amount of the catalyst (0.26 mg, Pt mass = 0.124 mg). Reaction conditions for furfural hydrogenation: Furfural/H₂/He = 0.023/11.4/8.6 mL/min, 160 °C.

As the conversion is too high to evaluate the actual stability of PtSn@mSiO₂, we decreased the amount of the catalyst (0.26 mg of PtSn@mSiO₂, containing 0.124 mg Pt) to tune the furfural conversion to ~ 20%. Again, the catalyst is stable for a 40 hour-test after an initial induction period (Figure 9b). Moreover, the low conversion data on PtSn@mSiO₂ shows that only one-tenth the amount of Pt is needed in the intermetallic catalyst compared to the pure Pt catalyst to achieve similar conversion of furfural.

This PtSn@mSiO₂ intermetallic catalyst demonstrates that greatly enhanced activity and selectivity in the hydrogenation of furfural to furfuryl alcohol can be achieved compared to pure Pt NPs with largely reduced usage of the precious metal. The other Pt-Sn composition, namely Pt₃Sn@mSiO₂ also demonstrated higher conversion and selectivity than Pt@mSiO₂. To prepare Pt₃Sn@mSiO₂, it's alloy (with a Pt:Sn molar ratio = 3:1) was first synthesized. After synthesis in tetraethylene glycol, the sample was first calcined at 500°C to remove any organic residues. This was then reduced in 10% H₂ for 6 hours to obtain intermetallic Pt₃Sn@mSiO₂. Intermetallic Pt₃Sn@mSiO₂, containing the same amount of Pt, also showed around 95% selectivity to furfuryl alcohol but deactivated over time (Figure 10a). However, it deactivated much slower in comparison to the unannealed PtSn alloy (Pt:Sn ratio = 1:0.3). We speculate that this is due to the greater degree of ordering in the intermetallic iteration of the compound than in the alloy. The other intermetallic catalysts, including PtZn, Pt₃Zn, and PtPb were also tested (Figure 11). All of them showed high selectivity to furfuryl alcohol, however, their conversions were lower than PtSn@mSiO₂ and Pt₃Sn@mSiO₂ for the same quantity of Pt employed.

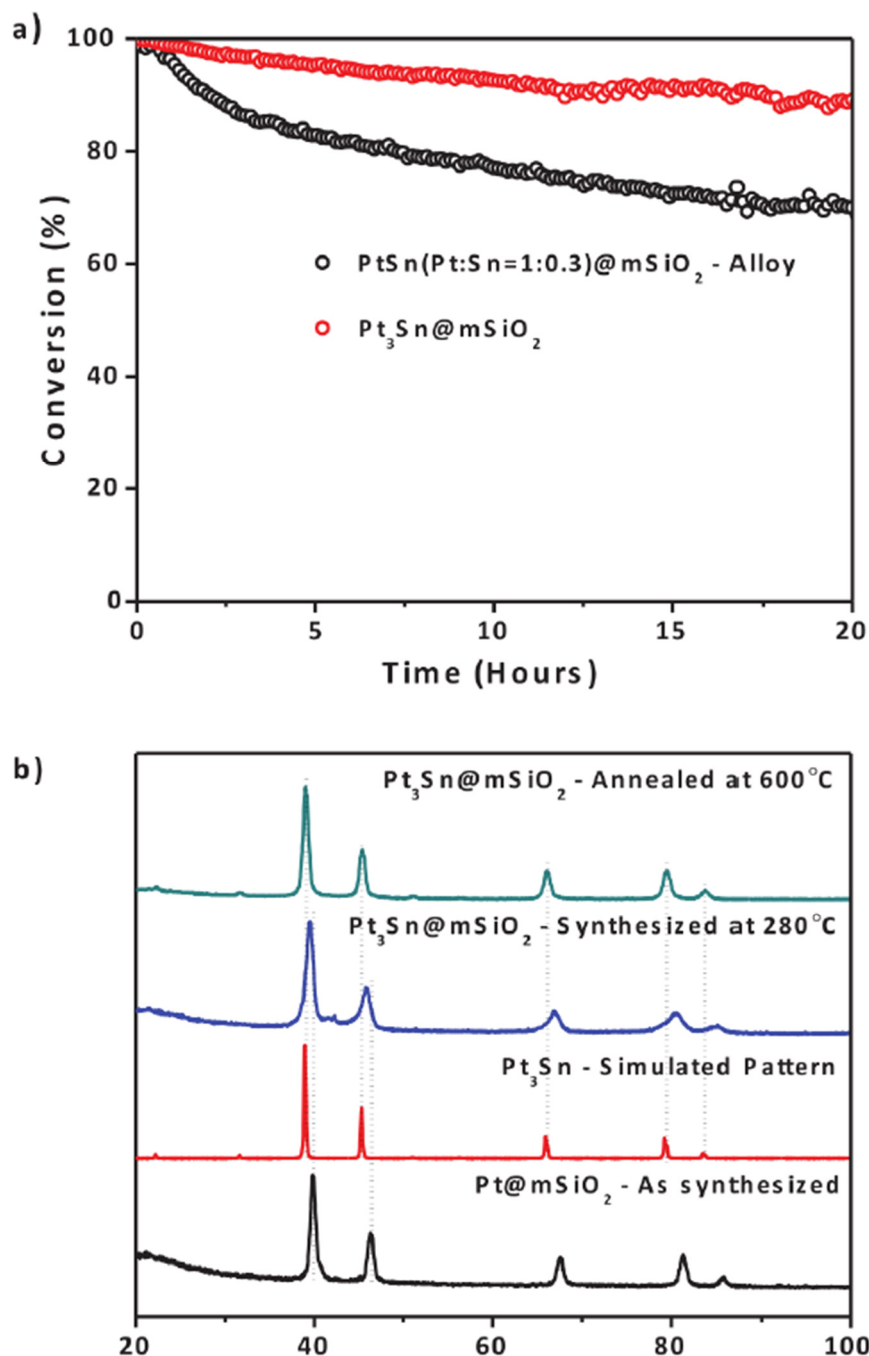


Figure 10. a) Activity of the $\text{Pt}_3\text{Sn@mSiO}_2$ and alloy PtSn@mSiO_2 (Pt:Sn ratio = 1:0.3). Selectivity is ~97% for the two catalysts. b) PXRD patterns of $\text{Pt}_3\text{Sn@mSiO}_2$ before and after reduction.

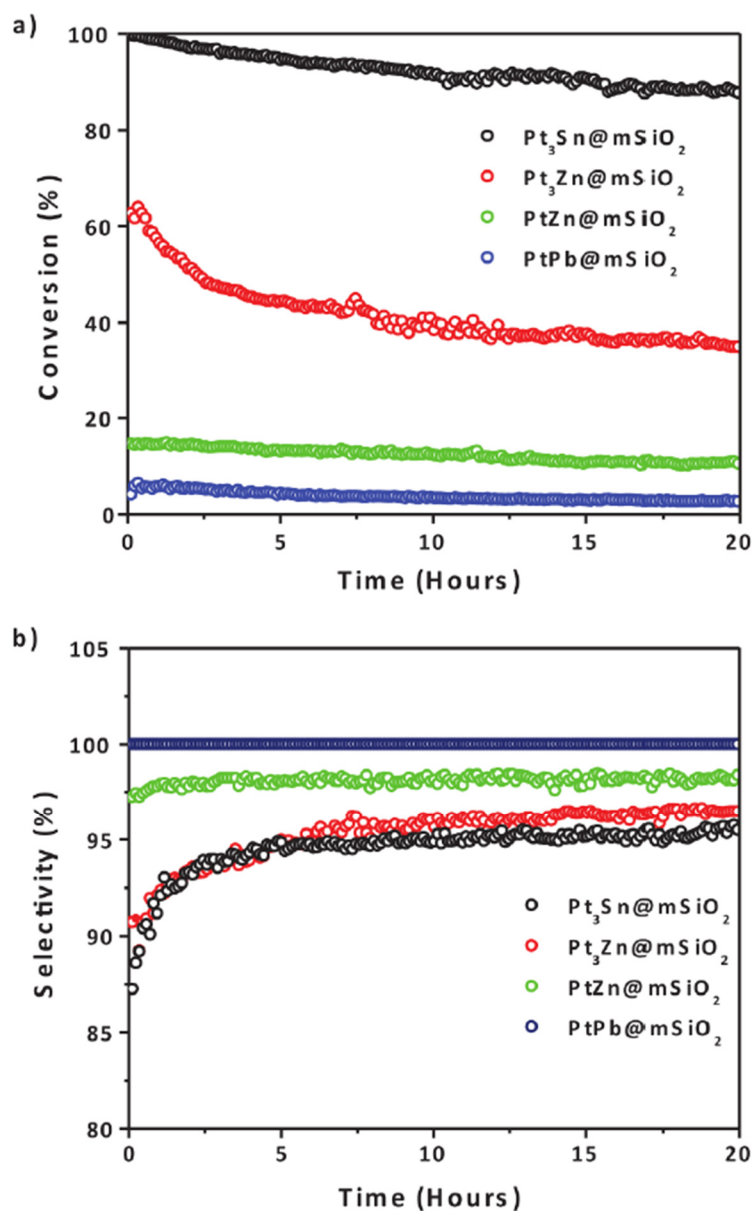


Figure 11. a) Conversion and b) selectivity for the other intermetallic Pt₃Sn, Pt₃Zn, PtZn, and PtPb NPs encapsulated in mSiO₂. The quantity of Pt was kept the same in all the above catalysts for a reasonable comparison with Pt@mSiO₂ and PtSn@mSiO₂. As can be observed, even with differing activity, all the intermetallic catalysts showed high selectivity towards furfuryl alcohol.

To indicate the importance of the mesoporous encapsulation, a control catalyst was also prepared by supporting the Pt colloidal NPs onto MCF-17 without the $m\text{SiO}_2$ coating and then converting it to PtSn/MCF-17, using the same synthetic conditions used to prepare PtSn@mSiO₂. The TEM images clearly depict aggregation for the final intermetallic compound on the support (Figure 12b).

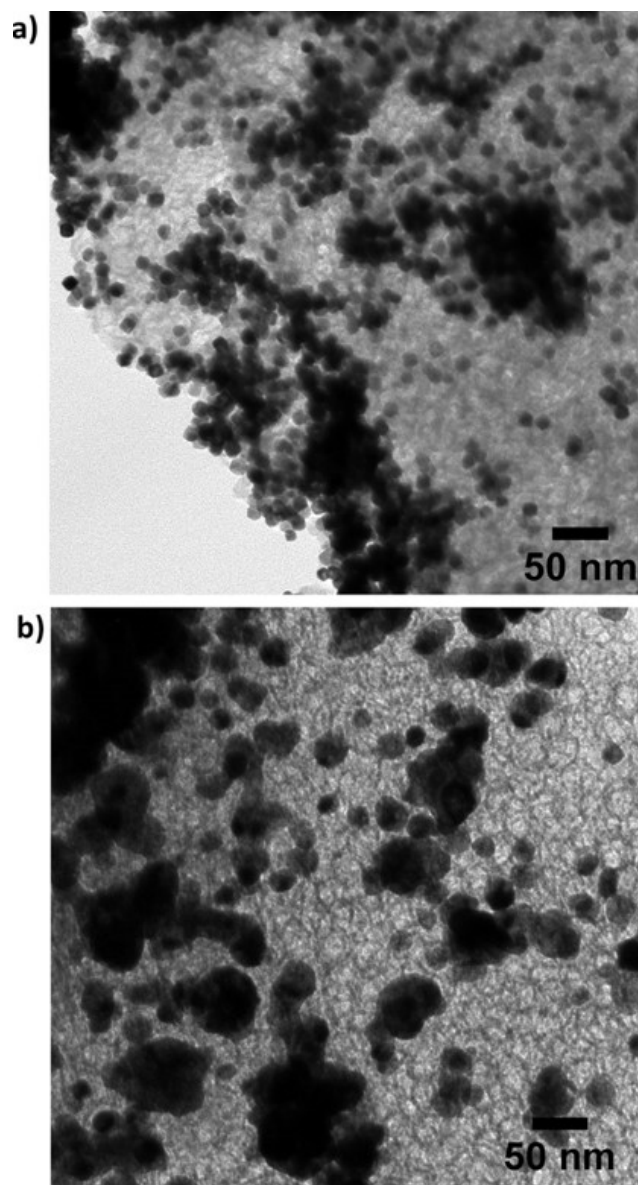


Figure 12: TEM images for a) Pt/MCF-17 - Pt NPs on MCF-17 b) PtSn/MCF-17

The conversion of furfural to furfuryl alcohol using the same quantity of Pt was far lower (stabilized at 4% after an induction period) for PtSn/MCF-17, although the selectivity is similar at around 96% to furfuryl alcohol (Figure S13a). Copper chromite, the industrial catalyst used for the hydrogenation of furfural, was also tested under our reaction conditions. High conversion and good selectivity are observed initially. However, the catalyst decays after 2 hours (Figure 14).

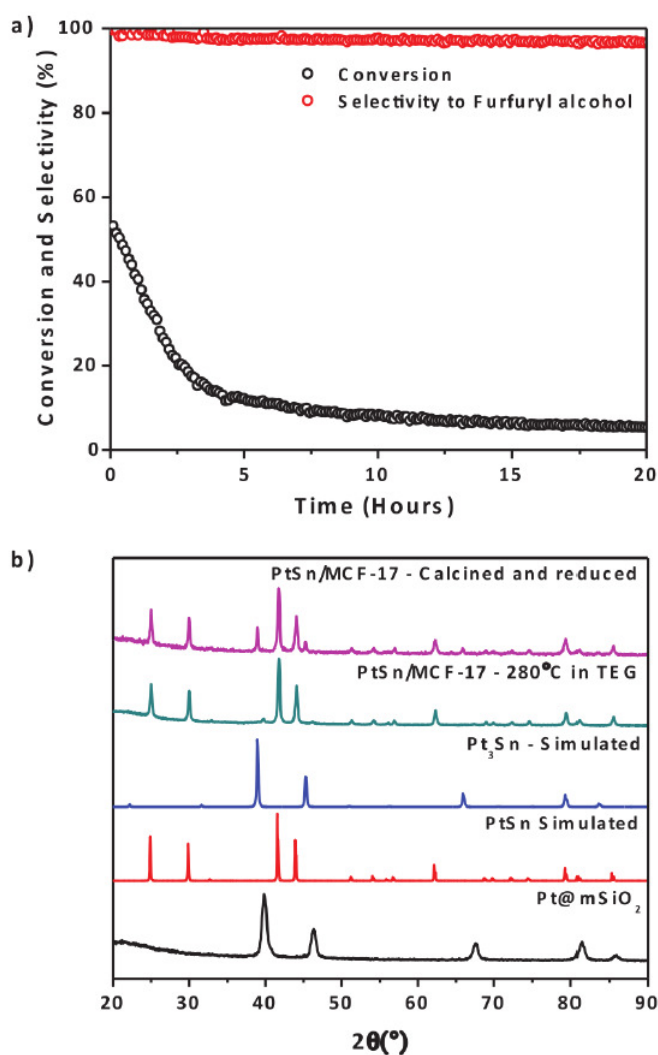


Figure 13. a) Furfural hydrogenation for PtSn/MCF-17. Amount of catalyst: 4.64 mg; Reaction conditions: Furfural/H₂/He = 0.023/11.4/8.6 mL/min, 160°C. b) PXRD patterns for the PtSn/MCF-17.

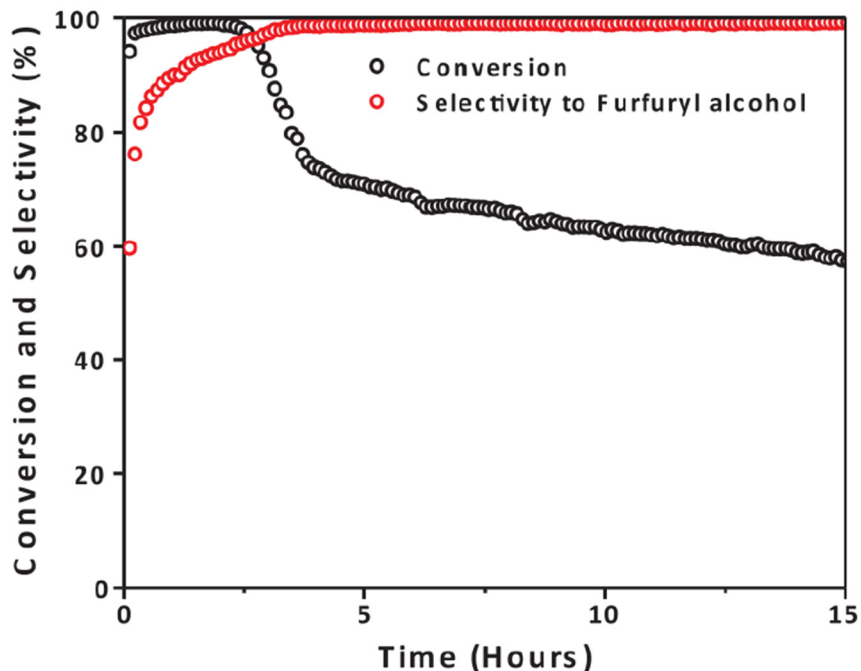


Figure 14. Furfural hydrogenation by Copper Chromite ($2\text{CuO}\cdot\text{Cr}_2\text{O}_3$); Amount of catalyst: 2.56 mg; Reaction conditions: Furfural/ H_2 / He = 0.023/11.4/8.6 mL/min, 160°C . Commercially available Copper Chromite has been considered the standard catalyst for furfural hydrogenation in the industry.

X-ray photoelectron Spectroscopy study of PtSn@mSiO_2 for furfural hydrogenation

Focusing on the best catalyst for furfural hydrogenation to understand the importance of the surface for activity and stability, X-ray photoelectron spectroscopy (XPS) studies were carried out on the intermetallic PtSn@mSiO_2 . Sn has been known to segregate to the surface readily upon exposure to air in PtSn bimetals due to its greater affinity for oxygen.³⁹⁻⁴² The freshly reduced sample showed higher conversion and greater stability compared to the sample that had not been reduced before reaction. The latter was a sample that had undergone typical synthesis, followed by calcination and reduction and then stored in a vial for two weeks. Their

selectivity to furfuryl alcohol was similar (96-98%) when furfural hydrogenation was carried out over a 10-hour period (Figure 15).

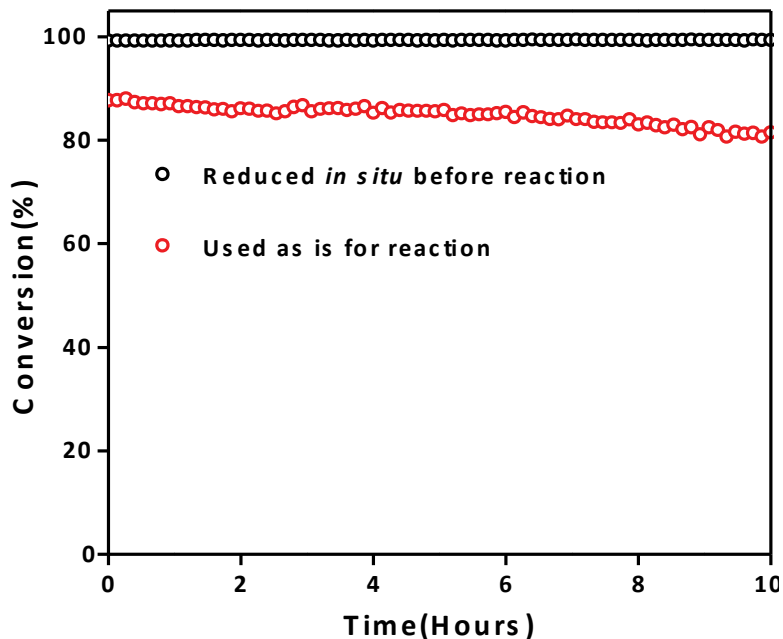


Figure 15. a) Conversion for reduced and unreduced PtSn@mSiO₂. The selectivity of both samples to furfuryl alcohol is between 96 to 98%. Reaction conditions: Furfural/H₂/He = 0.025/11.4/8.6 mL/min, 160 °C.

From the XPS spectra, the surface atomic concentration of Pt:Sn on the pre-reduced sample was 1:1.1, closer to the stoichiometry of the intermetallic compound (Pt:Sn ICP-MS ratio = 1:1.02; Table 1), while the PtSn sample that hadn't been reduced before XPS had a lower surface atomic concentration of Pt relative to Sn (Pt:Sn = 1:1.3, Table 1). Platinum in both the samples was in its metallic state, with a slight shift to higher binding energy (0.1~0.2 eV) for PtSn@mSiO₂ that had been reduced before XPS (Figure 6a). From the Sn spectra (Figure 6b), however, it is evident that the oxide component is greater than metallic tin in the sample that had not been reduced just before the reaction. The percentage of reduced Sn on this sample is only 52% of the total Sn on the surface.

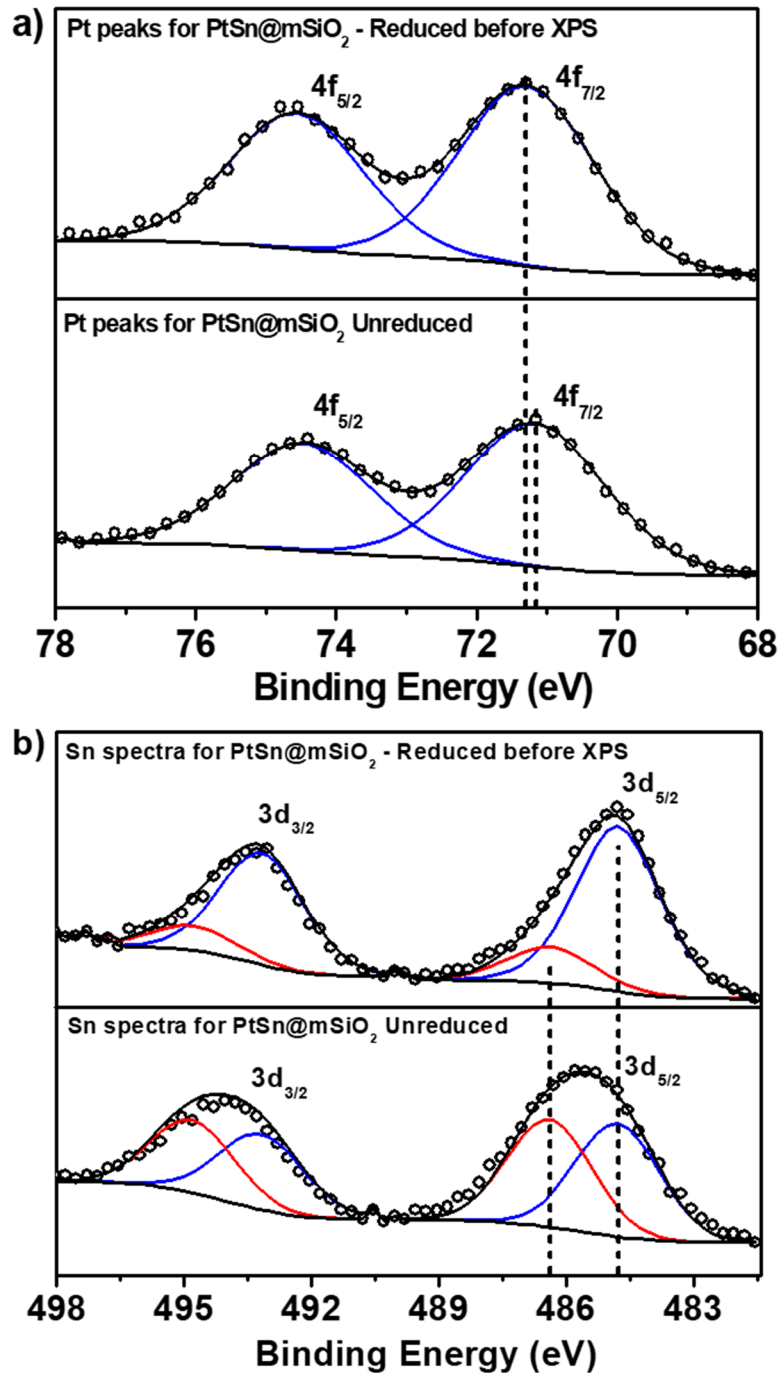


Figure 16. a) Pt XPS spectra for PtSn@mSiO₂ with and without reduction before XPS. b) Sn XPS spectra for PtSn@mSiO₂ that with and without reduction before XPS. Blue peaks correspond to the elements in their metallic state, while red components correspond to their oxides.

A higher percentage of reduced Sn on the surface (84% of the total Sn on the surface, Table 1) and a surface atomic ratio that represents the stoichiometry of the intermetallic compound seemed to contribute to the enhanced conversion by the catalyst that was reduced prior to furfural hydrogenation. This was further verified by initially running a freshly reduced catalyst for a short period, following which the catalyst was calcined in air. The conversion of furfural drops drastically from ~100% to ~30% after calcination (Figure 17). Hence although adding Sn to Pt improves the selectivity of the catalyst, the presence of excess Sn with respect to Pt on the surface reduces the conversion of the catalyst for furfural hydrogenation.

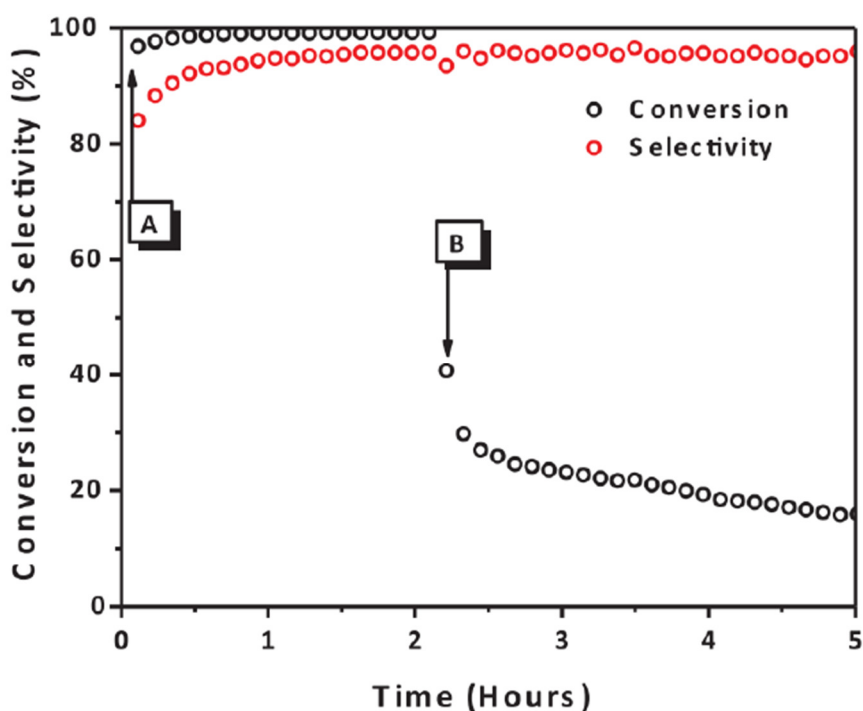


Figure 17. Furfural hydrogenation of PtSn@mSiO₂ under different pretreatment conditions: A – Calcined at 500°C in air and reduced at 300°C in 10% Hydrogen before hydrogenation; B – Calcined at 500°C before hydrogenation was resumed.

From the XPS measurements carried out on the calcined sample, Pt is still in the metallic state, while Sn exists solely as its oxides (Figure 18). The surface atomic ratio of Pt:Sn indicates that Sn is 5.5 times higher than Pt on the surface (Table 3).

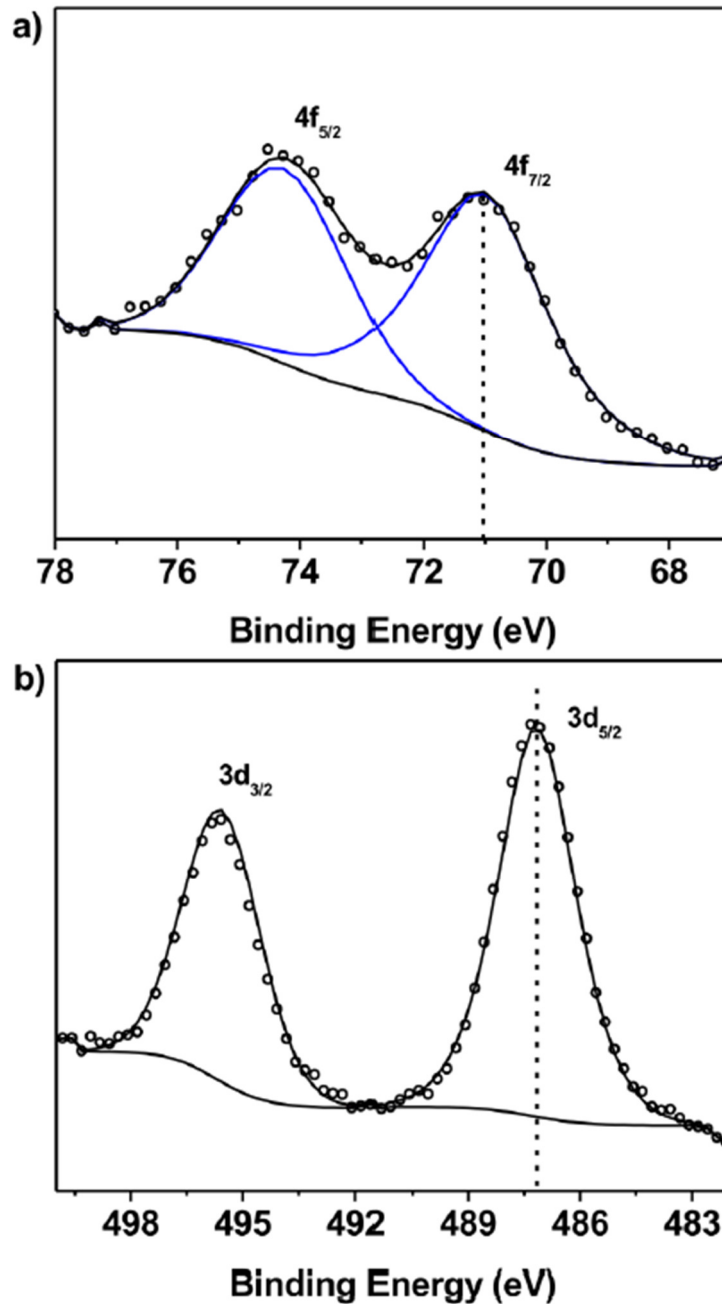


Figure 18. a) Pt peaks for the calcined sample (only metallic Pt observed). b) Sn peaks for the calcined sample (only Sn oxides observed via the fitting).

Table 3. XPS summary of the various PtSn@mSiO₂ samples

Sample	Pt:Sn by ICP- MS	Pt 4f _{7/2} (eV)	Sn 3d _{5/2} (Sn(0)) (eV)	Sn 3d _{5/2} (Sn(II,IV)) (eV)	Surface Pt:Sn	Sn(0)/Sn _{Total}
PtSn@mSiO ₂ unreduced	1:1.02	71.2	484.8	486.4	1:1.3	0.52
PtSn@mSiO ₂ reduced ^a	1:1.02	71.3	484.8	486.4	1:1.1	0.86
PtSn@mSiO ₂ calcined	1:1.02	71.3	N/A	487.1	1:5.5	N/A
PtSn@mSiO ₂ (Pt:Sn =1:1.1) reduced ^a	1:1.12	71.5	484.8	486.4	1:1.4	0.75

^a The samples were reduced at 300 °C in 10% H₂ right before XPS measurements.

Some reports we had resorted to for the synthesis of nanoscale intermetallic PtSn used significantly excess Sn.^{10,13} We wanted to observe the effect of adding slightly excess Sn during our synthesis of PtSn. PtSn_{1.1}@mSiO₂ with excess Sn (Pt:Sn = 1:1.12 measured by ICP-MS) was thus synthesized. We found that this 10% increase in the bulk Sn composition induced a 40% increase in the surface Sn concentration of the PtSn NPs, even when XPS was measured immediately after the sample had been reduced at 300°C in 10% Hydrogen (Pt:Sn surface ratio by XPS = 1:1.4, Table 3).

As seen in the Sn XPS in Figure 19b although reduction for PtSn_{1.1}@mSiO₂ was employed under similar conditions to PtSn@mSiO₂, the oxide component was more prominent. Additionally, from Table 3, PtSn@mSiO₂ (Pt:Sn = 1:1.1) also had a lower fraction of reduced Sn on the surface at 75%, compared to 86% reduced Sn in PtSn@mSiO₂ (Pt:Sn = 1:1) with respect to the total surface Sn. Increased surface Sn and a high percentage of oxidized Sn on the intermetallic surface may have contributed to the rapid decay in activity during furfural hydrogenation (Figure 20).

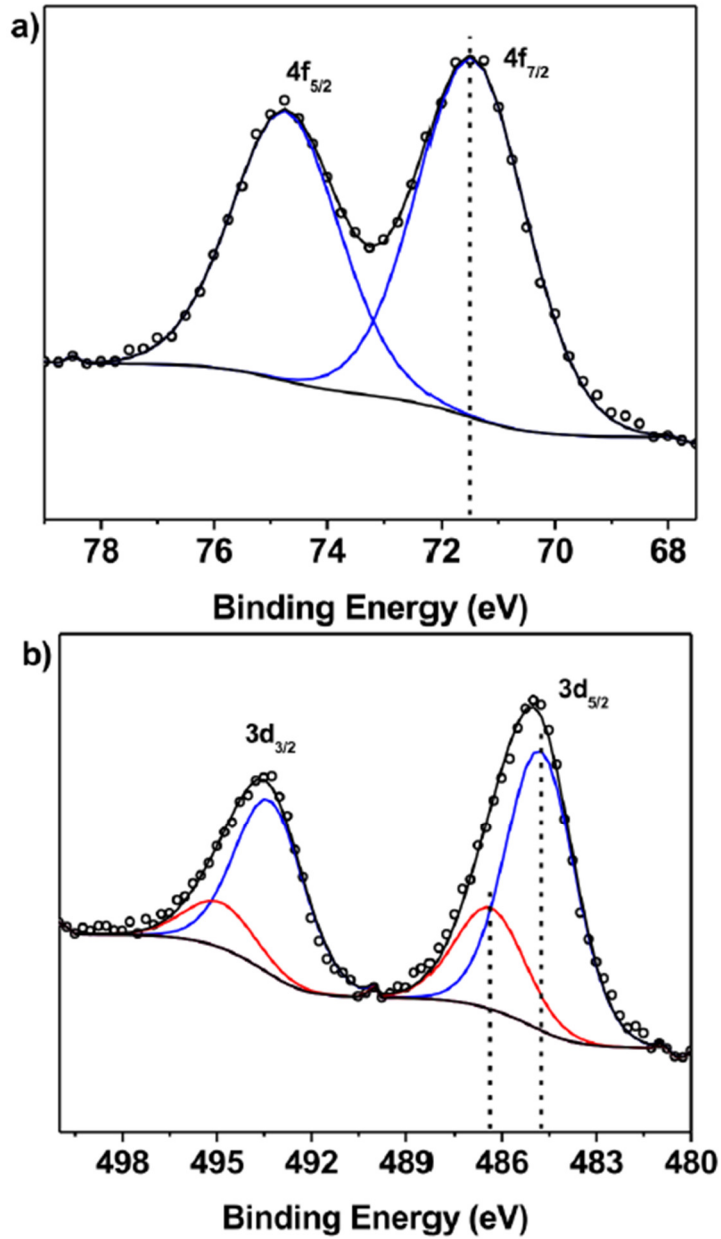


Figure 19. a) Pt and b) Sn peaks for PtSn@mSiO₂ (Pt:Sn = 1:1.1). The sample was reduced at 300°C in 10% H₂ before XPS.

Hence although adding Sn was beneficial to the performance of the catalyst via the formation of intermetallic PtSn, Sn added beyond the required amount accumulated on the

surface. The extra Sn on the intermetallic surface was susceptible to oxidation and detrimental to the stability of the catalyst in furfural hydrogenation.

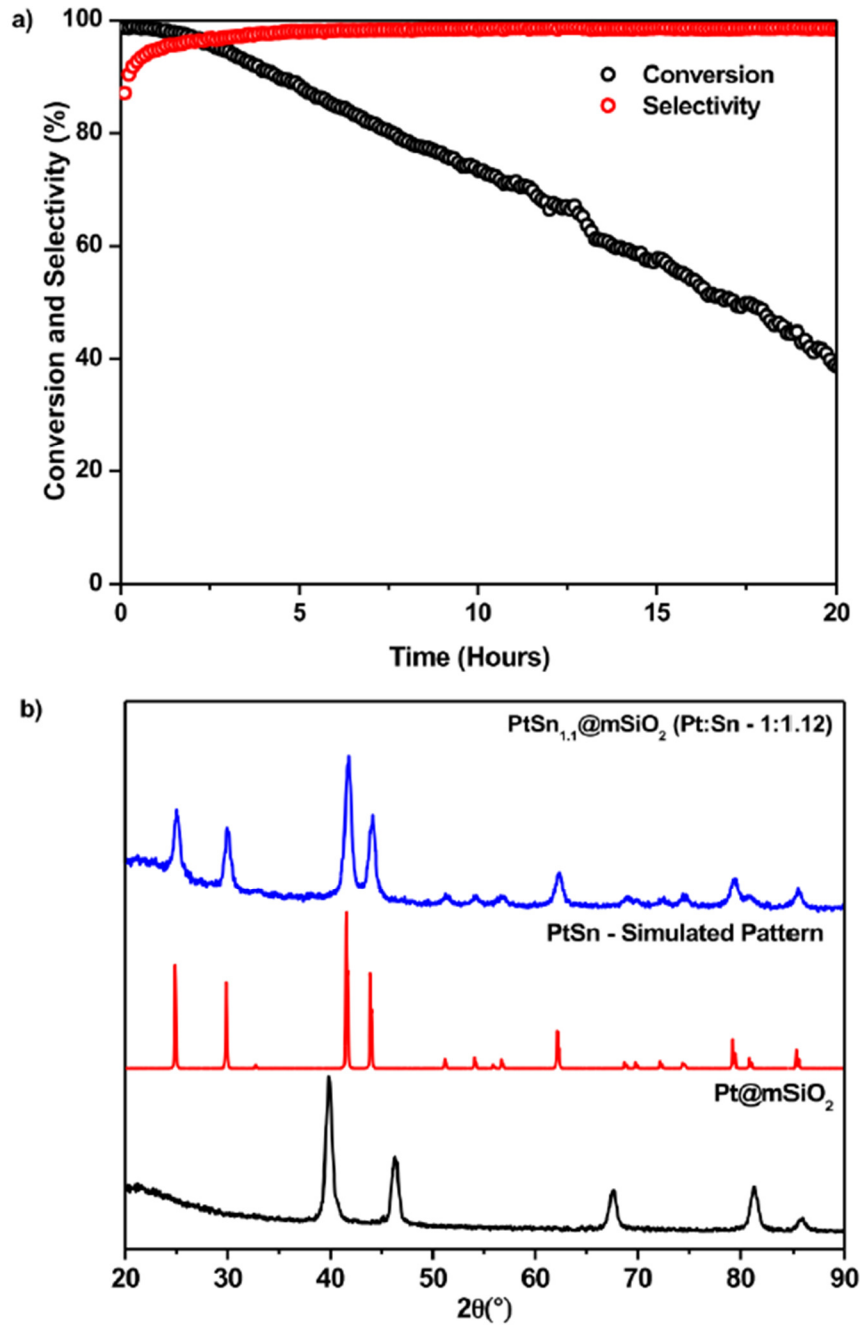


Figure 20. a) Furfural hydrogenation by PtSn@mSiO₂ (Pt:Sn = 1:1.12). b) PXRD pattern of the same sample.

We also tried to measure if there is any surface segregation of Pt or Sn on the PtSn@mSiO₂ using ambient pressure XPS (AP-XPS). AP-XPS measurements were carried out at different reduction temperatures to observe if the Pt:Sn surface atomic ratio would be affected by an increase in the reduction temperature. Using 0.2 Torr H₂ for the reduction of samples dispersed on pyrolytic graphite using ethanol, they were then examined by X-ray analysis after they were taken out to a manipulator in an ultrahigh vacuum. Pt:Sn atomic surface ratios indicate the intermetallic stoichiometry of bulk PtSn is maintained on the surface under reduction conditions.

The atomic percentage of Pt and Sn, as well as their ratios to Si, could be found in Table 4. The atomic ratio of surface Pt to Sn (1:1.1) is consistent with the bulk ratio. Annealing PtSn@mSiO₂ in H₂ at elevated temperatures, the composition of Pt and Sn barely changes, suggesting there is no segregation of Pt or Sn in the PtSn core under these reduction conditions. The ratios of Pt and Sn to Si are rather small, consistent with the fact that PtSn nanoparticle is encapsulated in the SiO₂ shell. The ratios of Pt and Sn to Si under these pretreatment conditions do not change much, indicating that the PtSn core still stays in the SiO₂ shell after 500 °C reduction.

Table 4. Compositional information of PtSn@mSiO₂ obtained from AP-XPS

Sample	Pt%	Sn%	Pt/Si	Sn/Si	Pt+Sn/Si
Fresh sample	47.7	52.3	0.0192	0.0211	0.0403
Sample reduced (H ₂ -300°C-0.5h)	47.6	52.4	0.0194	0.0214	0.0408
Sample reduced (H ₂ -500°C-0.5h)	48.5	51.5	0.0220	0.0236	0.0456

Catalyst Regeneration

A regeneration experiment was carried out to demonstrate the extra benefit of having the mSiO₂ shell protection for the iNPs. As demonstrated earlier, PtSn@mSiO₂ can be calcined at 500 °C and reduced at 300 °C to regenerate its intermetallic phase. Performing the same treatment on deactivated catalysts due to carbon deposition, we should be able to remove the deposited carbon and regenerate the intermetallic catalysts. To test this hypothesis, PtSn@mSiO₂ was first reduced at 300 °C *in situ* in the flow reactor using 10% H₂, followed by furfural hydrogenation for 35 minutes with the vapor composition being Furfural/H₂/He = 0.025/11.4/8.6 mL/min at 160 °C. Then the catalyst was deactivated intentionally by increasing the ratio of furfural to hydrogen such that Furfural/H₂/He = 0.025/2.86/17.2 mL/min. Following this deactivation, the catalyst was calcined at 500 °C for 30 minutes in air to remove deposited carbon and then reduced at 300 °C for 30 minutes. This constituted a single regeneration cycle and the catalyst showed completely recovered activity in furfural hydrogenation. In total 6 cycles were carried out to demonstrate the ability to regenerate the catalyst (Figure 21).

DFT Studies

To explain the high hydrogenation selectivity toward furfuryl alcohol on the PtSn NPs, we performed DFT-PBE calculations to compare the adsorption of furfural on PtSn surfaces versus Pt(111). PtSn at 1:1 ratio forms a line compound of hexagonal NiAs structure with Pt-Pt atomic chains, which is more open than the close-packed face-centered cubic (FCC) structure. Among the three cleaving planes, we found that (110) and (100) have lower energy cost than (001) because the former preserves while the latter breaks the strong interaction in

Pt-Pt chains. This behavior agrees with our earlier study on PtPb and PtBi compounds in the same NiAs structure.⁴⁴

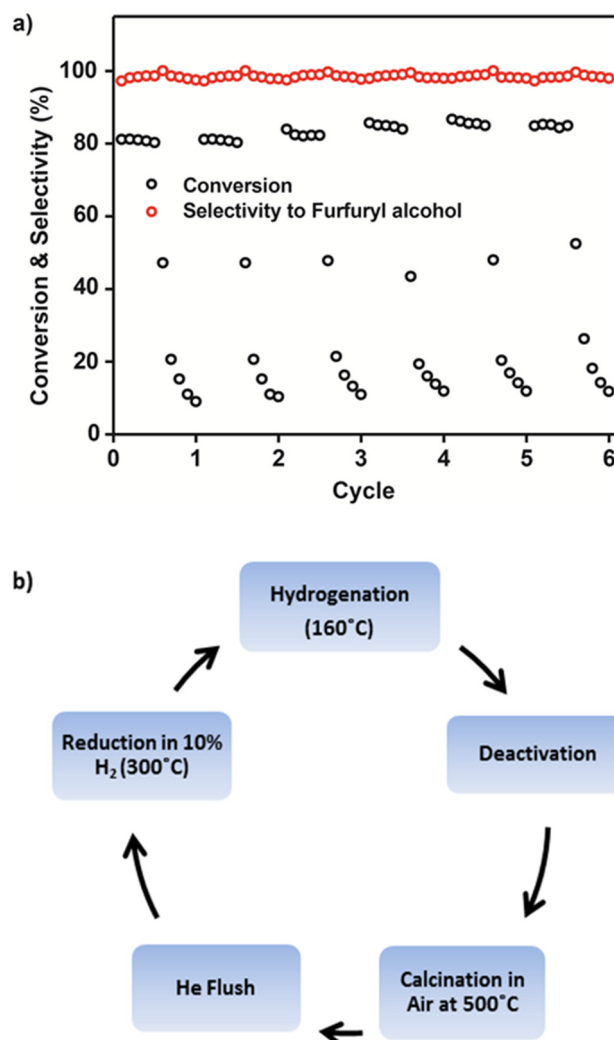


Figure 21. a) Regeneration cycles of PtSn@mSiO₂ in the hydrogenation of furfural; b) A schematic comprising all the steps in one regeneration cycle. The conversion was tuned to 80% on purpose to show the activity of the catalysts is fully retained after each deactivation-regeneration cycle.

For the adsorption of furfural, the most stable configurations on Pt(111) and PtSn(110) are shown in Figure 22a and b respectively, with their corresponding projected density of states

(PDOS) shown in (c). On Pt(111) the most preferred configuration is flat with the two C=C bonds in the furan ring and the C=O bond sitting along three different Pt-Pt bridge sites, agreeing with other studies.^{45,46} The adsorption energy is 0.87 eV. In contrast, on PtSn(110), the most preferred configuration is tilted with the O in C=O group sitting on top of Sn site. The PtSn(110) surface can be characterized as Pt-Pt chains decorated with Sn to form Pt-Pt-Sn trimers locally. Even though Pt-Pt bridge sites are still available, which can accommodate the adsorption of H and CO, the relatively larger furfural molecule does not have its C=C and C=O bond sit along these bridge sites (they are unstable) and become tilted after relaxation. The adsorption energy is reduced significantly to 0.33 eV. On PtSn(100) surface, the adsorption energy for furfural is even weaker at 0.18 eV with also the tilt configuration being preferred on top of the protruded Sn atoms.

The reduction in adsorption energies is expected from our earlier study of H and CO adsorption on PtPb and PtBi surfaces⁴⁴ having the same NiAs structure because the Pt *d*-band center on (110) is pushed toward lower energy and further away from the Fermi level due to the charge transfer from the *p*-metals. From PDOS (Figure 22c), this is clearly shown by furfural on PtSn (110) retaining the molecular HOMO-1 (-3.5 eV), HOMO (-2.5 eV), LUMO (0.5 eV) and LUMO+1 (3.0 eV) states with part of the broadened LUMO-derived band shifted below the Fermi level and filled by charge transfer from Sn. In contrast, there is a strong band hybridization between furfural and Pt(111) in the flat configuration is due to the direct C-Pt bonds. The tilt configuration on Cu(111) versus flat on Pd(111) has been used to explain⁴⁶ the high selectivity toward hydrogenation on Cu(111) because the channel for the activation of C=C is effectively closed.

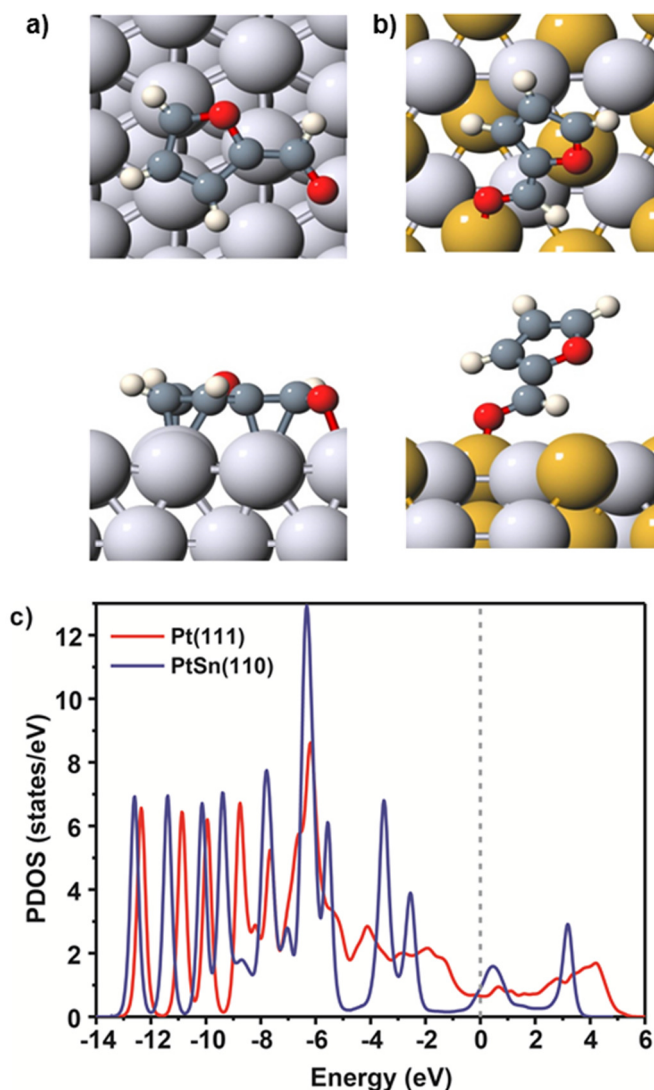


Figure 22. Most preferred adsorption configuration for furfural a) flat on Pt(111) and b) tilt on PtSn(110) surfaces with c) the corresponding projected density of states (PDOS). Large grey (brown) spheres are Pt (Sn) atoms in the surfaces; small gray, red and white spheres are C, O and H atoms in furfural. The top (bottom) panel is the top (side) view. Similarly here, enhanced selectivity for furfural hydrogenation with PtSn intermetallic NPs should be also due to its preferred tilted configuration on PtSn(110) and (100). To confirm, a future study will investigate the reaction pathway and kinetic barriers, including other surface terminations of PtSn.

Conclusions

Using this *ship-in-a-bottle* strategy, we have synthesized a series of monodisperse silica shell-encapsulated, Pt-based intermetallic NPs, including PtSn, Pt₃Sn, PtPb, PtZn, and Pt₃Zn. As demonstrated in the hydrogenation of furfural, the PtSn@mSiO₂ with a molar ratio of Pt:Sn = 1:1 phase exhibited superior activity and selectivity to furfuryl alcohol in comparison to Pt@mSiO₂. In intermetallic compounds, Pt benefits from an ordered environment and is deemed responsible for the observed enhanced activity and selectivity. From XPS studies, a stoichiometric surface ratio of Pt-to-Sn is found to be the most optimal for catalyst longevity. Using AP-XPS, we found that the surface Pt-to-Sn ratio remains constant under reduction conditions. DFT calculations suggest the enhanced furfuryl alcohol selectivity in furfural hydrogenation on PtSn over Pt is correlated to the different adsorption configuration of furfural in these two systems. Our work demonstrates that greatly enhanced activity and selectivity can be achieved using intermetallic NP catalysts, while reducing precious metal usage, and silica encapsulation can effectively prevent aggregation of PtSn NPs during catalyst synthesis and regeneration. This *ship-in-a-bottle* strategy provides an easy route to synthesize efficient intermetallic NPs heterogeneous catalysts with a broad spectrum of compositions and use.

Experimental Section

Materials and Synthesis

Synthesis of Pt@mSiO₂ NPs. Pt@mSiO₂ was prepared according to reported methods with a slight modification.¹⁹ Around 5 mL of a 10 mM K₂PtCl₄ (Acros Organics, 46-47% Pt) was added to 12.5 mL of a 400 mM aqueous solution of tetradecyltrimethylammonium bromide (TTAB, ≥99%, Sigma-Aldrich). Additionally, 29.5 mL of distilled water was added. After

stirring for 10 minutes at room temperature, a cloudy solution was obtained, which was then heated in an oil bath at 50 °C for another 10 minutes resulting in a clear solution. A freshly prepared ice-cold 500 mM (3 mL) aqueous solution of sodium borohydride (Alfa Aesar, 98%) was then added. Stirring for 15-20 hours at 50 °C resulted in a dark brown colloidal solution of Pt NPs. This was centrifuged at 3000 rpm four times for 30 minutes, discarding the residue after each session. Finally, the supernatant was centrifuged at 14000 rpm for 15 minutes, twice, collected and dispersed in 35 mL of water. About 1 mL of a 0.05 M sodium hydroxide solution was added to obtain a pH between 11 and 12. While stirring, 500 μ L of a 10% tetraethylorthosilicate (TEOS, Aldrich, reagent grade, 98%) solution in methanol was added dropwise and stirred. After 24 hours the sample was centrifuged at 14000 rpm twice and the coated particles were redispersed in methanol. The surfactant was removed via an acidic methanol refluxing session (6% hydrochloric acid solution) at 90 °C for 24 hours. The platinum content in Pt@mSiO₂ was identified using ICP-MS. This synthesis could conveniently be scaled up to generate more Pt@mSiO₂.

Synthesis of Intermetallic-Pt@mSiO₂ NPs. For a typical synthesis of an intermetallic compound, the Pt@mSiO₂ solution was centrifuged and redispersed in 40 mL of tetraethylene glycol (Alfa Aesar, 99%) in a 100 mL two-neck flask. The amount of Pt in a typical synthesis of Pt@mSiO₂ particles was 0.18 mmol. The salt of the corresponding metal (Sn, Pb or Zn) was then added prior to sonication of the mixture to obtain a homogeneous mixture. After removing air from the flask and refilling with Argon, the flask was heated using a temperature-controlled heating mantle for 2 hours. PtSn@mSiO₂ was made by adding SnCl₂·2H₂O (Alfa Aesar, 98%), with a molar ratio of Pt:Sn=1:1, heating the solution to 280 °C for 2 hours. Pt₃Sn@SiO₂ was made ensuring a Pt:Sn molar ratio of 3:1, heating the solution to 280 °C. The obtained alloy

was centrifuged, washed, dried and annealed at 600 °C in a 10% H₂ flow in a tube furnace to obtain intermetallic Pt₃Sn@SiO₂. PtPb@SiO₂ utilized Pb(CH₃COO)₂.3H₂O (Alfa Aesar, 99%), with a Pt:Pb molar ratio = 1:1, and a temperature of 260 °C. PtZn@SiO₂ and Pt₃Zn@SiO₂ were made using Zn(acac)₂ (Alfa Aesar, 98%) as the precursor with the corresponding ratios to obtain the desired intermetallic compound. Here a mixture of 15 mL oleyl amine (70%, technical grade, Aldrich) and 2.5 mL of oleic acid (EMD) was used as the reaction solvent. The mixture was heated to 350 °C. The as-obtained samples were washed, dried, and annealed in a 10% H₂ flow at 600 °C in a tube furnace to obtain the intermetallic phases. After their synthesis ICP-MS measurements were also carried out on the powdered samples to confirm their stoichiometry as per the synthesis.

A control experiment was also carried out to synthesize PtSn supported on MCF-17. Pt colloids synthesized earlier were not coated with the silica shell and instead dispersed directly on MCF-17 to obtain loadings similar to Pt@mSiO₂ (40-50%). The loading eventually obtained was around 38% of Pt in Pt/MCF-17. This was then dried and dispersed in tetraethylene glycol. Tin (II) Chloride was then added to the solution before heating it at 280 °C for 2 hours. The resultant solution was then diluted with acetone for easier centrifugation.

Instrumentation

Transmission electron microscopy (TEM) and energy dispersive X-ray spectrometry (EDS) analysis were carried out using a TECNAI G2 F20 with EDS analyzer (Oxford INCA EDS) at an acceleration voltage of 200 kV. Samples were prepared by the drop-cast method. Around 200 particles were measured for each sample to get the overall particle size, the metal core diameter, and the silica shell thicknesses. Histograms were then made using these size measurements. Powder X-ray diffraction (PXRD) patterns were collected at room temperature

using an STOE Stadi P powder diffractometer equipped with an image plate and a Cu $K_{\alpha 1}$ radiation source ($\lambda = 1.5406 \text{ \AA}$). Inductively-coupled plasma mass spectrometry (ICP-MS) measurements were carried out using a Thermo Fisher Scientific X Series 2 ICP-MS. Typically, powdered samples were dissolved in 5 mL of aqua regia to dissolve all metal content before the addition of around 100-300 μL 30% HF solution to dissolve the mesoporous silica completely. These samples were diluted with 2% Nitric acid before the ICP-MS measurements. BET Surface area measurements of Pt@mSiO₂ and PtSn@mSiO₂ were performed by nitrogen sorption isotherms using a Micromeritics 3Flex surface characterization analyzer at 77 K. Prior to surface area measurements both samples were calcined at 500 °C in air and reduced at 300 °C under 50 mL/min 10% H₂/He.

X-ray photoelectron spectroscopy (XPS) measurements were performed using a PHI 5500 Multi-technique system (Physical Electronics, Chanhassen, MN) with a monochromatized Al K_{α} X-ray source ($h\nu = 1486.6 \text{ eV}$). For both the Pt 4f and Sn 3d peaks theoretical values for the peak area ratios were used (0.75 for the Pt peaks and 0.67 for the Sn peaks) while fitting using CasaXPS. Peak widths (FWHM values), when comparing samples for the same elements, were also made as similar as possible, keeping within acceptable limits of $\pm 0.2 \text{ eV}$. For the Pt peaks, a peak width between 2.20 and 2.35 eV was maintained. For Sn peaks, a peak width was maintained between 2.35 and 2.45 eV.

Ambient-Pressure X-ray Photoelectron Spectroscopy (AP-XPS) was also carried out on PtSn@mSiO₂. The sample was dispersed in ethanol and then dropped on pyrolytic graphite. The reducing treatments to the sample were carried out in an incorporated high-pressure cell in the vacuum chamber of AP-XPS, in which 0.2 Torr H₂ was introduced at different temperatures for a certain amount of time. After the treatment, H₂ was purged out and the

sample was taken out to a manipulator in ultrahigh vacuum for X-ray analysis. Due to the existence of SiO₂ shell, significant surface charging was encountered. As a result, a flux of low energy electrons (8.5 eV, 60 mA) generated by a flood gun was used for each analysis.

Catalysis Studies

Furfural (Acros Organics, 99%) was hydrogenated by dispersing the catalysts on 1.2 g of quartz sand and then loading them into a quartz-glass plug flow reactor. The Pt content in all catalysts was maintained at a fixed value (1.25 mg or 6.4 μmol). All the catalysts were calcined in an oven at 500 °C in air – to remove any organic substances, such as solvent residues and surfactant, not been removed during the methanol reflux. Subsequently, the catalysts were reduced in 10% H₂ in situ (He = 45 mL/min, H₂ = 5 mL/min) at an appropriate temperature, i.e., 300 °C for PtSn@mSiO₂ and PtPb@mSiO₂; 600 °C for Pt₃Sn@mSiO₂, Pt₃Zn@mSiO₂ and PtZn@mSiO₂ to regenerate the intermetallic phase. All the catalysts were reduced at 300 °C again for 4 hours in 10% H₂ before furfural hydrogenation was carried out. The reaction gas mixture was composed of 8.6 mL/min He through a bubbler containing furfural (Actual furfural flow = 0.023 mL/min), and 11.4 mL/min H₂ at 1 atm, passed through the catalyst bed in a fritted quartz U-tube flow reactor. The vapor from the reactor was monitored on-line using an HP 5890 gas chromatograph equipped with a capillary column (DB-5, 30 m x 0.32 mm x 0.25 μm) and a Flame Ionization Detector. The products were further identified using an on-line mass spectrometer (Agilent 5973N) connected to the outlet of the capillary column installed in the HP 5890. Additional analysis of products was done using a GC-MS (Agilent 6890N-5975N) to identify products from washed catalysts.

DFT Calculations

All density functional theory (DFT) calculations were performed with the PBE exchange-correlation functional, a plane-wave basis set and projector augmented wave method, as implemented in the Vienna Ab initio Simulation Package (VASP). The Pt(111) surface was modeled as a three-layer slab with a surface supercell of $(2\sqrt{3}\times 3)$. The PtSn(110) and (100) surfaces (the lowest energy structure for these intermetallic compounds) are modeled as a four- and six-layer slab with a surface supercell of (2×2) , respectively. Various flat and tilt configurations with different molecular orientations of furfural on the surfaces were tried, and thermal annealing with *ab initio* molecular dynamics was used to search for the most stable adsorption configurations on each surface. All the atoms (except for the bottom two layers in the slab fixed at bulk positions) are relaxed until the absolute values of forces were below 0.02 eV/Å. A kinetic energy cutoff of 400 eV for the plane-wave basis and a $(5\times 5\times 1)$ *k*-point mesh with a Gaussian smearing of 0.05 eV was used.

Abbreviations

NPs, Nanoparticles; LDH, layered double hydroxide; TTAB, tetradecyltrimethylammonium bromide; TEOS, Tetraethylorthosilicate; ICP-MS, Inductively coupled plasma mass spectrometry; TEM, Transmission electron microscopy; EDS, energy dispersive X-ray spectrometry; PXRD, Powder X-ray diffraction; DFT-PBE, Density Functional Theory-Perdew, Burke and Ernzerhof; XPS, X-ray Photoelectron Spectroscopy; AP-XPS, Ambient-Pressure X-ray Photoelectron Spectroscopy.

References

- (1) Studt, F.; Abild-Pedersen, F.; Bligaard, T.; Sørensen, R. Z.; Christensen, C. H.; Nørskov, J. K. *Science* **2008**, *320*, 1320-1322.

- (2) Xiao, C.; Wang, L.-L.; Maligal-Ganesh, R. V.; Smetana, V.; Walen, H.; Thiel, P. A.; Miller, G. J.; Johnson, D. D.; Huang, W. *J. Am. Chem. Soc.* **2013**, *135*, 9592-9595.
- (3) Studt, F.; Sharafutdinov, I.; Abild-Pedersen, F.; Elkjaer, C. F.; Hummelshoj, J. S.; Dahl, S.; Chorkendorff, I.; Norskov, J. K. *Nat. Chem.* **2014**, *6*, 320-324.
- (4) Armbrüster, M.; Kovnir, K.; Friedrich, M.; Teschner, D.; Wowsnick, G.; Hahne, M.; Gille, P.; Szentmiklósi, L.; Feuerbacher, M.; Heggen, M.; Girgsdies, F.; Rosenthal, D.; Schlögl, R.; Grin, Y. *Nat. Mater.* **2012**, *11*, 690-693.
- (5) Armbrüster, M.; Schlögl, R.; Grin, Y. *Sci. Tech. Adv. Mater.* **2014**, *15*, 1-17.
- (6) Armbrüster, M.; Kovnir, K.; Behrens, M.; Teschner, D.; Grin, Y.; Schlögl, R. *J. Am. Chem. Soc.* **2010**, *132*, 14745-14747.
- (7) Armbrüster, M.; Wowsnick, G.; Friedrich, M.; Heggen, M.; Cardoso-Gil, R. *J. Am. Chem. Soc.* **2011**, *133*, 9112-9118.
- (8) Schaak, R. E.; Sra, A. K.; Leonard, B. M.; Cable, R. E.; Bauer, J. C.; Han, Y. F.; Means, J.; Teizer, W.; Vasquez, Y.; Funck, E. S. *J. Am. Chem. Soc.* **2005**, *127*, 3506-3515.
- (9) Leonard, B. M.; Bhuvanesh, N. S.; Schaak, R. E. *J. Am. Chem. Soc.* **2005**, *127*, 7326-7327.
- (10) Cable, R. E.; Schaak, R. E. *Chem. Mater.* **2005**, *17*, 6835-6841.
- (11) Sra, A. K.; Schaak, R. E. *J. Am. Chem. Soc.* **2004**, *126*, 6667-6672.
- (12) Leonard, B. M.; Schaak, R. E. *J. Am. Chem. Soc.* **2006**, *128*, 11475-11482.

- (13) Bauer, J. C.; Chen, X.; Liu, Q.; Phan, T.-H.; Schaak, R. E. *J. Mater. Chem.* **2008**, *18*, 275-282.
- (14) Li, C.; Chen, Y.; Zhang, S.; Xu, S.; Zhou, J.; Wang, F.; Wei, M.; Evans, D. G.; Duan, X. *Chem. Mater.* **2013**, *25*, 3888-3896.
- (15) Ge, J.; Zhang, Q.; Zhang, T.; Yin, Y. *Angew. Chem., Int. Ed.* **2008**, *47*, 8924-8928.
- (16) Zhang, T.; Zhao, H.; He, S.; Liu, K.; Liu, H.; Yin, Y.; Gao, C. *ACS Nano* **2014**, *8*, 7297-7304.
- (17) Huang, X.; Guo, C.; Zuo, J.; Zheng, N.; Stucky, G. D. *Small* **2009**, *5*, 361-365.
- (18) Qiao, Z.-A.; Zhang, P.; Chai, S.-H.; Chi, M.; Veith, G. M.; Gallego, N. C.; Kidder, M.; Dai, S. *J. Am. Chem. Soc.* **2014**, *136*, 11260-11263.
- (19) Joo, S. H.; Park, J. Y.; Tsung, C.-K.; Yamada, Y.; Yang, P.; Somorjai, G. A. *Nat. Mater.* **2009**, *8*, 126-131.
- (20) Feldmann, C. *Adv. Funct. Mater.* **2003**, *13*, 101-107.
- (21) Kang, Y.; Pyo, J. B.; Ye, X.; Gordon, T. R.; Murray, C. B. *ACS Nano* **2012**, *6*, 5642-5647.
- (22) Lange, J.-P.; van der Heide, E.; van Buijtenen, J.; Price, R. *ChemSusChem* **2012**, *5*, 150-166.
- (23) Yan, K.; Wu, G.; Lafleur, T.; Jarvis, C. *Renew. Sust. Energ. Rev.* **2014**, *38*, 663-676.

- (24) Gürbüz, E. I.; Gallo, J. M. R.; Alonso, D. M.; Wettstein, S. G.; Lim, W. Y.; Dumesic, J. A. *Angew. Chem., Int. Ed.* **2013**, *52*, 1270-1274.
- (25) Gonzalez Maldonado, G. M.; Assary, R. S.; Dumesic, J.; Curtiss, L. A. *Energy Environ. Sci.* **2012**, *5*, 6981-6989.
- (26) Zhang, Z.; Dong, K.; Zhao, Z. *ChemSusChem* **2011**, *4*, 112-118.
- (27) Radhakrishnan, L.; Reboul, J.; Furukawa, S.; Srinivasu, P.; Kitagawa, S.; Yamauchi, Y. *Chem. Mater.* **2011**, *23*, 1225-1231.
- (28) Wang, H.; Yao, J. *Ind. Eng. Chem. Res.* **2006**, *45*, 6393-6404.
- (29) Liu, D.; Zemlyanov, D.; Wu, T.; Lobo-Lapidus, R. J.; Dumesic, J. A.; Miller, J. T.; Marshall, C. L. *J. of Catal.* **2013**, *299*, 336-345.
- (30) Pang, S. H.; Medlin, J. W. *ACS Catal.* **2011**, *1*, 1272-1283.
- (31) Pang, S. H.; Schoenbaum, C. A.; Schwartz, D. K.; Medlin, J. W. *Nat. Comm.* **2013**, *4*, 2448.
- (32) Pang, S. H.; Schoenbaum, C. A.; Schwartz, D. K.; Medlin, J. W. *ACS Catal.* **2014**, *4*, 3123-3131.
- (33) Pushkarev, V. V.; Musselwhite, N.; An, K.; Alayoglu, S.; Somorjai, G. A. *Nano Lett.* **2012**, *12*, 5196-5201.
- (34) Baker, L. R.; Kennedy, G.; Van Spronsen, M.; Hervier, A.; Cai, X.; Chen, S.; Wang, L.-W.; Somorjai, G. A. *J. Am. Chem. Soc.* **2012**, *134*, 14208-14216.

- (35) Kijeński, J.; Winiarek, P.; Paryjczak, T.; Lewicki, A.; Mikołajska, A. *Appl. Catal., A* **2002**, *233*, 171-182.
- (36) Park, S.-J.; Kim, Y.-J.; Park, S.-J. *Langmuir* **2008**, *24*, 12134-12137.
- (37) Grzelczak, M.; Correa-Duarte, M. A.; Liz-Marzán, L. M. *Small* **2006**, *2*, 1174-1177.
- (38) Roca, M.; Haes, A. J. *J. Am. Chem. Soc.* **2008**, *130*, 14273-14279
- (39) Tsung, C.-K.; Kuhn, J. N.; Huang, W.; Aliaga, C.; Hung, L.-I.; Somorjai, G. A.; Yang, P., *J. Am. Chem. Soc.* **2009**, *131*, 5816-5822.
- (40) Yu, K.; Wu, Z.; Zhao, Q.; Li, B.; Xie, Y. *J. Phys. Chem C* **2008**, *112*, 2244-2247.
- (41) Jugnet, Y.; Loffreda, D.; Dupont, C.; Delbecq, F.; Ehret, E.; Cadete Santos Aires, F. J.; Mun, B. S.; Aksoy Akgul, F.; Liu, Z. *J. Phys. Chem. Lett.* **2012**, *3*, 3707-3714.
- (42) Tao, F.; Zhang, S.; Nguyen, L.; Zhang, X. *Chem. Soc. Rev.* **2012**, *41*, 7980-7993.
- (43) Wang, X.; Stöver, J. r.; Zielasek, V.; Altmann, L.; Thiel, K.; Al-Shamery, K.; Bäumer, M.; Borchert, H.; Parisi, J. r.; Kolny-Olesiak, J. *Langmuir* **2011**, *27*, 11052-11061.
- (44) Wang, L. L.; Johnson, D. D. *J. Phys. Chem. C* **2008**, *112*, 8266-8275.
- (45) Liu, B.; Cheng, L.; Curtiss, L.; Greeley, J. *Surf. Sci.* **2014**, *622*, 51-59.
- (46) Vorotnikov, V.; Mpourmpakis, G.; Vlachos, D. G. *ACS Catal.* **2012**, *2*, 2496-2504.

CHAPTER 3. ENHANCED CHEMOSELECTIVITY IN BIMETALLIC NANOPARTICLES IN THE ABSENCE OF SURFACE MODIFYING LIGANDS

Raghu V. Maligal-Ganesh, Kyle Brashler, Xuechen Luan, Tian Wei Goh, Jeffrey Gustafson, Jiashu Wu, Wenyu Huang

Abstract

Noble metal-based bimetallic nanoparticles (NPs) synthesized using colloidal methods always contain organic capping agents. These NPs show high selectivities in many chemoselective hydrogenation reactions benefitting from both capping agents and secondary metals. However, it is challenging to separately identify the role of the second metal and the capping agents in the bimetallic NPs because the complete removal of the capping agents can often cause aggregation or structural/compositional changes. Herein we report the synthesis of Pt₅Fe_x (x = 1, 2 and 4) bimetallic NPs capped by an inorganic mesoporous silica (mSiO₂) shell, which could prevent NP aggregation during high-temperature treatment to remove capping agents. Using these Pt₅Fe_x@mSiO₂ NPs with a clean surface, we could demonstrate the role played independently by the bimetallic composition in the selective hydrogenation of cinnamaldehyde and furfuraldehyde. Understanding the functions of the second metal and the surface modifying ligands on the selectivity enhancement of bimetallic NPs is necessary for the design of high-performance chemoselective catalysts.

Introduction

Bimetallic NPs have been of considerable interest because of their enhanced activity/selectivity in heterogeneous catalysis.¹⁻³ The general colloidal synthesis of NPs requires surface capping ligands to lower the high surface energy of NPs, and exert control on their size and shape.⁴⁻⁶ Moreover, these surface modifying ligands can interestingly control catalytic activity and selectivity of NPs in chemical reactions by tuning the electronic structure of bimetallic surfaces.⁷⁻¹¹ However, bimetallic NPs are usually complicated catalytic systems because the secondary metals can also affect the electronic structure of the bimetallic surface.¹²⁻¹⁵ There are contradictory reports that attribute the enhanced catalytic selectivity of many bimetallic NPs to either the surface-modifying ligands or the addition of the secondary metals. For example, on bimetallic Pt₃Co, surface adsorbed alkylamine ligands enhance the selective hydrogenation of the C=O bond in α,β -unsaturated aldehydes to form the corresponding unsaturated alcohols.¹⁶ However, on oleylamine-capped PtCo NPs with similar selectivity in the same reaction, the enhanced selectivity was attributed solely to the electronic modification of undercoordinated Pt sites via the decoration of Co.¹⁷ In the many bimetallic systems, the roles of secondary metals or surface capping agent are not clearly differentiated, thus hindering the rational design of bimetallic catalysts.

We wanted to analyze the role of the secondary metal alone in bimetallic catalysts in the absence of surface capping ligands. However, the lack of surface-modifying ligands in general colloidal synthesis or the thermal removal of these ligands tend to result in the aggregation of NPs.^{18,19} To overcome this difficulty, advances in mesoporous silica encapsulated bimetallic NPs have provided ample scope to facilitate the synthesis of metallic NPs in the absence of surface-modifying ligands.²⁰⁻²⁴ We report the synthesis of mesoporous

silica encapsulated $\text{Pt}_5\text{Fe}_x@m\text{SiO}_2$ ($x=1,2$ and 4) bimetallic NPs via colloidal synthesis, beginning with encapsulated $\text{Pt}@m\text{SiO}_2$ NPs. Since the mesoporous silica encapsulation prevents aggregation of NPs, these PtFe bimetallic NPs can be calcined at $550\text{ }^\circ\text{C}$ to remove the surface-modifying ligands and reduced at temperatures as high as $850\text{ }^\circ\text{C}$ to introduce alloy and intermetallic Pt-Fe phases.

Further studies on the role of Fe surface segregation alone under high-temperature reduction treatment and how it alters catalytic properties of $\text{Pt}_5\text{Fe}_x@m\text{SiO}_2$ without the aid of the ligand help elucidate the surface structure-catalytic property relationship of these bimetallic NPs. Rodionov et al. reported Pt-Fe bimetallic NPs capped with decanoic acid and perfluorodecanoic acid for cinnamaldehyde hydrogenation,²⁵ whose enhanced activity and selectivity in hydrogenating the C=O bond preferentially over the -C=C- bond were attributed to the presence of the organic capping agents. The role of Fe is to provide the adsorption site for the long chain carboxylic acids. However, beyond functioning as a coordination site for the capping carboxylic ligands, Fe could also affect the catalysis of Pt-Fe bimetallic NPs in cinnamaldehyde hydrogenation.

In this study, we demonstrated the catalytic performance of $\text{Pt}_5\text{Fe}_x@m\text{SiO}_2$ ($x = 1, 2$ and 4) in the absence of organic capping agents for cinnamaldehyde hydrogenation. Increasing the amount of Fe in the Pt-Fe NPs can consistently increase their catalytic selectivity to cinnamyl alcohol and concomitantly decrease the activity, providing evidence of a bimetallic synergistic effect between Pt and Fe. We further added decanoic acid and perfluorodecanoic acid as surface modifying ligands to the clean Pt_5Fe surface. Both ligands enhanced the selectivity, and the fluorinated ligand also enhanced the activity, agreeing with Rodionov's

observation.²⁵ These results differentiated the role of the second metal and the surface-modifying ligand in tuning the catalytic property of bimetallic NPs.

Results and discussion

Bimetallic Pt-Fe@mSiO₂ NPs was synthesized by reducing the desired amount of Fe(acac)₃ on pre-synthesized Pt@mSiO₂ NPs in tetraethylene glycol at elevated temperatures, where encapsulated Pt cores act as the seeds and mSiO₂ shells serve as the inorganic capping.²⁶ The Fe incorporation efficiency (incorporated/added precursor) is around 70-85% for all the three bimetallic systems, measured by ICP-MS (Table 1). Hence the compositions of the final NPs are denoted as Pt₅Fe_x@mSiO₂ where x (x = 1, 2, and 4) is the molar amount of Fe with respect to Pt. After colloidal synthesis, washing and calcination-reduction cycles, the Pt₅Fe_x@mSiO₂ bimetallic NPs with a clean surface free of surface organic modifying ligands, were obtained as confirmed by FTIR measurements (Figure 1),.

Table 1. Pt/Fe ratios of synthesized Pt-Fe bimetallic NPs

Sample	Targeted Pt/Fe	Actual Pt/Fe	% Wt Pt in catalyst	% Wt Fe in catalyst	% Fe incorporated
Pt ₅ Fe@mSiO ₂	1/0.33	1/0.23	46.2	3.0	~70
Pt ₅ Fe ₂ @mSiO ₂	1/0.50	1/0.39	44.5	4.8	~78
Pt ₅ Fe ₄ @mSiO ₂	1/1	1/0.85	31.8	7.7	~85

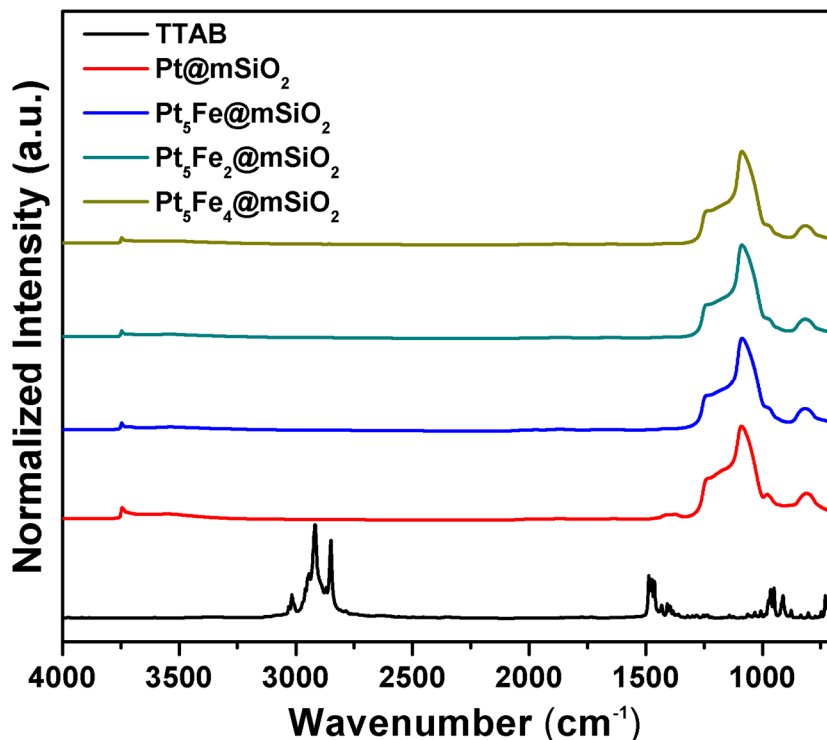


Figure 1. Pt@mSiO₂, Pt₅Fe@mSiO₂, Pt₅Fe₂@mSiO₂, and Pt₅Fe₄@mSiO₂ after calcination (550 °C) and reduction (700 °C). For comparison TTAB (black) has also been measured. All the catalysts only display features on the spectra exclusive to the mSiO₂ encapsulation. Bands between 1000 and 1100 cm⁻¹ are due to internal Si-O asymmetric stretching vibrations, while those in the 1200-1250 cm⁻¹ region are due to external Si-O vibrations.

The PXRD pattern (Figure 2) of Pt₅Fe_x@mSiO₂ materials (x=1, 2 and 4) reduced at 700 °C displays characteristics of the Pt₃Fe alloy phase, with the corresponding superlattice peaks ($2\theta = 23^\circ$ and 32°) associated with ordered Pt-Fe alloys.²⁷ The diffraction peaks at $\sim 40^\circ$ and 47° shift towards higher angles in comparison to those of Pt@mSiO₂, owing to the contraction of the fcc lattice by the addition of iron, whose atomic radius is smaller than Pt. With the increase of Fe in Pt₅Fe_x@mSiO₂, the major peak ($\sim 40^\circ$) demonstrates a consistent

high angle shift due to more Fe in the lattice, going from the ordered Pt₃Fe alloy to that of fct PtFe in the case of Pt₅Fe₄@mSiO₂ reduced at 700 °C.²⁸

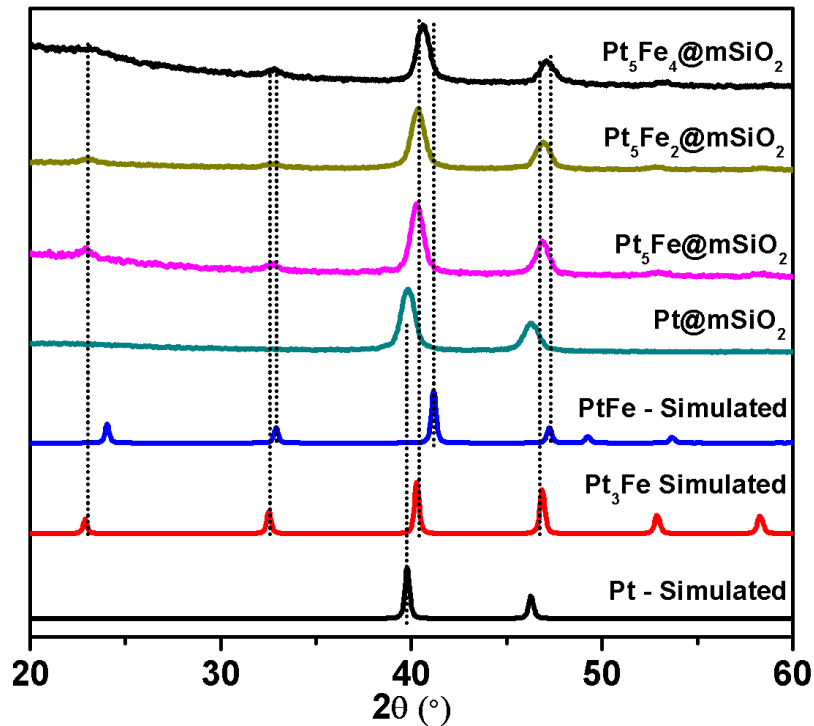


Figure 2. Powder XRD pattern for Pt@mSiO₂, Pt₅Fe@mSiO₂, and Pt₅Fe₂@mSiO₂ post a 550 °C calcination and 700°C reduction cycle.

Pt₅Fe₄@mSiO₂ could be further reduced at 850 °C to obtain fct PtFe (Figure 3). TEM images from the samples (Figure 4) were collected to confirm the thermal stability of the Pt@mSiO₂ and Pt₅Fe_x@mSiO₂ (x = 1, 2 and 4) samples after the calcination-reduction treatment cycles (Figure 1 b, c and d). The mesoporous silica shell has an average thickness of 9.1 ± 0.9 nm. The core metallic NPs show sizes ranging from 12.6 nm for Pt NPs to 15.8 nm for the Pt₅Fe₄ NPs (Table 2). All samples show high thermal stability and no obvious NP aggregations. Table 2 further summarizes information gleaned from the synthesis conditions, TEM images, and PXRD patterns for the various samples treated under different reduction

temperatures. During catalysis, $\text{Pt}_5\text{Fe}_4@\text{mSiO}_2$ was inactive for both cinnamaldehyde and furfural hydrogenation. Therefore, further discussion focuses only on $\text{Pt}@\text{mSiO}_2$, $\text{Pt}_5\text{Fe}@\text{mSiO}_2$ and $\text{Pt}_5\text{Fe}_2@\text{mSiO}_2$ and their role in catalysis.

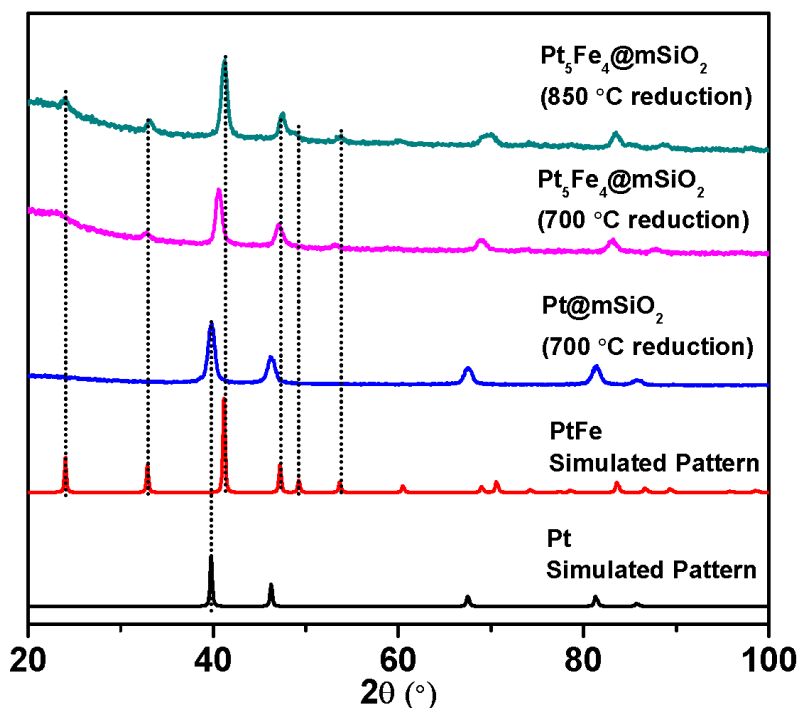


Figure 3. $\text{Pt}_5\text{Fe}_4@\text{mSiO}_2$ reduced at 700 and 850 °C.

Table 2. Summary of TEM and XRD characterization of Pt and Pt_5Fe_x NPs.

Sample	Oxidation Temperature (°C) ^a	Reduction Temperature (°C) ^b	Reduction Time (h)	Particle Size by TEM (nm)	2θ Peak for Pt or Pt_5Fe_x (111) (°)
$\text{Pt}@\text{mSiO}_2$	550	700	6	12.6 ± 0.2	39.78
$\text{Pt}_5\text{Fe}@\text{mSiO}_2^c$	550	700	6	13.2 ± 0.2	40.28
$\text{Pt}_5\text{Fe}_2@\text{mSiO}_2^c$	550	700	6	13.9 ± 0.3	40.25
$\text{Pt}_5\text{Fe}_4@\text{mSiO}_2^c$	550	700	6	15.8 ± 0.3	40.49
$\text{Pt}_5\text{Fe}_4@\text{mSiO}_2^c$	550	850	1	15.8 ± 0.3	40.78

^aSamples calcined in air at 550 °C with a rate of 1 °C/min, and kept at 550 °C for 6 hrs.

^bSamples were reduced in 10% H_2/Ar with a rate of 1 °C/min. ^cSamples were made from the same large mixed batch of $\text{Pt}@\text{mSiO}_2$.

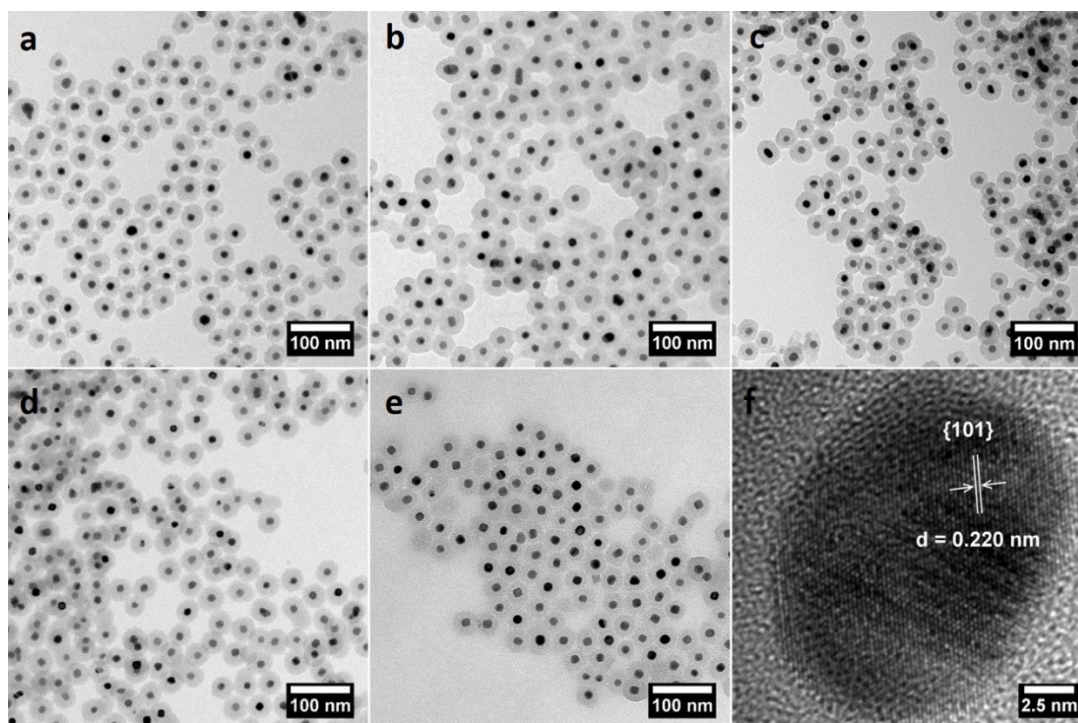


Figure 4. TEM of a) Pt@mSiO₂, b) Pt₅Fe@mSiO₂, c) Pt₅Fe₂@mSiO₂ after calcination at 550 °C and reduction at 700 °C d) Pt₅Fe₄@mSiO₂ synthesized in TEG at 200 °C e) Pt₅Fe₄@mSiO₂ after calcination at 500 °C followed by reduction at 700 °C for 6 h and then reduction at 850 °C for 1 h. f) HRTEM image of Pt₅Fe₄@mSiO₂ with the lattice spacing corresponding to the {101} plane of the PtFe fct intermetallic phase.

In a previous report,²⁴ we had indicated that the mesoporous silica encapsulation around the NPs does not hinder substrate access to the metal nanoparticle at its core while performing the important function of preventing the aggregation of NPs. Nitrogen physisorption measurements were carried out on Pt@mSiO₂ and Pt₅Fe@mSiO₂ and Pt₅Fe₂@mSiO₂ (Figure 5) to characterize the porous structure of the silica shell. All the samples display a Type IV isotherm (Figure 5a) indicating the mesoporous nature of the silica shell. The BET surface areas (550-580 m²/g), pore sizes (between 2.4-2.5 nm) and mesopore volumes (between 0.91-

0.97 cm³/g) of all samples are almost identical within measurement errors (Table 3), demonstrating the similar mesoporous structures after the incorporation and reduction of Fe at high temperatures at the Pt nanoparticle.

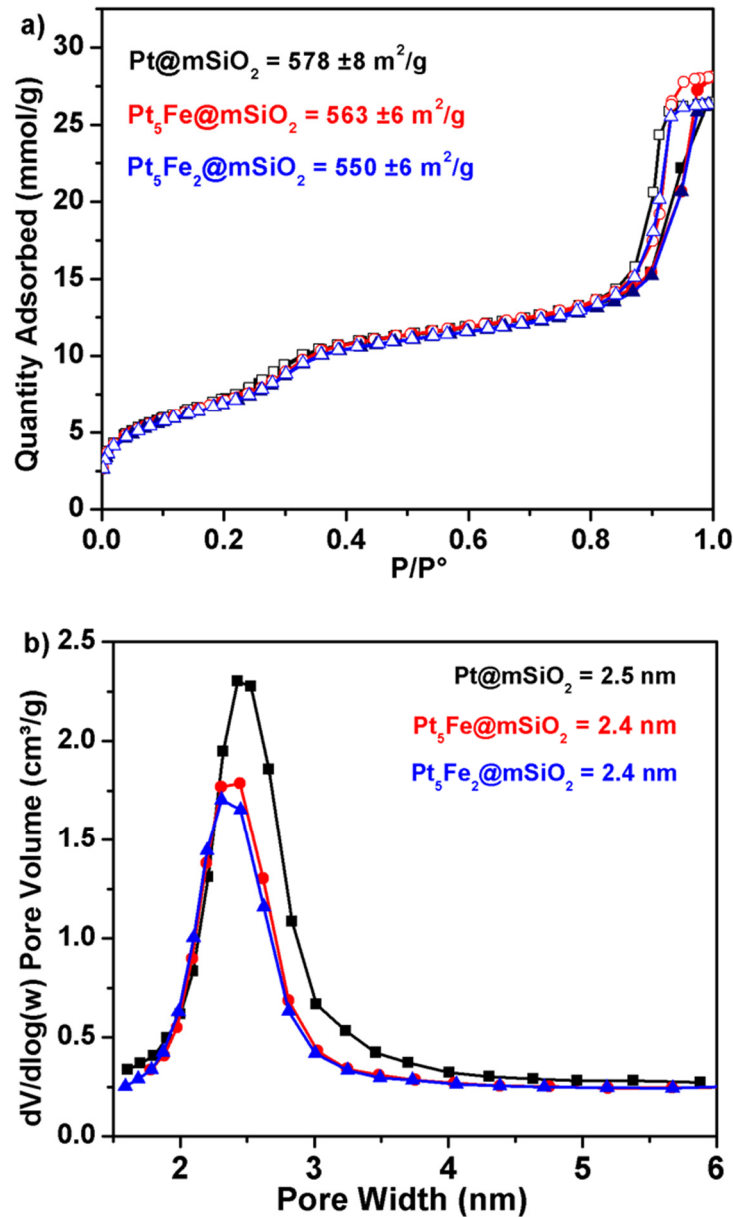


Figure 5. a) Surface area and b) pore size distribution measured by N₂ physisorption. All samples were calcined at 550 °C in air and reduced at 700 °C before the measurements.

Table 3. Summary of N₂ Physisorption measurements

Sample	BET Surface Area (m ² /g)	Pore Volume (cm ³ /g)	Pore Width (nm)
Pt@mSiO ₂	578 ± 8	0.96	2.5
Pt ₅ Fe@mSiO ₂	563 ± 6	0.97	2.4
Pt ₅ Fe ₂ @mSiO ₂	550 ± 6	0.91	2.4

Surface studies were also conducted to understand how Pt and Fe surface atomic ratios and oxidation states may influence catalysis. The binding energy for Pt increases in Pt₅Fe_x@mSiO₂ (x = 1, 2) with the addition of Fe at the surface when compared to pure Pt@mSiO₂ (Table 1). While Pt is shown to be predominantly in the metallic state, the XPS spectra for Fe only contains characteristics of FeO, and Fe₂O₃ and a multiplet splitting feature.²⁹ It is possible that the surface of Pt₅Fe_x@mSiO₂ (x = 1, 2) mainly consists of Fe₂O₃, on observing the binding energy of the Fe on the surface to be between 710 – 710.6 eV (Fig. 2b). Even though we freshly reduced the sample (300 °C, 10% H₂/Ar, 4h) before the XPS measurements according to a previously reported temperature programmed reduction study,³⁰ we cannot completely exclude the possibility of re-oxidation of Fe upon exposure to air during the sample transfer. In Pt₅Fe₂@mSiO₂, we observed more surface Fe oxides in comparison to Pt₅Fe@mSiO₂, which reflects the more Fe-rich surface of Pt₅Fe₂ compared with Pt₅Fe (regardless of the oxidation state of Fe in the working catalysts).

Table 1. XPS results of Pt@mSiO₂ and Pt₅Fe_x@mSiO₂ samples.

Sample	Pt 4f _{7/2} B.E. (eV)	Fe 2p _{3/2} B.E. (eV)	Pt/Fe surface ratio
Pt@mSiO ₂	70.9	-	-
Pt ₅ Fe@mSiO ₂	71.3	709.9	0.55
Pt ₅ Fe ₂ @mSiO ₂	71.4	710.3	0.18

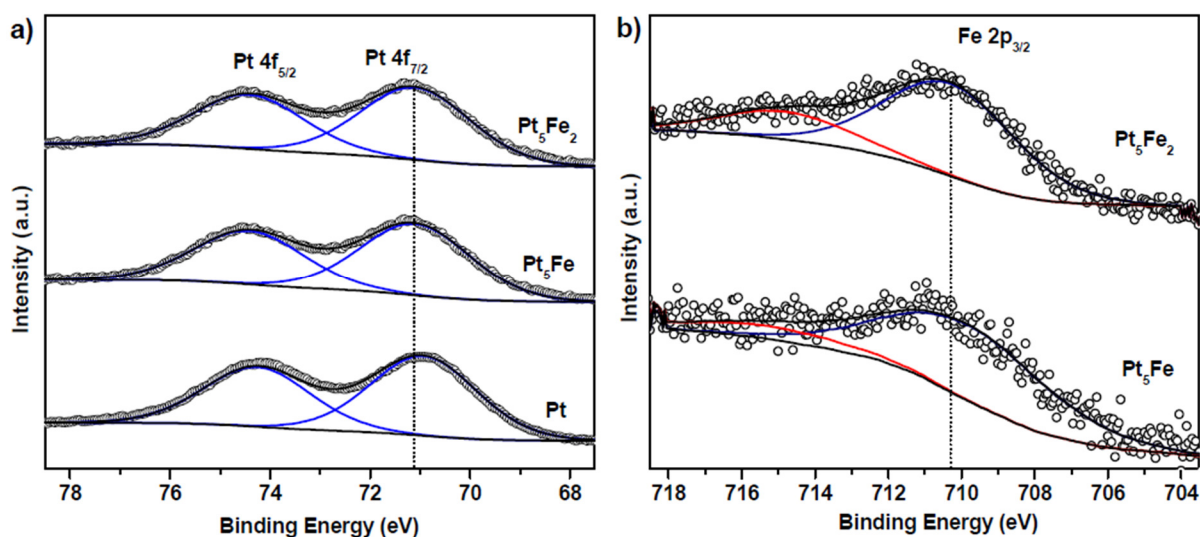


Figure 6 a) Pt XPS spectra of Pt, Pt₅Fe, and Pt₅Fe₂. b) Fe XPS spectra of Pt₅Fe@mSiO₂ and Pt₅Fe₂@mSiO₂. All samples were freshly reduced at 300 °C for 4h in 10% H₂/Ar

Chemoselective hydrogenation of cinnamaldehyde was tested over Pt@mSiO₂ and Pt₅Fe_x@mSiO₂ (x = 1, 2, 4), and their catalytic results are summarized in Table 2. We used thermal treatments to clean off the surface organic capping agents on these mSiO₂ encapsulated NPs to understand the effect of the Fe addition alone on their catalytic properties. After reduction at 300 °C, Pt@mSiO₂ showed a dismal selectivity to cinnamyl alcohol at 8.9% (Table 2), which is much lower than Pt₅Fe@mSiO₂ (42.5 %) and Pt₅Fe₂@mSiO₂ (75.1 %). The higher C=O hydrogenation selectivity with the increase of Fe content in the Pt-Fe NPs is demonstrated

more clearly if we take the ratio of all C=O bond hydrogenation (COL + HCOL) and C=C bond hydrogenation (HCAL + HCOL). The ratios for Pt₅Fe₂, Pt₅Fe, and Pt are 3.40, 1.23, and 0.63, respectively. The higher C=O hydrogenation selectivity with an increase in Fe was attributed to the synergistic effect of Pt and Fe with the higher alloying in the bimetallic Pt-Fe surface that tunes the preferential adsorption of the polar C=O group in comparison to C=C in cinnamaldehyde. Previous studies of Pt and Pt-Fe, supported on a zeolitized pumice support and zeolite P, also showed similar improvements in the selective hydrogenation of the carbonyl bond in campholenic aldehyde and cinnamaldehyde.³¹⁻³³ The improved carbonyl hydrogenation selectivity was attributed to the addition of Fe, which could inhibit C=C bond adsorption while polarizing the carbonyl bond to make its hydrogenation more facile.

In our study increasing Fe content also decreased the conversion when comparing Pt₅Fe@mSiO₂ and Pt₅Fe₂@mSiO₂ that were both reduced at 300 °C prior to cinnamaldehyde hydrogenation. The decreased conversion is likely due to the higher surface fraction of Fe which is less active for the hydrogenation. The surface fraction of Fe as determined by XPS earlier seems to corroborate this. Pt₅Fe₂@mSiO₂ displays the best compromise between conversion and selectivity after reduction at 300 °C, with a conversion of 36.9 % and a cinnamyl alcohol selectivity of 75.1 % after 3h.

We also carried out additional experiments with surface adsorbed carboxylic ligands utilized by the Rodionov group to validate the hypothesis, whether the addition of surface modifying ligands can affect their catalysis.²⁵ The ligands, decanoic acid and perfluorodecanoic acid could be simply added post the synthesis of the Pt₅Fe_x@mSiO₂ materials, as detailed in the experimental section. Pt₅Fe@mSiO₂ with decanoic acid adsorbed at the catalyst surface improves carbonyl hydrogenation selectivity (62.6 %) although

conversion is decreased from 50.4 to 27.0%. Using perfluorodecanoic acid as the surface modifying ligand, we obtained improved conversion (61.8%) and selectivity (69.6%) to cinnamyl alcohol. Perfluorodecanoic acid enhances the performance of the catalysts, as demonstrated by the Rodionov group. It is worth noting that the use of surface modifying ligands enhancing the catalytic performance depends heavily on the intrinsic structures of ligands and their interactions with metal surfaces.

Table 3. Cinnamaldehyde hydrogenation by the catalysts

Catalyst	Conversion (%)	Hydrogenation Selectivity					
		HCAL (%)	COL (%)	HCOL (%)	All C=O (%)	All C=C (%)	C=O/C=C ratio
Pt@mSiO ₂	53.3	41.4	8.9	47.6	56.5	89	0.63
Pt ₅ Fe@mSiO ₂	50.4	30.3	42.5	21.7	64.2	52	1.23
Pt ₅ Fe ₂ @mSiO ₂	36.9	15.4	75.1	9.5	84.6	24.9	3.40
Pt ₅ Fe@mSiO ₂ + DA	27.0	23.7	62.6	13.7	76	37.4	2.03
Pt ₅ Fe@mSiO ₂ + PFDA	61.8	13.6	69.6	16.9	86.5	30.5	2.83

Reaction conditions: 1 mL hexane as the solvent, 20 mg cinnamaldehyde, 1 atm H₂, mesitylene as an internal standard with a temperature of 50 °C for the reaction carried out for 3 hours. Pt content was kept constant at 1.5 mg (Cinnamaldehyde/metal ratio = 20); All catalysts were reduced 300 °C in 10% H₂ prior to catalysis. DA = Decanoic acid; PFDA – Perfluorodecanoic acid

Besides being able to differentiate the roles of Fe and the ligands in this system, it is also important to ensure that the reaction was heterogeneous and neither Pt nor Fe active species were released into the solution facilitating the reaction. Hence, a leaching test was carried out using the Pt₅Fe₂@mSiO₂ catalyst. After a typical 3-hour run the catalyst was removed by centrifugation, and the solution was transferred to a fresh vial. Hydrogen was

purged through the vial for 10 seconds via the septum, and then a hydrogen balloon was inserted. As observed in Fig. 7, the conversion of the reaction did not increase, and the selectivity to cinnamyl alcohol was also maintained. Additionally, we tested the recyclability of $\text{Pt}_5\text{Fe}_2@m\text{SiO}_2$, and the catalyst could be recycled for 5 runs without any loss in activity and selectivity (Figure 8).

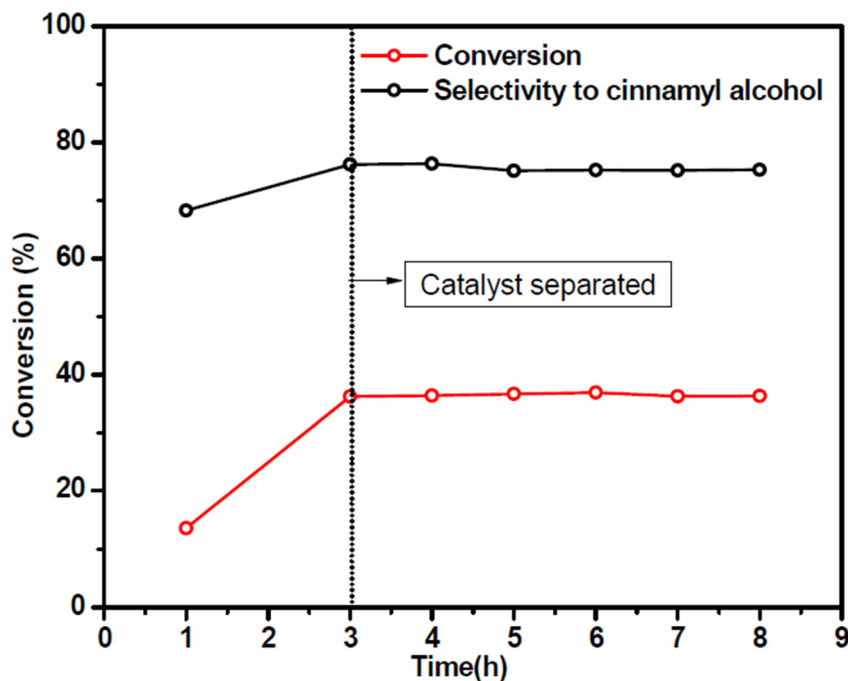


Figure 7. Leaching test for the $\text{Pt}_5\text{Fe}_2@m\text{SiO}_2$ catalyst. Reaction conditions: 1 mL hexane as the solvent, 20 mg cinnamaldehyde, mesitylene as an internal standard, 1 atm H_2 , 50 °C, 3 h. Pt content was kept constant at 1.5 mg (Cinnamaldehyde/metal ratio = 20). The catalyst was separated from the solution after 3 h.

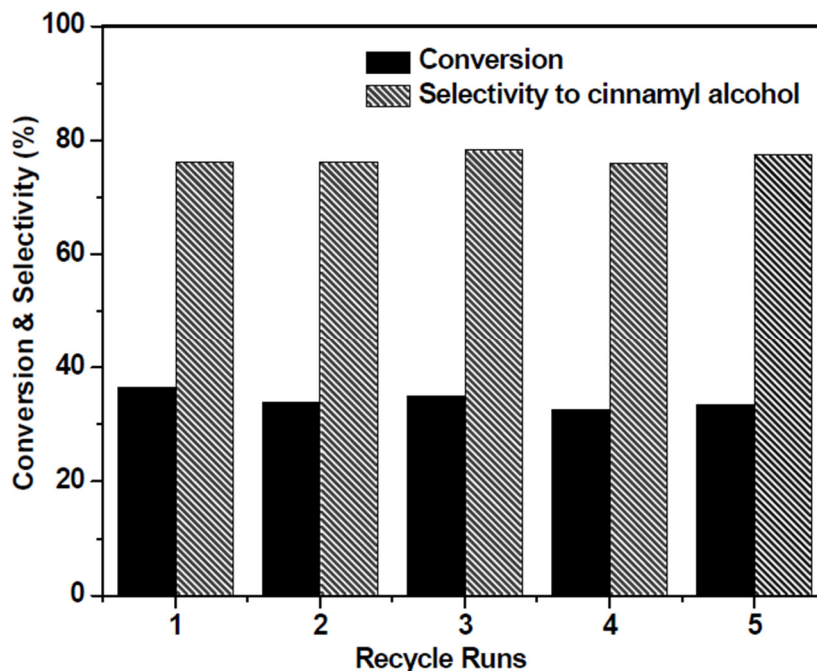


Figure 8. Recycling test for the $\text{Pt}_5\text{Fe}_2@\text{mSiO}_2$ catalyst. Reaction conditions: 1 mL hexane as the solvent, 20 mg cinnamaldehyde, 1 atm H_2 , mesitylene as an internal standard with a temperature of 50 °C for the reaction carried out for 3 h for each run. Pt content was kept constant at 1.5 mg (Cinnamaldehyde/metal ratio = 20).

To further test the efficacy of the Pt-Fe catalysts, vapor phase furfural hydrogenation was carried out, and the selectivity to furfuryl alcohol was compared at the similar conversion of furfural. As shown in Figure 6, selectivity to furfuryl alcohol increased with the addition of Fe, with $\text{Pt}_5\text{Fe}_2@\text{mSiO}_2$ showing the highest selectivity. The $\text{Pt}_5\text{Fe}_x@\text{mSiO}_2$ catalysts show the same catalytic trend for furfural hydrogenation in the vapor phase as that for hydrogenation of cinnamaldehyde in the liquid phase. In the case of the vapor phase hydrogenation of furfural, the presence of Fe alone is enough to ensure higher selectivity to the desired product, namely furfuryl alcohol.

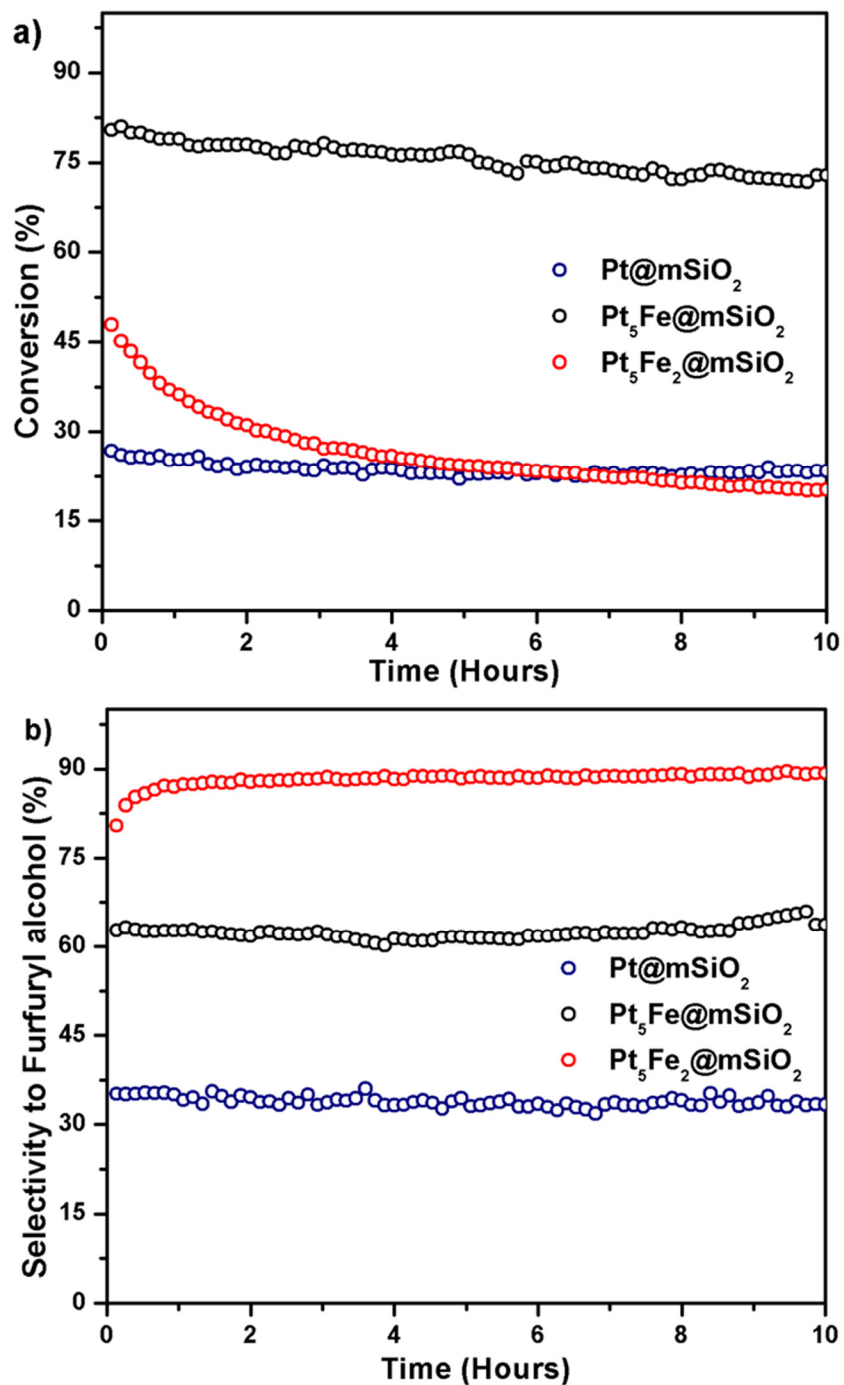


Figure 6 a) Conversion of furfural to furfuryl alcohol for Pt, Pt₅Fe and Pt₅Fe₂ reduced at 300 °C. b) Selectivity to furfuryl alcohol for Pt₅Fe@mSiO₂ and Pt₅Fe₂@mSiO₂ at 160 °C. In the above catalysts, the amount of Pt was kept constant at 1.26 mg.

Conclusions

Pre-synthesized Pt@mSiO₂ NPs were used as a platform to synthesize bimetallic Pt₅Fe_x@mSiO₂ NPs, free from surface modifying ligands. Using the selective hydrogenation of cinnamaldehyde as a model reaction, we elucidated the roles of Fe content on cinnamaldehyde hydrogenation over the Pt₅Fe_x@mSiO₂ catalysts. We found that selectivity to cinnamyl alcohol during cinnamaldehyde hydrogenation is enhanced by adding Fe to the Pt. Vapor phase hydrogenation of furfural selectively to furfuryl alcohol further confirmed the beneficial aspects of adding Fe to the Pt@mSiO₂ NPs, with higher selectivity to furfuryl alcohol being observed with greater Fe content. Although surface modifying ligands help the expression of remarkable selectivity in chemical reactions such as the hydrogenation of the C=O bond in α , β -unsaturated aldehydes, they are not suited to reaction conditions that are not conducive to their presence. Bimetallic and intermetallic nanoparticles designed via such porous encapsulation methods could sidestep the need for complex ligands used to perform such catalyst synthesis. Besides offering size and shape control, this encapsulation method enables the study of myriad other conditions of the catalysis facilitated by metal NPs alone.

Experimental section

Materials. Decanoic acid (99%), HF (48-51% in H₂O), K₂PtCl₄ (46-47% Pt), mesitylene (99%), and tetraethylene glycol (99%) were purchased from Acros Organics. NaBH₄ (98%), perfluorodecanoic acid (97%), tetraethylene glycol, and trans-cinnamaldehyde (98%) were purchased from Alfa Aesar. NaOH (99.0 – 100%) was purchased from EMD. Acetone (HPLC grade), acetone (Optima purity), CH₂Cl₂ (Optima purity), HCl (trace metal grade, 34 – 37%), HNO₃ (67-70%), and methanol (ACS grade) were purchased from Fisher Scientific. Fe(acac)₃

was purchased from Lancaster Synthesis Ltd. Hexanes (95% n-hexane) was purchased from Macron. Ar (99.995%) and H₂ (99.99%) were purchased from Matheson. Tetradecyltrimethylammonium bromide (TTAB, ≥99%) and tetraethyl orthosilicate (TEOS, reagent grade, 98%) were purchased from Sigma Aldrich. Hydrocinnamyl alcohol (HCOL, ≥98.0%), hydrocinnamaldehyde (HCAL, ≥90%), and cinnamyl alcohol (COL, ≥97.0%) were purchased from TCI. Materials were used as received.

Synthesis of Pt NPs. Platinum NPs were synthesized according to a previously reported procedure.^{20, 24} To a 500 mL round bottom flask containing 150 mL of DI water, 8.4 mg of TTAB was added and dissolved via sonication. An additional volume of water was added to obtain a total volume of 200 mL of the TTAB solution. To 25 mL of DI water in a centrifuge tube, 100 mg of K₂PtCl₄ was added and mixed thoroughly. This was then added to the TTAB solution, and the flask was stirred for 10 minutes. The flask was then transferred to an oil bath maintained at 50 °C and heated for 15 min until the cloudy solution became clear. The molar ratio of Pt to the surfactant is 1:100. We then added 25 mL ice-cold solution of 0.3 M sodium borohydride to the 500 mL flask. The molar ratio of Pt to the reducing agent was 1:30. A needle was inserted through the septum on the flask to relieve excess H₂ generated by the sodium borohydride dissolution for 20 min. The sample was stirred at 50 °C for 24 h. The resultant brown colloidal solution was centrifuged at 4500 × g for 4 times, each time the supernatant was collected while gathered residue was discarded as they contain bigger NPs that weren't desired. The final supernatant solution was then centrifuged at 18300 × g twice to concentrate the colloidal Pt NPs to a 20 mL solution.

Coating the Pt NPs with Silica (Pt@mSiO₂). The Pt NP solution was then further diluted with 180 mL of DI water, transferred to a 500 mL round bottom flask, and sonicated for 10

seconds. While stirring at 600 rpm, 8 mL of 0.05 M NaOH was added to the round bottom flask, and the sample was stirred for 10 min. Next, 3 mL of a 10 vol% tetraethyl orthosilicate (TEOS) in methanol solution was added dropwise to the solution over the course of 5 min. The sample was stirred at room temperature for 36 h and then centrifuged at $18300 \times g$ for 30 min at 30 °C. The supernatant was removed and the sample was dispersed in 20 mL of deionized water.

Surfactant removal through methanol reflux (Pt@mSiO₂). The Pt@mSiO₂ NPs were transferred to a 500 mL round bottom flask and diluted with 180 mL of methanol with sonication to obtain a homogeneous mixture. Next, 15 mL of concentrated HCl was slowly added while swirling the flask to mix the solution. The solution was then refluxed at 90 °C under stirring overnight. After the refluxing procedure, the solution was centrifuged at $18300 \times g$ for 30 min. The sample was washed and centrifuged with 20 mL of acetone twice, then diluted to 40 mL with acetone and the exact amount of Pt in the batch was determined using inductively coupled plasma mass spectrometry (ICP-MS). In a typical synthesis around 0.15 to 0.18 mmol of Pt was obtained.

Synthesis of Pt-Fe@mSiO₂ bimetallic NPs. In a typical synthesis, three batches of the as-synthesized Pt@mSiO₂ (with each synthetic batch confirmed to contain around 0.15 mmol of Pt), containing approximately 0.45 mmol of Pt, was centrifuged at $18300 \times g$ for 30 min. The residue was then redispersed in 5 mL of acetone and transferred to a 2-neck 250 mL round bottom flask. The Pt/Fe ratios used during the synthesis were 3 and 2 and 1 for Pt₃Fe@mSiO₂, Pt₂Fe₂@mSiO₂, and Pt₁Fe₄@mSiO₂, respectively. The appropriate Fe(acac)₃ amount in Optima purity acetone was transferred to the 250 mL round bottom flask. We then added 100 mL of tetraethylene glycol to this flask. The sample was then degassed at 100 °C under vacuum

to remove acetone for 1 h with stirring. After backfilling the flask with Ar, we attached an Ar balloon to the flask and heated the solution to 170 °C over 28 min, then to 200 °C over 12 min, and then held at 200 °C for 2 h. The solution was cooled to r.t. and diluted with 100 mL of acetone and centrifuged at $15200 \times g$ for 30 min at 30 °C. The sample was washed 3 more times with acetone, transferred to a 5 mL vial using acetone, and then dried using a rotary evaporator.

Calcination and Reduction of $Pt_5Fe_x@mSiO_2$. The samples were first dried for 2 h at 100 °C, then calcined in air at 550 °C for 6 h. The samples were then reduced using 10% H_2/Ar at 700 °C for 6 h in a tube furnace. The tube furnace was heated to 700 °C at a ramping rate of 5 °C/min. Before catalysis study, the samples were freshly reduced at 300 °C in 10% H_2/Ar for 2 h.

Ligand Introduction. In 100 μL of Optima purity acetone, 8.61 mg of decanoic or 25.70 mg of perfluorodecanoic acid were dissolved. To the reduced catalysts, first 1 mL of dichloromethane was added. The decanoic acid or perfluorodecanoic acid was added to the catalyst suspension in dichloromethane. After sonicating the mixture for 1 h, the samples were centrifuged, and the dichloromethane was discarded.

Characterization. Elemental analysis was performed using a Thermo Fisher Scientific X Series 2 ICP-MS. For Fe content analysis, 1 mL of the DI water diluted sample was diluted to 50 mL with 0.05 wt % HNO_3 and analyzed using the cold plasma mode. Powder X-ray diffraction (PXRD) patterns were collected at room temperature using an STOE Stadi P powder diffractometer equipped with an image plate and a Cu $K\alpha_1$ radiation source ($\lambda = 1.54056 \text{ \AA}$). All PXRD patterns were calibrated using a Si standard after measurements were complete. Transmission electron microscopy (TEM) samples were prepared using the drop

cast method and images were collected using a TECNAI G2 F20 microscope at an acceleration voltage of 200 kV. The particle size distributions for all imaged particles was calculated using the Particle Size Analyzer macro on ImageJ software by measuring at least 100 randomly chosen particles. Nitrogen physisorption analyses were performed at 77 K using a Micromeritics 3Flex surface characterization analyzer. Before analysis, the samples were degassed at 250 °C for 12 h under vacuum ($\sim 5 \times 10^{-5}$ Torr). The desorption branch of the isotherm was used to calculate the BJH pore sizes and BET surface areas. X-ray photoelectron spectroscopy (XPS) was performed on a Kratos Amicus/ESCA 3400 instrument. The sample was irradiated with 240 W unmonochromated Mg $K\alpha$ x-rays ($\lambda = 1253.6$ eV), and photoelectrons emitted at 0° from the surface normal were energy analyzed using a DuPont type detector. The pass energy was set at 150 eV. All data was energy calibrated with Si 2p at a binding energy of 103.5 eV as observed in SiO₂.

Cinnamaldehyde Hydrogenation in Liquid Phase. To either ligand-free catalysts or catalysts that underwent the ligand addition process, 1 mL of n-hexane, 20 μ L of cinnamaldehyde, and 10 μ L of mesitylene as internal standard were added to the test tubes. The tubes were capped with a septum and purged for 10 seconds using H₂, then protected with an H₂ balloon. The samples were heated at 50 °C for 3 h while stirring. The samples were centrifuged at $4500 \times g$ for 10 min at 30 °C, and the top layer was transferred to a vial for immediate analysis. The products were analyzed on an Agilent 6890N gas chromatograph (GC) equipped with a flame ionization detector (FID) and an HP-5 capillary column (30 m \times 0.320 mm \times 0.25 μ m). The products are also characterized using an Agilent 6890N GC equipped with a 5975 inert gas mass selective detector (MSD) and an HP-5ms capillary column

(30 m × 0.250 mm × 0.25 μm). The response factors of each component were determined using standard samples and were used to calculate the conversion and selectivity.

Leaching Tests for Cinnamaldehyde Hydrogenation. For the leaching test, Pt₅Fe₂@mSiO₂ was chosen as the catalyst. The catalyst was used under the same reaction conditions as the typical liquid phase cinnamaldehyde hydrogenation. After the 3-hour reaction, the solution mixture was isolated from the catalyst by centrifugation. The supernatant was then transferred to a fresh vial that was capped with a septum and purged with H₂ for 10 seconds. A hydrogen balloon was inserted and the reaction was carried out for another 5 h. Aliquots were taken every hour and quantified by GC.

Recycling Tests for Cinnamaldehyde Hydrogenation. Prior to the first run, the catalyst was reduced at 300 °C for 4 h under 10% H₂/Ar. Then the catalyst was transferred to a vial containing hexane, cinnamaldehyde, and mesitylene (internal standard). Hydrogen was purged through the vial for 10 seconds ahead of adding a hydrogen balloon. After each run, the solution was centrifuged to separate the catalyst. Acetone was added to the catalyst to wash it and further centrifuged to remove any traces of the solvents and substrate. The catalyst was then transferred to a fresh vial to which the substrate, internal standard, and solvent were added. Hydrogen was again purged through the septum for 10 seconds before adding a hydrogen balloon to the vial. The reaction was then carried out for 3h as before. Additional 3 (total 5) recycle runs were performed.

Furfural Hydrogenation in Vapor Phase. The catalysts were mixed with quartz sands and placed in a plug-flow quartz reactor. Ahead of the vapor phase hydrogenation, all catalysts were reduced at 300 °C for 2 h in a 10% H₂/He in a temperature controlled oven. Furfural was introduced into the flow system via a bubbler with He at a flow rate of 8.6 mL/min (actual

volume of furfural = 0.023 mL/min), while hydrogen was set at 11.4 mL/min. The oven was set to 160 °C for the hydrogenation reaction. At the outlet, the contents of the vapor were identified by an HP 5890 GC equipped with an FID detector and a capillary column (DB-5, 30 m x 0.32 mm x 0.25 μm).

References

1. Yu.W.; Porosoff M.D.; Chen J.G.; *Chem. Rev.* **2012**, *112*, 5780-5817.
2. Singh AK, Xu Q.; *ChemCatChem* **2013**, *5*, 652-676.
3. Alonso D.M.; Wettstein S.G.; Dumesic J.A.; *Chem Soc Rev*, **2012**, *41*, 8075-8098.
4. Mourdikoudis S.; Liz-Marzán L.M., *Chem Mater* **2013**, *25*, 1465-1476.
5. Kang Y.; Pyo J.B.; Ye X.; Gordon T.R.; Murray C.B.; *ACS Nano* **2012**, *6*, 5642-5647.
6. Lopez-Sanchez J.A.; Dimitratos N.; Hammond C.; Brett GL, Kesavan L, White S.; Miedziak P.; Tiruvalam R.; Jenkins R.L.; Carley A.F.; Knight D.; Kiely C.J.; Hutchings G.J., *Nat Chem*, **2011**, *3*, 551-556.
7. Marshall S.T.; O'Brien M.; Oetter B.; Corpuz A.; Richards R.M.; Schwartz D.K.; Medlin J. W., *Nat Mater* **2010**, *9*, 853-858.
8. Kwon SG, Krylova G, Sumer A, Schwartz MM, Bunel E.E.; Marshall C.L.; Chattopadhyay S.; Lee B.; Jellinek J.; Shevchenko E.V., *Nano Lett* **2012**, *12*, 5382-5388.
9. Li G, Jiang D-e, Kumar S, Chen Y, Jin R (2014). *ACS Catal* **2014**, *4*, 2463-2469.
10. González-Gálvez, D.; Nolis, P.; Philippot, K.; Chaudret, B.; van Leeuwen, P. W. N. M., *ACS Catal* **2012**, *2*, 317-321.
11. Pang SH, Schoenbaum CA, Schwartz DK, Medlin JW., *Nat Commun* **2013**, *4*, 2448.
12. Stamenkovic, V. R., Mun, B. S.; Mayrhofer, K. J. J.; Ross, P.N.; Markovic, N.M., *J Am Chem Soc* **2006**, *128*, 8813-8819.

13. Stamenkovic, V. R.; Mun, B.S.; Arenz, M.; Mayrhofer, K. J. J.; Lucas, C. A.; Wang, G.; Ross, P.N.; Markovic, N.M., *Nat Mater* **2007**, 6, 241-247.
14. Tao, F; Grass, M.E.; Zhang, Y.; Butcher, D.R.; Aksoy, F; Aloni, S.; Altoe, V.; Alayoglu, S.; Renzas, J.R.; Tsung, C-K.; Zhu, Z.; Liu, Z.; Salmeron, M.; Somorjai, G.A., *J Am Chem Soc* **2010**, 132, 8697-8703.
15. Kim, D.; Resasco, J.; Yu, Y.; Asiri, A.M.; Yang, P.; *Nat Commun* **2014**, 5, 4948.
16. Wu, B.; Huang, H.; Yang, J.; Zheng, N.; Fu G., *Angew Chem Int Ed* **2012**, 51, 3440-3443.
17. Tsang, S.C.; Cailuo, N.; Oduro, W.; Kong, A. T. S.; Clifton, L.; Yu, K. M. K.; Thiebaut, B.; Cookson, J.; Bishop, P., *ACS Nano* **2008**, 2, 2547-2553.
18. Astruc, D.; Lu, F.; Aranzaes, J.R., *Angew Chem Int Ed* **2005**, 44, 7852-7872.
19. Wang, D.; Li, Y.; *Adv Mater* **2011**, 23, 1044-1060.
20. Joo, S. H.; Park, J.Y.; Tsung, C-K.; Yamada, Y.; Yang P.; Somorjai G. A., *Nat Mater* **2009**, 8, 126-131.
21. Lee, I.; Albiter, M. A.; Zhang, Q.; Ge, J; Yin, Y; Zaera, F., *Phys Chem Chem Phys* **2011**, 13, 2449-2456.
22. Wang, G-H.; Hilgert, J.; Richter, F. H.; Wang, F.; Bongard, H-J.; Spliethoff, B.; Weidenthaler, C; Schüth, F.; *Nat Mater* **2014**, 13, 293-300.
23. Pei, Y.; Maligal-Ganesh, R.V.; Xiao, C.; Goh, T-W.; Brashler, K; Gustafson, J.A.; Huang, W., *Nanoscale* **2015**, 7, 16721-16728.
24. Maligal-Ganesh, R.V., Xiao, C.; Goh, T.W.; Wang, L-L.; Gustafson, J.; Pei, Y.; Qi, Z.; Johnson, D. D., Zhang, S.; Tao, F; Huang, W.; *ACS Catal* **2016**, 6, 1754-1763.
25. Vu, K. B.; Bukhryakov, K. V.; Anjum, D. H.; Rodionov, V. O.; *ACS Catal* 2015, 5, 2529-2533.

26. Bauer, J.C.; Chen, X.; Liu Q.; Phan, T-H.; Schaak, R.E., *J Mater Chem* **2008**, 18, 275-282.
27. Hyie, K.M.; Yaacob, I. I., *Mater Res Innovations* **2009**, 13, 214-216.
28. Sun, S.; Murray, C.B.; Weller, D.; Folks, L.; Moser, A., *Science* **2000**, 287, 1989-1992.
29. Groot, Fd.; *Coord Chem Rev*, **2005**, 249, 31-63.
30. Sirijaruphan, A.,; Goodwin, J.G.; Rice, R. W.; *J Catal* **2004**, 224, 304-313.
31. Neri, G.; Rizzo, G.; De Luca, L.; Corigliano, F.; Arrigo, I.; Donato A., *Catal Comm* **2008**, 9, 2085-2089.
32. Neri, G.; Rizzo, G.; De Luca, L.; Corigliano, F.; Arrigo, I.; Aricò, A. S.; Donato, A., (2008) *Appl Catal A-Gen* **2008**, 350, 169-177.
33. Neri, G.; Arrigo, I.; Corigliano, F.; De Luca, L.; Donato, A., *Catal Lett* **2011**, 141, 1590.

**CHAPTER 4. SELECTIVE HYDROGENATION OF ACETYLENE OVER SUB-5 NM
INTERMETALLIC NANOPARTICLES ENCAPSULATED IN MESOPOROUS
SILICA WELLS**

Raghu V. Maligal-Ganesh, Chaoxian Xiao, Yuchen Pei, Tian Wei Goh, Weijun Sun,
and Wenyu Huang

Abstract

We report the synthesis and catalytic application of intermetallic PtSn@MSWs (Mesoporous Silica Wells) in the semi-hydrogenation of acetylene. Platinum nanoparticles with a size of 2.9 nm supported on amine-functionalized ~180 nm SiO₂ spheres were enmeshed in a mesoporous silica shell, before the addition of tin via polyol synthesis, leading to the final PtSn@MSWs. Owing to the mesoporous encapsulation the sub-5 nm bimetallic particles are shown to be monodisperse and well protected against individual bimetallic nanoparticles on the SiO₂ sphere even under high-temperature treatment procedures. In the gas phase semi-hydrogenation of acetylene, the PtSn@MSWs with Sn/Pt molar ratios greater than 1, displayed higher selectivity to ethylene. However, increased Sn also led to the lower conversion of acetylene. The intermetallic PtSn@MSW catalysts also displayed long-term stability.

Introduction

The discovery of metal nanoparticles as efficient bridges between homogeneous and heterogeneous catalysis has led to their greater exploration over the last three decades.¹⁻³ Thus size,⁴⁻⁶ morphology,⁷⁻¹⁰ surface modifying organic ligands¹¹⁻¹³ and specific reaction environments¹⁴⁻¹⁸ have been under intense scrutiny to grasp the extensive implications of how catalysis is affected by nanoparticles. An important class of nanoparticles is bimetallic alloy nanoparticles, which have been demonstrated to be superior catalysts to their monometallic iterations.¹⁹⁻²¹

Due to the operation of unique electronic and structural effects on their surfaces, bimetallic nanoparticles offer tunability of the catalytic reactions for improved activity and selectivity in chemical transformations.²² However, there is significant room for improvement due to the random arrangement of their constituent atoms at the surface, which are also subject to change under reaction conditions.²³⁻²⁴ Hence, a recent direction has been the study of the catalytic properties of structurally ordered bimetallic compounds, intermetallic compounds, which are less susceptible to such changes.

Intermetallic compounds are ordered alloys formed by metals in specific compositions with substantially different chemical properties.²⁵⁻²⁶ They possess unique crystal structures and chemical properties quite distinct from their parent metals. Recent reports have detailed the role the structural and electronic properties of both bulk and nanoscale intermetallic compounds can potentially play in catalysis.²⁷⁻²⁸ Nanoscale intermetallic compounds containing precious metals have shown great promise as efficient catalysts.²⁹⁻³¹ Previously, we synthesized intermetallic nanoparticles (iNPs) of Pt in a confined silica environment and demonstrated their ability as efficient catalysts.³² However,

the size of these iNPs was in the 16-20 nm range, which significantly reduces the active metal surface area. Concurrently we had developed a core-shell strategy to load pre-synthesized smaller Pt nanoparticles (~2.9 nm) on a silica support ahead of providing a mesoporous silica shell, denoted as Pt@MSWs, to prevent aggregation of the nanoparticles.³³ These Pt@MSWs catalysts were thermally stable at high reaction temperatures.

In this report, we used the Pt@MSWs as seeds to prepare PtSn@MSWs with varying Sn/Pt ratios using colloidal chemistry methods. The thermally stable PtSn@MSWs were thus synthesized via this confinement strategy. At Sn/Pt ratios equal to or greater than 1, intermetallic PtSn@MSWs was obtained. The semi-hydrogenation of acetylene was used as a model reaction to demonstrate the efficiency of the ordered intermetallic PtSn@MSWs. While Pt@MSWs and the alloys of Pt-Sn@MSWs had poor selectivity to desired ethylene, the intermetallic PtSn@MSWs showed vastly improved selectivity. The intermetallic catalyst could be conveniently regenerated for reuse without any loss in activity or selectivity.

Results and discussion

The Pt-Sn bimetallic catalysts were synthesized by a colloidal seeded growth method, converting Pt seeds to Pt-Sn bimetallic nanoparticles, as shown in Figure 1.

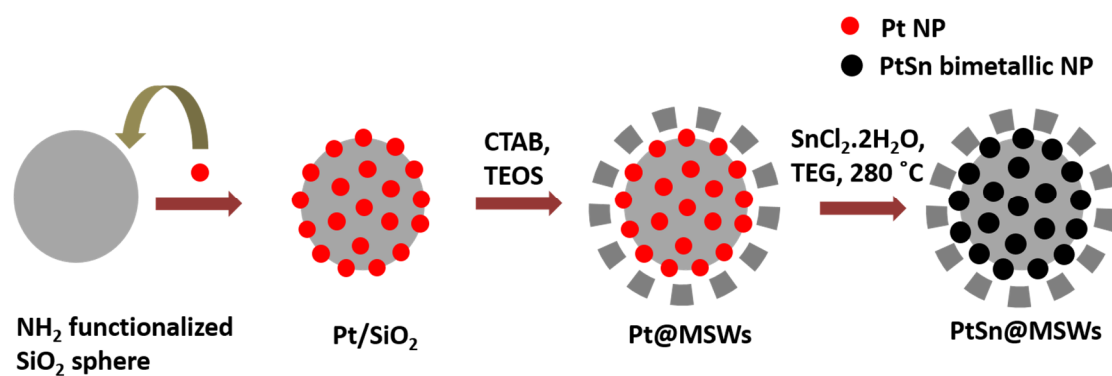


Figure 1. Schematic synthesis of Pt-Sn bimetallic catalysts encapsulated in mesoporous silica well.

We prepared the Pt@MSWs as Pt seeds following reported literature. Bare silica spheres with an average size of ~180 nm were prepared with a modified Stöber method, and then functionalized with the -NH₂ group to facilitate the loading efficiency and uniformity of metal NPs.³⁴ Pre-synthesized PVP-capped Pt nanoparticles (2.9 ± 0.3 nm) were loaded onto NH₂-functionalized silica spheres to give the Pt-SiO₂ composite. Following the deposition of the Pt nanoparticles, a mesoporous silica shell was coated on the Pt-SiO₂ composite by hydrolyzing TEOS in ammonia solution where CTAB performs the role of a pore-directing template.^{33,35} The template CTAB was removed by using methanol-HCl reflux for the access of reactants/products to MSW-coated Pt NPs. We controlled the MSW shell thickness at 20 nm in this work.³³

The final Pt-Sn bimetallic nanoparticles were obtained by reducing SnCl₂.2H₂O in the presence of Pt@MSWs in tetraethylene glycol (TEG). To maintain the compositional control of Pt/Sn, the exact Pt loading was determined by ICP-MS to adjust the necessary amount of SnCl₂ precursor. As shown in Table 1, the Pt-Sn samples are denoted as PtSn_x@MSW (where x = 0.3, 0.5, 0.7, 1.0 and 2.0). The actual Sn content as measured by ICP-MS in the samples is close to the added amount of Sn precursor during synthesis for the samples with Sn/Pt ≤ 1.0, but slightly lower when Sn/Pt = 2. All samples were then calcined at 500 °C to remove carbonaceous species and then reduced at 300 °C to obtain the bimetallic Pt-Sn composites.

Table 1. Pt and Sn loading in Pt-Sn samples measured with ICP-MS.

Sample	Sn/Pt ratio during synthesis	Measured Pt (wt% by ICP-MS)	Measured Sn (wt% by ICP-MS)	Sn/Pt (Molar ratio)
PtSn _{0.3} @MSW	0.3	1.11	0.24	0.35
PtSn _{0.5} @MSW	0.5	1.10	0.31	0.47
PtSn _{0.7} @MSW	0.7	1.12	0.50	0.74
PtSn _{1.0} @MSW	1.0	1.34	0.80	1.02
PtSn _{2.0} @MSW	2.0	1.10	1.22	1.85

To characterize the mesoporous nature of the MSWs encapsulating the NPs, nitrogen sorption measurements were carried out on the Pt@MSW sample (Figure 2). BET surface area of Pt@MSWs was measured to be $598 \pm 8 \text{ m}^2/\text{g}$, and the pore diameter was determined to be 2.7 nm based on the desorption branch of the isotherms by using the Barrett–Joyner–Halenda (BJH) method.

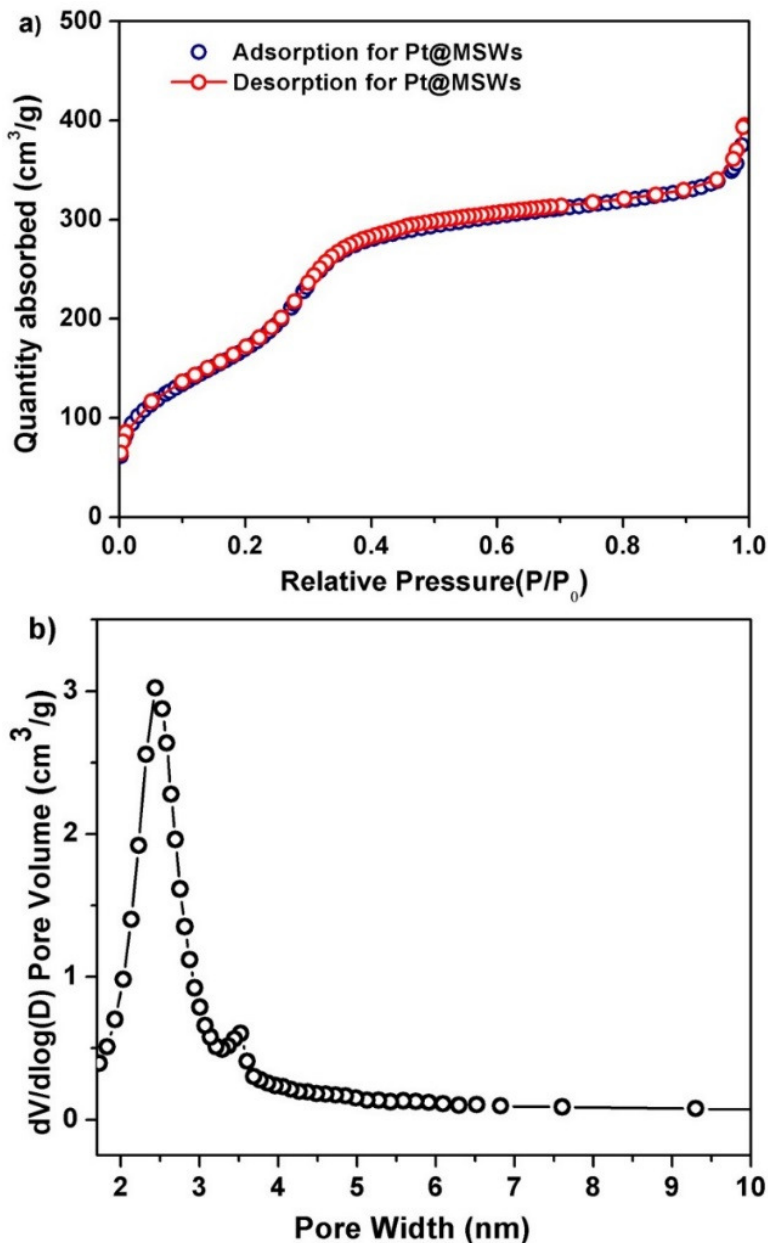


Figure 2 a) Nitrogen sorption isotherm and b) BJH pore diameter assessment of Pt@MSWs.

From the PXRD patterns (Figure 3), Pt-Sn alloy phase was observed with a slight low-angle peak shift consistent with the addition of Sn for all Sn/Pt ratios varying from 0.3 to 0.7. When Sn/Pt ratios were controlled at 1 and 2, a NiAs type PtSn intermetallic compound was formed as the primary phase where the observed pattern lines up with the standard PtSn pattern.

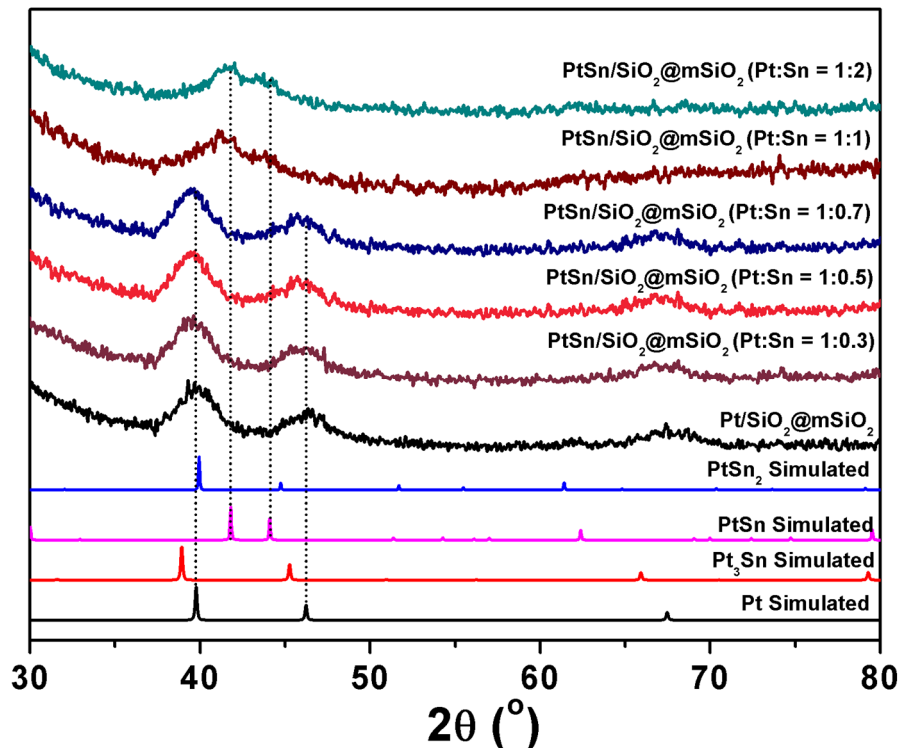


Figure 3. PXRD patterns of Pt-Sn@SiO₂ catalysts with various Sn/Pt ratio. The simulated patterns for the standards (generated from JCPDS data) used for comparison are also shown.

The TEM image of the various stages of the synthesis of PtSn@MSWs is shown in Figure 4. Figure 4a-d depicts the morphology of respective PVP-capped 2.9 nm Pt NPs, Pt/SiO₂, Pt@MSWs, and 1:1 PtSn@MSWs. The average particle size of the as-formed Pt-Sn nanoparticles in Figure 3d is measured to be ~4 nm.

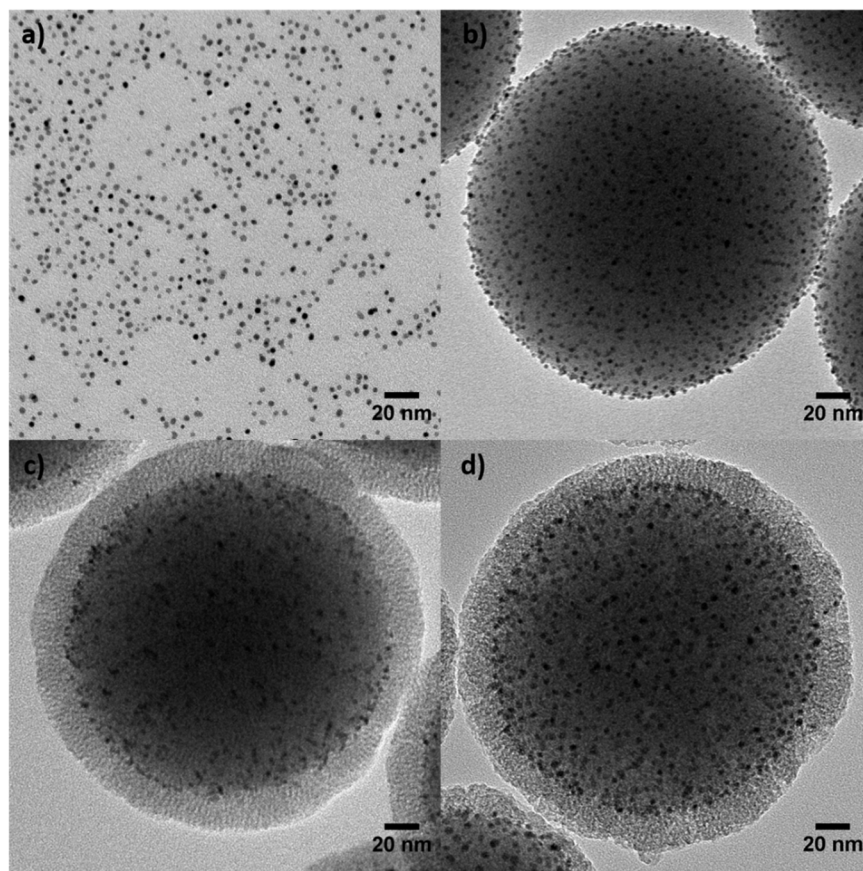


Figure 4. TEM images of a) 2.9 nm Pt nanoparticles protected by PVP, b) 2.9 nm Pt/SiO₂, c) 2.9 nm Pt@MSWs, and d) PtSn@MSWs of a Pt:Sn molar ratio of 1:1. The PtSn particles in d) have an average size of ~4 nm.

Semi-hydrogenation of acetylene by the Pt-Sn/SiO₂@mSiO₂ catalysts

Semi-hydrogenation of acetylene was chosen as a model reaction to evaluate the catalytic efficiency of as-synthesized PtSn@MSWs. Using a feed mixture of 0.5% C₂H₂, 50% C₂H₄, 5% H₂ in He for a total flow of 30 mL/min, the reaction was initially screened at 200 °C for all the catalysts. The results for the semi-hydrogenation of acetylene for these catalysts are shown in Figure 5. Pt@MSWs is not selective, with complete conversion observed for the trace acetylene and as well partial conversion of feed ethylene to ethane. PtSn@MSWs with Sn/Pt ratios from 0.3-0.7 also indicated the poor selectivity, exhibiting behavior similar to

Pt@MSWs. The low selectivity of PtSn@MSWs with Sn/Pt ratios from 0.3-0.7 is attributed to the Pt dominance in these PtSn alloys as evidenced by the powder XRD patterns. However, intermetallic PtSn phase can be formed at Sn/Pt ratios =1 and 2, which eliminates contiguous Pt domains at the surface responsible for complete hydrogenation. PtSn@MSWs with Sn/Pt ratios of 1 and 2, indeed displayed higher selectivity to ethylene. For PtSn@MSWs with a Sn/Pt ratio of 2, there was a decrease in the activity probably due to the presence of inactive Sn species on the surface.

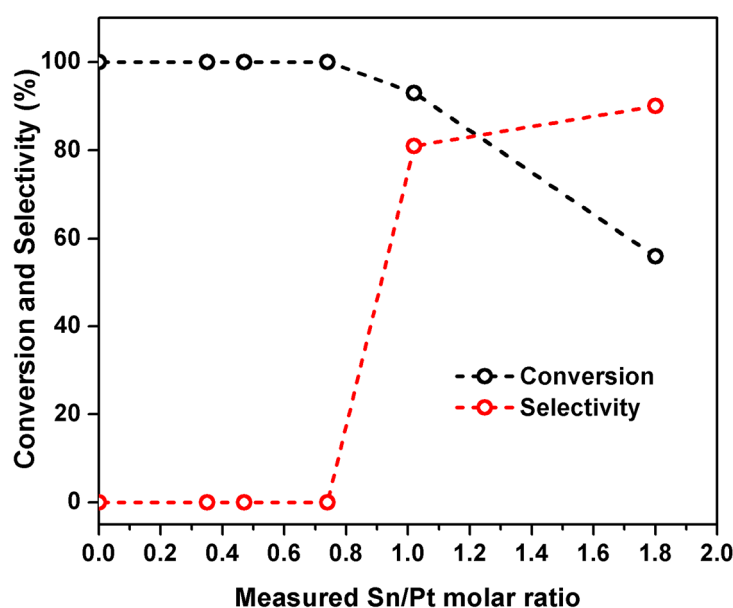


Figure 5. The influence of Sn/Pt molar ratio (measured by ICP-MS) on the catalytic performance of PtSn@MSWs. Reaction conditions: He/H₂/C₂H₄/C₂H₂ = 13.5/1.5/15/0.15 mL/min. The mass of Pt used was kept constant at 1.4 mg.

In previous work carried out in our group (also reported in chapter 2 of this thesis) we have observed that increased surface Sn can result in the decreased activity for PtSn@mSiO₂ catalysts in the hydrogenation of furfuraldehyde selectively to furfuryl alcohol.³² The catalytic

screening confirms the structural advantages of intermetallic PtSn in enhancing the selectivity of acetylene semi-hydrogenation.

Intermetallic PtSn@MSWs with a Sn/Pt ratio of 1 was then run for the stability evaluation under similar on-stream conditions for an extended period. Over a 40-hour period, the catalyst only shows slight deactivation for the first 15 h while the selectivity to ethylene was maintained at 81%. Besides ethylene, the byproducts were majorly ethane (10%) and dimerized C₄ hydrocarbons (7-9%).

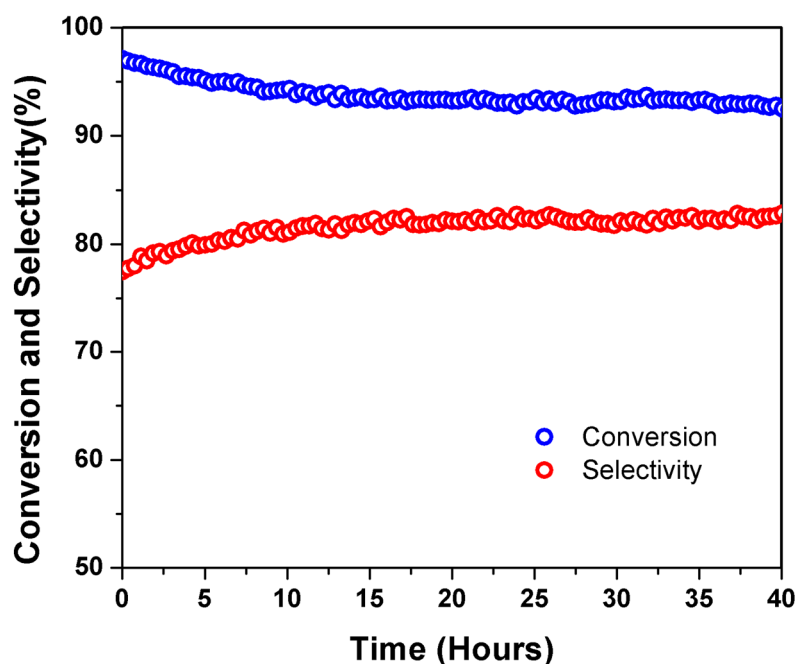


Figure 6. Acetylene semi-hydrogenation stability of 1% PtSn@MSWs with a Sn/Pt ratio = 1. Reaction conditions: He/H₂/C₂H₄/C₂H₂ = 13.5/1.5/15/0.15 mL/min, 200 °C. Mass of Pt used = 1.4 mg.

A stability study was also conducted for intermetallic PtSn@MSWs with a Sn/Pt ratio of 2 containing the same amount of Pt. Although the conversion was lower at 56% at the same temperature of 200 °C, higher selectivity to desired ethylene was observed at 91%. The decrease in activity for Pt-Sn systems at higher concentrations of Sn for the semi-

hydrogenation of acetylene has been alluded to in a study by Gao et al.³⁶ Their study points to the need for optimal concentrations of Sn at the surface, as all hydrocarbon species bind only to Pt with Sn only affecting the extent of this adsorption on Pt. Previous studies have also demonstrated that at higher concentrations of Sn, the density of Pt surface sites at the surface decline owing to the lower surface energy of tin and tin oxide species compared to that of platinum.³⁷⁻³⁸

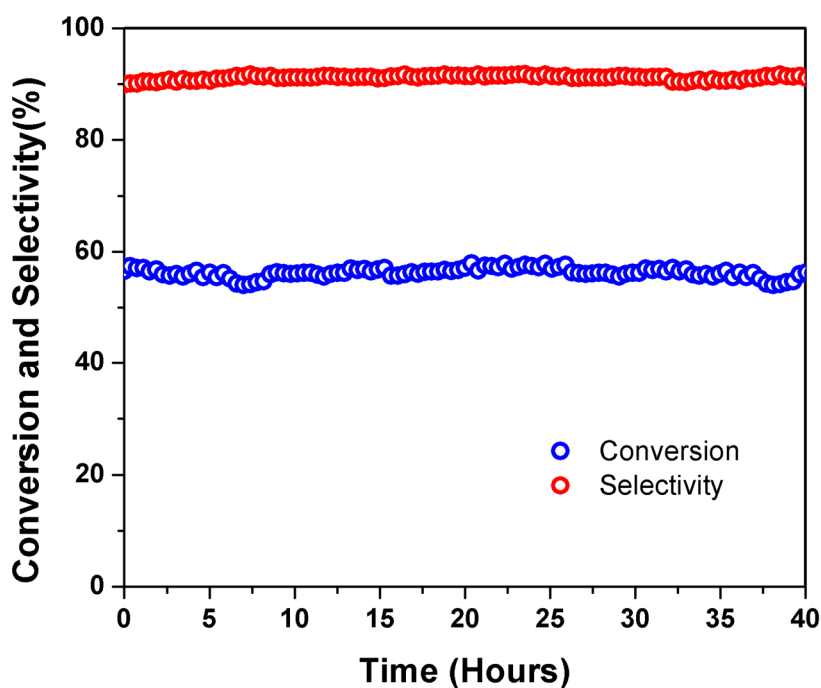


Figure 7. Acetylene semi-hydrogenation stability of 1% PtSn@MSWs with a Sn/Pt ratio = 2. Reaction conditions: He/H₂/C₂H₄/C₂H₂ = 13.5/1.5/15/0.15 mL/min, 200 °C. Mass of Pt used = 1.4 mg.

The size of the PtSn@MSWs iNPs plays an important role in their catalytic performance. To illustrate the importance of the size of the iNPs we also ran the reaction for ~20 nm PtSn@mSiO₂ iNPs, with a Sn/Pt molar ratio of 1 (reported in chapter 2 of this thesis), as demonstrated in figure 8. Although the selectivity to ethylene was comparable at 79%, the

conversion was considerably lower at around 18% for the same quantity of Pt (1.4 mg). As reported in chapter 2, from CO chemisorption measurements of PtSn@mSiO₂ we obtained a Pt metal surface area of only 1.8%. Similar CO chemisorption measurements on the PtSn@MSWs were not successful at elucidating the metal surface area, however from their catalytic performance it can be clearly observed that the sub-5 nm PtSn@MSWs catalysts offer 5-fold enhanced conversion for the same quantity of platinum in comparison to PtSn@mSiO₂.

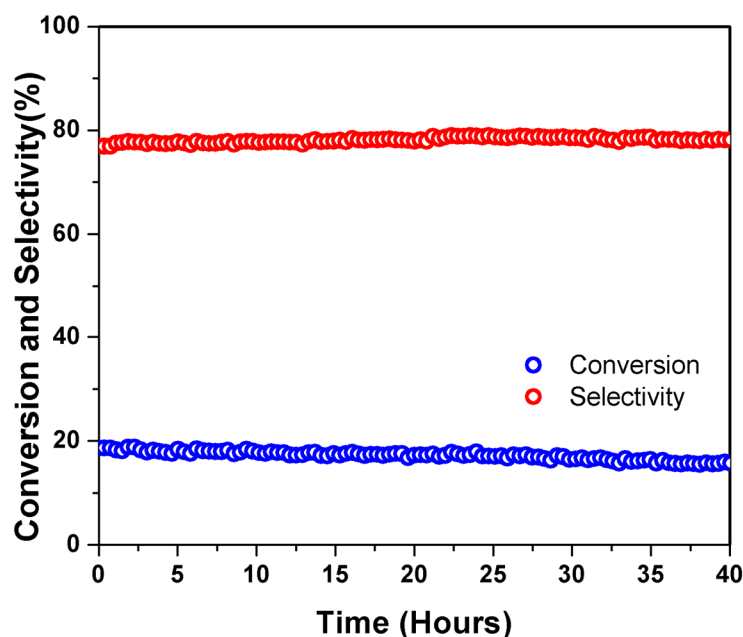


Figure 8. Acetylene semi-hydrogenation over PtSn@mSiO₂ with a Sn/Pt ratio = 1. Reaction conditions: He/H₂/C₂H₄/C₂H₂ = 13.5/1.5/15/0.15 mL/min, 200 °C. Mass of Pt used = 1.4 mg.

While the intermetallic PtSn@MSWs demonstrated enhanced selectivity during catalysis in comparison to Pt and PtSn alloys, it is important to note that the high selectivity of the catalyst relied on the seed-mediated synthesis of the intermetallic compounds to ensure the homogenous composition and accurate structure of intermetallic PtSn@MSWs.³⁹ To demonstrate the importance of this homogeneity in our PtSn@MSWs, we synthesized a control

catalyst by a conventional wetness impregnation technique. We co-impregnated Pt and Sn precursor solutions (K_2PtCl_4 and $SnCl_2 \cdot 2H_2O$) to pre-weighed SBA-15 (denoted as PtSn/SBA-15). To minimize the compositional heterogeneity in PtSn/SBA-15, we used the sequential addition of each precursor following a drying process overnight at 100 °C to exclude the adsorption difference of two precursors. We controlled the Pt loading to 1 wt.% with a ratio of Pt/Sn=1 in PtSn/SBA-15 like our PtSn@MSWs.

The PXRD pattern of PtSn/SBA-15 (Figure 8a) indicates the formation of PtSn intermetallic phase predominantly, with some traces of the Pt_3Sn alloy phase after the reduction treatment. From the TEM images of PtSn/SBA-15, the average size of PtSn NPs was calculated as ~ 7 nm, close to the PtSn NPs in PtSn@MSWs. PtSn/SBA-15 was then used as a control catalyst for the semi-hydrogenation of acetylene at 200 °C. As shown in Figure 9, the catalyst has poor selectivity to ethylene with the major product being ethane. Previous reports have indicated that heterogeneous domains can be present in catalysts prepared by the co-impregnation of metallic precursors due to the inhomogeneous dispersion of metals on supports.⁴⁰⁻⁴¹ This is partially evident in our PXRD for the sample, as shown in Figure 8a.

Hence although the desired intermetallic phase was formed via this conventional wetness impregnation method, Pt_3Sn alloy particles may have also formed, leading to the lower selectivity for this control catalyst. Tanaka et al. demonstrated through XAFS studies that their PtSn/SiO₂ (with a Sn/Pt ratio = 1) catalyst prepared by the same impregnation technique we used, consisted of PtSn, Pt_3Sn , and tin oxide nanoclusters even at high reduction temperatures of 1000 °C.⁴² From our study on the PtSn@MSWs catalyst with a Sn/Pt ratio of 0.3, we have already demonstrated that this is a poor catalyst for the semi-hydrogenation of acetylene.

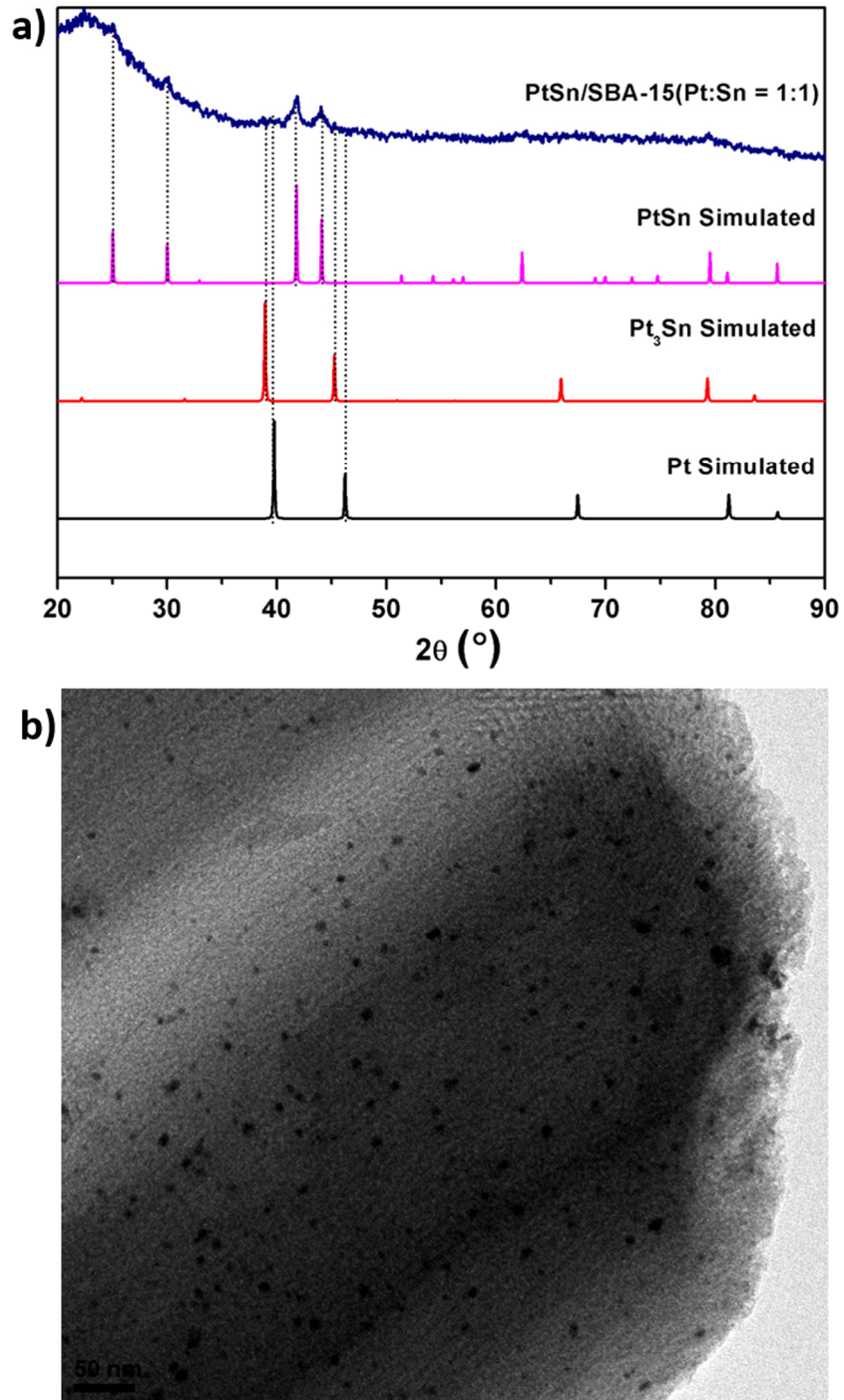


Figure 8. a) PXRD of 1% PtSn/SBA-15, with a Sn/Pt ratio = 1; PtSn particle size calculated from PXRD is ~ 7 nm. b) A TEM image of 1% PtSn/SBA-15, the particle size was measured to be 6-8 nm.

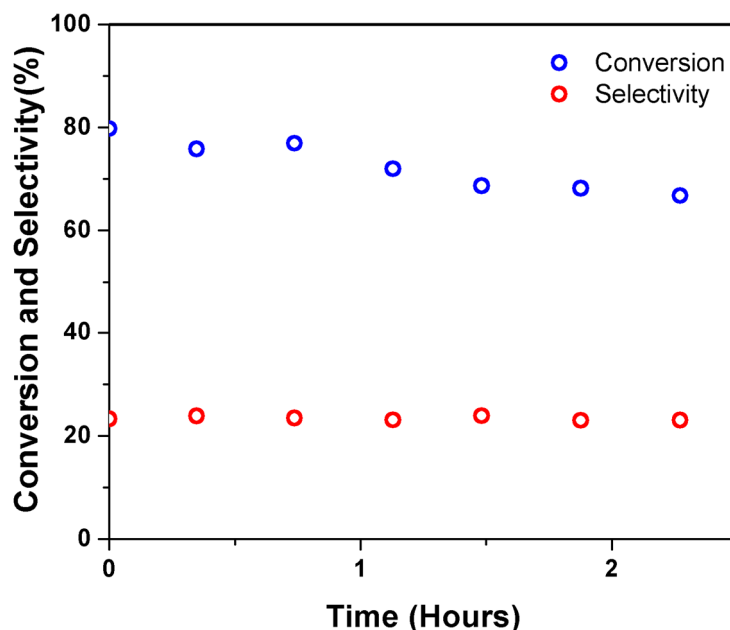


Figure 9. Acetylene semi-hydrogenation by 1% PtSn/SBA-15 of a Sn/Pt ratio = 1; Reaction conditions: He/H₂/C₂H₄/C₂H₂ = 13.5/1.5/15/0.15 mL/min, 200 °C. Mass of Pt used = 1.4 mg.

Regeneration of the PtSn@MSW catalyst

A regeneration experiment was also carried out to demonstrate the high thermal stability of the PtSn@MSW catalyst due to the presence of MSW shells. The catalyst could be conveniently recycled by an oxidation/reduction cycle, in the same fashion as our previous report on a PtSn@mSiO₂ catalyst.³² In a typical cycle, the pre-reduced catalyst (reduced at 300 °C in a flow of 10% H₂ in He) was first run for the reaction for 1.5 h, following which it was deactivated (details in the experimental section). The deactivated catalyst was then regenerated by calcination in an 80% oxygen flow in helium for half an hour at 500 °C and a subsequent reduction in 10% H₂ flow at 300 °C. The next cycle was then started. PtSn@MSWs showed a complete recovery of activity and selectivity in the semi-hydrogenation of acetylene for at least 5 cycles after the regeneration. (Figure 10).

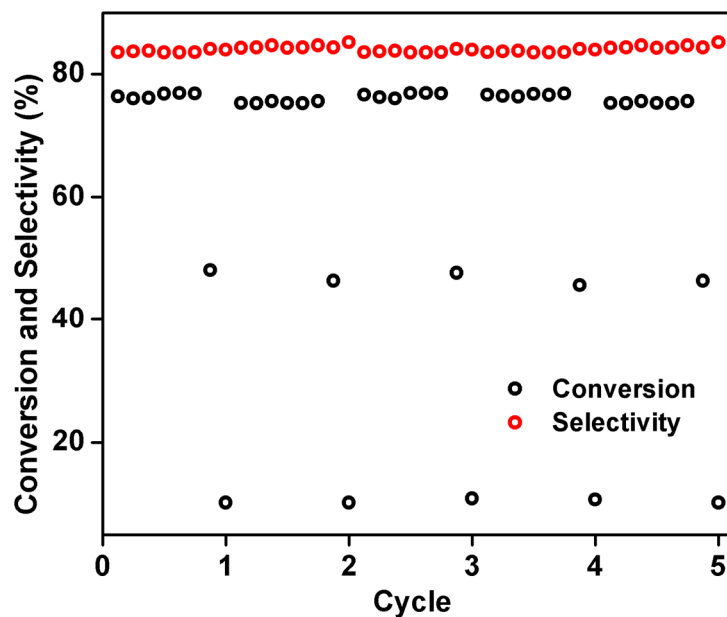


Figure 10. Regeneration experiment performed on PtSn@MSWs with a Sn/Pt ratio of 1:1.

PXRD and TEM measurements of the sample post the regeneration cycles indicate the PtSn NPs are still well encapsulated in the mesoporous silica wells (Figure 11).

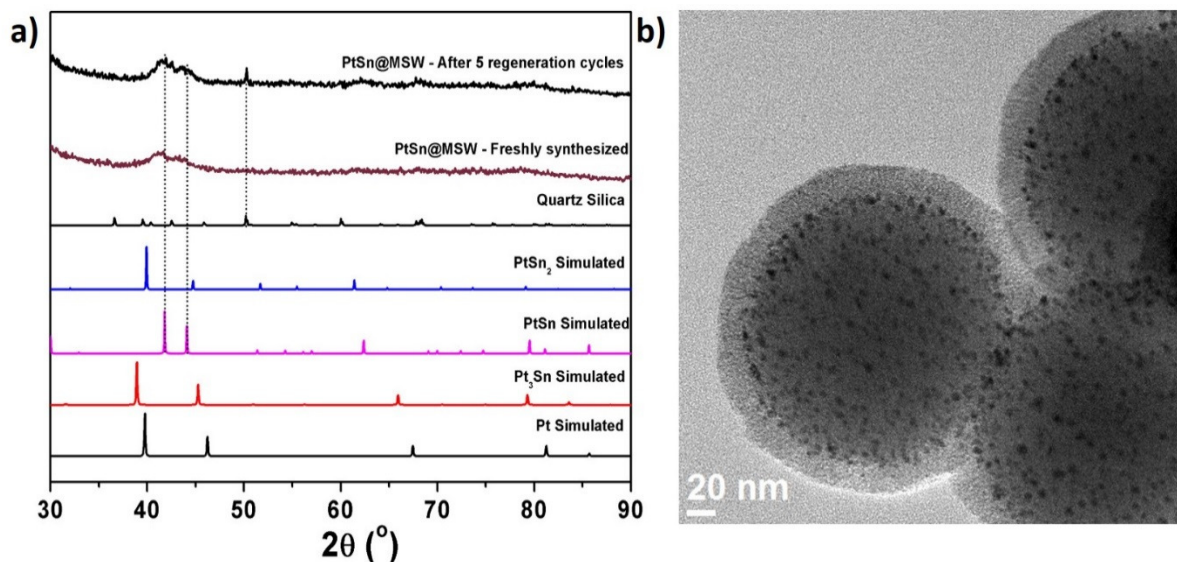


Figure 11. a) PXRD pattern of PtSn@MSW before and after reaction b) TEM image of the same catalyst after the reaction.

Conclusions

Intermetallic compounds hold great promise for enhanced heterogeneous catalysis. Improved synthetic methodologies can enhance the homogeneity of iNPs, and further increase their catalytic efficiency. In this report, we have demonstrated the synthesis of sub-5 nm thermally stable intermetallic PtSn@MSW as selective catalysts for the semi-hydrogenation of acetylene. Moreover, the catalysts can be conveniently regenerated via an oxidation/reduction cycle, because the presence of the MSW shells can prevent the aggregation of PtSn iNPs under high temperatures. We hope to generalize this seeded growth method in preparing various PtM@MSWs intermetallic structures for other selective hydrogenation reactions in future studies.

Experimental section

Chemicals

Methanol, ethanol, isopropanol, ammonium hydroxide (28%) and ethylene glycol (EG), cyclohexane were purchased from Fisher Scientific. 3-aminopropyltriethoxysilane (APTS, 99%), was obtained from Alfa Aesar. K_2PtCl_4 was obtained from Acros Organics. Tetraethyl orthosilicate (TEOS, 98%), L-arginine, polyvinylpyrrolidone (PVP, K30 MW~29000), myristyltrimethylammonium bromide ($C_{14}TAB$) and hexadecyltrimethylammonium bromide ($C_{16}TAB$) were obtained from Sigma Aldrich.

The synthesis of 180 nm SiO_2 spheres with uniform particle size (deviation <5%)

The synthesis of the 180 nm SiO_2 spheres was carried out based on a previously reported four-step seeded growth approach.⁴³

Preparation of 24 nm SiO_2 seeds: A homogeneous mixture of 18.2 mg L-arginine (0.104 mmol) in 13.9 mL water was first made. Cyclohexane (0.9 mL) was then gently added to the water-arginine mixture, resulting in the formation of a double layer. The solution was heated

to 60.0 ± 0.2 °C for 30 min at 300 rpm stirring to mix the aqueous layer contents well, without disturbing the cyclohexane layer. This was followed by the addition of 1.10 mL TEOS (5.0 mmol) to the mixture. The reaction was kept for 20 hrs at 60 °C. After this, the aqueous layer was carefully removed and stored under refrigeration. This was named as Sample A.

Preparation of 45 nm SiO₂ seeds: Around 4 mL Sample A was taken and diluted with 14.4 mL ultrapure water. To this 2 mL cyclohexane was added. The aqueous layer was stirred with a magnetic stir bar at 300 rpm to homogeneously mix its contents while leaving the cyclohexane layer undisturbed. Then 1.408 mL TEOS was added to the top layer in its entirety, and the mixture was kept at 60°C for 30 hrs. Post this duration, the aqueous layer was carefully removed and stored under refrigeration as Sample B.

Preparation of 82 nm SiO₂ seeds using the Stöber method: Around 1 mL of Sample B was taken and diluted with 2.6 mL deionized water and 18 mL ethanol. Subsequently, 1.7 mL NH₃·H₂O (~28% assay) was added. This solution was mixed under ~ 500 rpm for 1 hr at room temperature. Around 0.8 mL TEOS was added to the solution dropwise three times at 30-minute intervals. The solution was stirred for 6 hrs and later stored under refrigeration as Sample C.

Preparation of 180 nm SiO₂ spheres using the Stöber method: From Sample C 1 mL was taken and diluted with 2.6 mL deionized water and 18 mL ethanol. To this 1.7 mL NH₃·H₂O (~28% assay) was added. The solution was mixed under ~ 500 rpm for 1 hr. A total volume of 0.44 mL TEOS was added to the solution dropwise twice at 30-minute intervals. After 6 hrs, ~180 nm SiO₂ spheres were obtained and kept in the refrigerator for further use as Sample D. This step could be easily scaled up to obtain >10 g silica spheres in a single batch. The size deviation is typically within ± 10 nm. The purification of SiO₂ spheres was conducted by

washing with ethanol/water solution (50/50 v/v) for 5 times. The purified SiO₂ spheres were stored in ethanol.

The synthesis of NH₂-SiO₂

The subsequent functionalization of the obtained spheres with an amine derivative of the silica precursor has been previously reported.⁴⁴⁻⁴⁵ Around 1.0 g SiO₂ spheres were centrifuged from the original ethanol solution and re-dispersed in 175 mL isopropanol. 200 μ L APTS was dissolved in 25 mL isopropanol and mixed with the above SiO₂-isopropanol solution. A round-bottom flask containing mixed solution was heated to 80 °C. The reaction was stopped after 2 hrs. NH₂-SiO₂ spheres were separated, washed with ethanol for 3 times and stored in 20 mL ethanol. As-synthesized NH₂-SiO₂ spheres were taken out from their ethanol solution and dried in vacuum at room temperature. The dried solids were annealed in an oven in air at 100 °C for 5 hrs, then cooled down to room temperature naturally.

The synthesis of 2.9 nm Pt NPs

Monodisperse 2.9 nm Pt NPs were synthesized according to reported methods.⁴⁶ In a typical experiment, PVP (266 mg, MW~29,000) was dissolved in methanol (360 mL) and deionized water (40 mL) in a 1000 mL round-bottomed flask. H₂PtCl₆ · 6H₂O (98.2 mg) was then added.

The mixture was heated to reflux at 100 °C in air for 3 h with vigorous magnetic stirring. A dark brown colloidal solution that contained monodisperse 2.9 nm Pt NPs was thus obtained.

The preparation of Pt/NH₂-SiO₂

Typically, 200 mg NH₂-SiO₂ (fresh or annealed) spheres were taken out and dispersed in 60 mL ethanol. The appropriate amount of Pt NPs solution (1.34 % Platinum by weight of the functionalized spheres) was taken out and diluted with ethanol to a final volume of 110 mL.

This diluted metal NPs solution was added to 60 mL $\text{NH}_2\text{-SiO}_2$ solution dropwise under vigorous magnetic stirring. The resulting Pt/ $\text{NH}_2\text{-SiO}_2$ solution was further sonicated for 30 min. After separation, the Pt/ $\text{NH}_2\text{-SiO}_2$ precipitate was washed with ethanol for 5 times and stored in ethanol.

Synthesis of Pt@MSWs

To prepare Pt@MSWs, first Pt/ $\text{NH}_2\text{-SiO}_2$ (200 mg) dispersed in ethanol (20 mL) was initially taken and sonicated for 10 minutes. To this around 300 mg of CTAB was added. Ammonium hydroxide (1.11 mL, 28% assay) was added to render the solution basic and the solution was stirred for half an hour. To this TEOS (250 μL in 10 mL of ethanol) was added dropwise under magnetic stirring to template a 20 nm MSW coating with the aid of the CTAB. After 6 hours of stirring, the solution was separated by centrifugation. This was then redispersed in 100 mL of methanol and concentrated HCl (6 mL, 36% assay) and heated under reflux at 90 °C to remove CTAB. The obtained Pt@MSWs were then washed with acetone to remove all traces of acid and finally redispersed in methanol, ahead of iNP synthesis.

Synthesis of PtSn@MSWs

The Pt-Sn bimetallic nanoparticle catalysts were synthesized using a procedure developed by R. Schaak.⁴⁷ In a typical experiment, a given amount of Pt@MSWs sample was dispersed in TEG (60 mL) in a two neck round bottom flask. $\text{SnCl}_2\cdot\text{H}_2\text{O}$ was then added depending on the required molar ratio of Pt:Sn into the solution and dispersed with sonication. The mixture solution was then heated to 230 °C and maintained at this temperature for 2h under Ar. After the reaction, the catalyst was separated by centrifugation and washed with ethanol five times. The sample was further dried at 60 °C in vacuum for 6h. Following this, the sample was

calcined at 500 °C to remove any organic residues and reduced at 300 °C under 10% hydrogen before catalysis.

Catalytic testing: Hydrogenation of acetylene

The hydrogenation of acetylene was carried out in a fritted quartz U-tube reactor. Typically ~100 mg catalyst was weighed, and mixed with 2.0 g quartz sands. The reaction gases were composed of 10.5 mL/min He (99.999%), 1.5 mL/min H₂ (99.995%), 15 mL/min C₂H₄ (99.9%), 0.15 mL/min C₂H₂ (99.9%) at 1 bar. The gas composition was monitored online by an HP 5890 gas chromatograph equipped with a capillary column (HP PLOT Q, 30 m × 0.25 mm × 0.25 μm) with a flame ionization detector. The catalytic activity was obtained when a steady state was observed.

Regeneration Experiment

PtSn@MSWs with a Sn/Pt ratio of 1 was first reduced at 300 °C in situ in the flow reactor using 10% H₂/He, followed by acetylene hydrogenation for around 1.5 hours at a reaction temperature of 200 °C. For the deactivation of the catalyst, H₂ flow was lowered from 1.5 mL/min to 0.15 mL/min and He flow was increased from 10.5 to 11.9 mL/min to maintain the total reaction gas flow at 30 mL/min. During the deactivation, cycle conversion was lowered to 10%. At this junction, the reaction sequence was paused and helium was flushed through the reactor at 40 mL/min. Following this, PtSn@MSWs were then oxidized in a He/O₂ flow of 10/40 mL/min at 500 °C for 30 min to remove carbon deposits, and reduced at 300 °C for 30 min in a 10% H₂ flow in He to prepare the catalyst for the next 1.5 h of acetylene hydrogenation run.

Characterization

The transmission electron micrographs (TEM) were taken on a TECNAI G² F20 at the acceleration voltage of 200 kV. Samples were prepared by drop-drying dilute particle suspensions in ethanol onto carbon film stabilized with formvar on 300 mesh Cu grids (Global Electron Microscopy Technology Co.). Particle size distribution was obtained by counting at least 300 randomly chosen particles. The powder X-ray diffraction (PXRD) patterns were collected at room temperature using an STOE Stadi P powder diffractometer, equipped with an image plate and Cu $K_{\alpha 1}$ radiation source ($\lambda = 1.540598 \text{ \AA}$). Nitrogen sorption was carried out on a Micromeritics 3Flex surface characterization analyser at 77 K. Each sample was degassed by heating in flowing N₂ at 200 °C for 5 h before the measurements. The surface area was calculated by using the Brunauer–Emmett–Teller method. Pore size distribution was obtained by using Barrett–Joyner–Halenda method. The metal loading amounts were determined with ICP-MS (Thermo Scientific, X Series II).

References

1. Zahmakran, M.; Ozkar, S., *Nanoscale* **2011**, *3*, 3462-3481.
2. Jose Climent, M.; Corma, A.; Iborra, S., *RSC Advances* **2012**, *2*, 16-58.
3. Witham, C. A.; Huang, W.; Tsung, C.-K.; Kuhn, J. N.; Somorjai, G. A.; Toste, F. D., *Nat Chem* **2010**, *2*, 36-41.
4. Shekhar, M.; Wang, J.; Lee, W.-S.; Williams, W. D.; Kim, S. M.; Stach, E. A.; Miller, J. T.; Delgass, W. N.; Ribeiro, F. H., *Journal of the American Chemical Society* **2012**, *134*, 4700-4708.
5. Nesselberger, M.; Ashton, S.; Meier, J. C.; Katsounaros, I.; Mayrhofer, K. J. J.; Arenz, M., *Journal of the American Chemical Society* **2011**, *133* (43), 17428-17433.

6. Joo, S. H.; Park, J. Y.; Renzas, J. R.; Butcher, D. R.; Huang, W.; Somorjai, G. A., *Nano Lett.* **2010**, *10*, 2709-2713.
7. Burda, C.; Chen, X.; Narayanan, R.; El-Sayed, M. A., *Chemical Reviews* **2005**, *105* (4), 1025-1102.
8. Wang, J.; Tan, H.; Yu, S.; Zhou, K., *ACS Catalysis* **2015**, *5* (5), 2873-2881.
9. Cheong, S.; Watt, J. D.; Tilley, R. D., *Nanoscale* **2010**, *2* (10), 2045-2053.
10. Bratlie, K. M.; Lee, H.; Komvopoulos, K.; Yang, P.; Somorjai, G. A., *Nano Letters* **2007**, *7* (10), 3097-3101.
11. Marshall, S. T.; O'Brien, M.; Oetter, B.; Corpuz, A.; Richards, R. M.; Schwartz, D. K.; Medlin, J. W., *Nat Mater* **2010**, *9*, 853-858.
12. Kwon, S. G.; Krylova, G.; Sumer, A.; Schwartz, M. M.; Bunel, E. E.; Marshall, C. L.; Chattopadhyay, S.; Lee, B.; Jellinek, J.; Shevchenko, E. V., *Nano letters* **2012**, *12*, 5382-5388.
13. Vu, K. B.; Bukhryakov, K. V.; Anjum, D. H.; Rodionov, V. O., *ACS Catalysis* **2015**, *5* (4), 2529-2533.
14. Kang, J.; Cheng, K.; Zhang, L.; Zhang, Q.; Ding, J.; Hua, W.; Lou, Y.; Zhai, Q.; Wang, Y., *Angewandte Chemie* **2011**, *123* (22), 5306-5309.
15. Guo, Z.; Xiao, C.; Maligal-Ganesh, R. V.; Zhou, L.; Goh, T. W.; Li, X.; Tesfagaber, D.; Thiel, A.; Huang, W., *ACS Catalysis* **2014**, *4* (5), 1340-1348.
16. Li, X.; Goh, T. W.; Li, L.; Xiao, C.; Guo, Z.; Zeng, X. C.; Huang, W., *ACS Catalysis* **2016**, 3461-3468.
17. Lee, J.; Farha, O. K.; Roberts, J.; Scheidt, K. A.; Nguyen, S. T.; Hupp, J. T., *Chemical Society Reviews* **2009**, *38*, 1450-1459.

18. Bhattacharjee, S.; Lee, Y.-R.; Puthiaraj, P.; Cho, S.-M.; Ahn, W.-S., *Catalysis Surveys from Asia* **2015**, *19* (4), 203-222.
19. Tao, F.; Zhang, S.; Nguyen, L.; Zhang, X., *Chem. Soc. Rev.* **2012**, *41* (24), 7980-7993.
20. Sankar, M.; Dimitratos, N.; Miedziak, P. J.; Wells, P. P.; Kiely, C. J.; Hutchings, G. J., *Chemical Society Reviews* **2012**, *41* (24), 8099-8139.
21. Wang, D.; Li, Y., *Adv. Mater.* **2011**, *23* (9), 1044-1060.
22. Singh, A. K.; Xu, Q., *ChemCatChem* **2013**, *5* (3), 652-676.
23. Small, M. W.; Sanchez, S. I.; Menard, L. D.; Kang, J. H.; Frenkel, A. I.; Nuzzo, R. G., *Journal of the American Chemical Society* **2011**, *133* (10), 3582-3591.
24. Abe, H.; Matsumoto, F.; Alden, L. R.; Warren, S. C.; Abruña, H. D.; DiSalvo, F. J., *Journal of the American Chemical Society* **2008**, *130* (16), 5452-5458.
25. Armbrüster, M., In *Encyclopedia of Catalysis*, John Wiley & Sons, Inc.: 2002.
26. Furukawa, S.; Komatsu, T., *ACS Catal.* **2017**, *7* (1), 735-765.
27. Armbrüster, M.; Schlögl, R.; Grin, Y., *Sci. Technol. Adv. Mater.* **2014**, *15* (3), 1-17.
28. Yan, Y.; Du, J. S.; Gilroy, K. D.; Yang, D.; Xia, Y.; Zhang, H., *Advanced Materials* **2017**, *29* (14), 1605997-n/a.
29. DeSario, D. Y.; DiSalvo, F. J., *Chem. Mater.* **2014**, *26* (8), 2750-2757.
30. Cui, Z.; Chen, H.; Zhao, M.; Marshall, D.; Yu, Y.; Abruña, H.; DiSalvo, F. J., *J Am Chem Soc* **2014**, *136* (29), 10206-10209.
31. Chen, H.; Wang, D.; Yu, Y.; Newton, K. A.; Muller, D. A.; Abruña, H.; DiSalvo, F. J., *J Am Chem Soc* **2012**, *134* (44), 18453-18459.
32. Maligal-Ganesh, R. V.; Xiao, C.; Goh, T. W.; Wang, L.-L.; Gustafson, J.; Pei, Y.; Qi, Z.; Johnson, D. D.; Zhang, S.; Tao, F.; Huang, W., *ACS Catalysis* **2016**, *6* (3), 1754-1763.

33. Xiao, C.; Maligal-Ganesh, R. V.; Li, T.; Qi, Z.; Guo, Z.; Brashler, K. T.; Goes, S.; Li, X.; Goh, T. W.; Winans, R. E.; Huang, W., *ChemSusChem* **2013**, *6* (10), 1915-1922.
34. Zhang, Q.; Lee, I.; Ge, J.; Zaera, F.; Yin, Y., *Advanced Functional Materials* **2010**, *20*, 2201-2214.
35. Chen, Z.; Cui, Z.-M.; Niu, F.; Jiang, L.; Song, W.-G., *Chemical Communications* **2010**, *46*, 6524-6526.
36. Gao, J.; Zhao, H.; Yang, X.; Koel, B. E.; Podkolzin, S. G., *ACS Catalysis* **2013**, *3*, 1149-1153.
37. Zhu, M.; Sun, G.; Xin, Q., *Electrochimica Acta* **2009**, *54* (5), 1511-1518.
38. Wang, X.; Stöver, J.; Zielasek, V.; Altmann, L.; Thiel, K.; Al-Shamery, K.; Bäumer, M.; Borchert, H.; Parisi, J.; Kolny-Olesiak, J., *Langmuir* **2011**, *2*, 11052-11061.
39. Schaak, R. E.; Sra, A. K.; Leonard, B. M.; Cable, R. E.; Bauer, J. C.; Han, Y. F.; Means, J.; Teizer, W.; Vasquez, Y.; Funck, E. S., *J Am Chem Soc* **2005**, *127* (10), 3506-15.
40. Soderberg, J. N.; Sirk, A. H. C.; Campbell, S. A.; Birss, V. I., *Journal of The Electrochemical Society* **2005**, *152* (10), A2017.
41. Schulenburg, H.; Müller, E.; Khelashvili, G.; Roser, T.; Bönnemann, H.; Wokaun, A.; Scherer, G. G., *The Journal of Physical Chemistry C* **2009**, *113* (10), 4069-4077.
42. Deng, L.; Miura, H.; Shishido, T.; Hosokawa, S.; Teramura, K.; Tanaka, T., *ChemCatChem* **2014**, *6* (9), 2680-2691.
43. Hartlen, K. D.; Athanasopoulos, A. P. T.; Kitaev, V., *Langmuir* **2008**, *24*, 1714-1720.
44. Pastoriza-Santos, I.; Gomez, D.; Perez-Juste, J.; Liz-Marzan, L. M.; Mulvaney, P., *Physical Chemistry Chemical Physics* **2004**, *6* (21), 5056-5060.

45. Xiao, C.; Maligal-Ganesh, R. V.; Li, T.; Qi, Z.; Guo, Z.; Brashler, K. T.; Goes, S.; Li, X.; Goh, T. W.; Winans, R. E.; Huang, W., *ChemSusChem* **2013**, *6* (10), 1915-22.
46. Teranishi, T.; Hosoe, M.; Tanaka, T.; Miyake, M., *The Journal of Physical Chemistry B* **1999**, *103* (19), 3818-3827.
47. Bauer, J. C.; Chen, X.; Liu, Q.; Phan, T.-H.; Schaak, R. E., *Journal of Materials Chemistry* **2008**, *18* (3), 275-282.

CHAPTER 5. CONCLUSIONS

Over the course of this thesis, we have demonstrated the use of encapsulation strategies to synthesize intermetallic nanoparticles. With a focus on Pt-based intermetallic compounds, we were further able to show evidence of their efficiency as selective catalysts that surpassed the catalytic performance of platinum. Additionally, the inert porous silica encapsulation afforded thermal stability to the iNPs under various reaction and treatment conditions.

In chapter 2, the feasibility of using previously synthesized core-shell materials to enable the seeded synthesis of intermetallic compounds was demonstrated. Various PtM@mSiO₂ iNPs (where M = Sn, Pb, Zn) were synthesized via previously reported solution chemistry methods. The porous silica environment enabled the conversion of the platinum NPs to the respective iNPs without subsequent aggregation, as was evident from TEM. All the iNPs were demonstrated to be stable at temperatures as high as 600 °C. Vapor phase furfural hydrogenation was tested for these catalysts and all the iNPs demonstrated drastic improvements in selectivity to the desired product, furfuryl alcohol, in comparison to platinum alone. For the same quantity of platinum, PtSn@mSiO₂ displayed complete conversion of furfural, with 98% selectivity to desired furfuryl alcohol, as opposed to 23% conversion and only 35% selectivity to furfuryl alcohol in the case of Pt@mSiO₂. Owing to the encapsulation the catalyst could be conveniently regenerated via an oxidation/reduction cycle after on-purpose deactivation.

DFT calculations further explained the selectivity in terms of the preferential binding mode of the furfural substrate via the oxygen in carbonyl bond alone on Sn atoms on the PtSn (110) surface. Meanwhile on Pt (111) furfural adsorbed in a flat configuration with the C=C

bonds of the furan ring and the C=O bond on Pt-Pt bridge sites, enabling the hydrogenation and breakdown of the furan ring, leading to lower selectivity to furfuryl alcohol.

This ship-in-a-bottle strategy to encapsulate Pt-based iNPs has also been expanded to palladium and gold-based intermetallic compounds. However, both palladium and gold initially required the synthesis of smaller seed NPs ahead of synthesizing the final NPs.^{1,2} These were then coated similarly to Pt@mSiO₂. Intermetallic compounds of palladium, PdM@mSiO₂ (where M = Cu, Zn, Ga, and Sn), and gold, AuM'@mSiO₂ (where M' = Cu, Zn, and Sn) were also successfully synthesized, via preliminary PXRD and TEM investigations. Further characterization of these iNPs and their catalytic properties will be the subject of future work in our group.

In chapter 3, the ship-in-a-bottle strategy was used to make Pt-Fe bimetallics, identified as Pt₅Fe_x@mSiO₂ (where x = 1, 2 and 4). In previous reports, surface-modifying ligands had been used to demonstrate that platinum NP surfaces could be modified to demonstrate chemoselectivity in heterogeneous catalytic reactions. However, some of these ligands required the presence of additional metals such as iron, whose role was not clarified.³ In our report, we used the advantages of our encapsulation strategy to synthesize Pt-Fe bimetallic compounds which could be oxidized or reduced at high temperatures as high as 850 °C. The catalyst could also be post-modified by simply mixing the ligands with Pt-Fe@mSiO₂, for additional improvements in selectivity. In the selective hydrogenation of both furfural and cinnamaldehyde, the Pt-Fe@mSiO₂ bimetallics showed improvements in both conversion and selectivity to the desired alcohols, furfuryl alcohol, and cinnamyl alcohol respectively. The impact of ligands such as perfluorodecanoic acid on the catalysis merits further investigation in other encapsulated bimetallic compounds that will be explored in our group. Changes in the

size of the core metallic NPs using the ship-in-a-bottle strategy will also be the focus of future studies.

In chapter 3, the ship-in-a-bottle strategy was used to make Pt-Fe bimetallics, identified as $\text{Pt}_5\text{Fe}_x@\text{mSiO}_2$ (where $x = 1, 2$ and 4). In previous reports, surface-modifying ligands had been used to demonstrate that platinum NP surfaces could be modified to demonstrate chemoselectivity in heterogeneous catalytic reactions. However, some of these ligands required the presence of additional metals such as iron, whose role was not clarified.³ In our report, we used the advantages of our encapsulation strategy to synthesize Pt-Fe bimetallic compounds which could be oxidized or reduced at high temperatures as high as $850\text{ }^\circ\text{C}$. The catalyst could also be post-modified by simply mixing the ligands with $\text{Pt-Fe}@\text{mSiO}_2$, for additional improvements in selectivity. In the selective hydrogenation of both furfural and cinnamaldehyde, the $\text{Pt-Fe}@\text{mSiO}_2$ bimetallics showed improvements in both conversion and selectivity to the desired alcohols, furfuryl alcohol, and cinnamyl alcohol respectively. The impact of ligands such as perfluorodecanoic acid on the catalysis merits further investigation in other encapsulated bimetallic compounds that will be explored in our group. Changes in the size of the core metallic NPs using the ship-in-a-bottle strategy will also be the focus of future studies.

In Chapter 4, we endeavored to further decrease the size of our iNPs to maximize precious metal usage via the intermetallic compounds of noble metals. Using platinum as an example and a previously reported $\text{Pt}@\text{MSWs}$ (mesoporous silica wells) architecture,⁴ we again used seed-mediated solution chemistry to synthesize Pt-Sn bimetallics and intermetallic compounds. The intermetallic compounds with Sn/Pt ratio greater than 1, demonstrated high selectivity to desired ethylene. Additionally, the catalyst could be regenerated in a similar

fashion to PtSn@mSiO₂ catalysts via a simple oxidation/reduction cycle. Compared to a conventional wetness impregnation catalyst intermetallic PtSn@MSWs were more efficient for the semi-hydrogenation of acetylene to ethylene.

Future Directions

Although we have shown that alloying of precious metals such as Pt and Pd can result in catalysts that are more efficient at evincing selectivity in chemical transformation, especially via iNPs, a more important goal is to rely even less on noble metal nanoparticles. Transition metals such as Fe, Co, Ni, and Cu have long been known as catalytically active metals. However, nanoparticles of these pose a significant challenge owing to the difficulty in preventing their oxidation.

Seed-mediated strategies to synthesize Ni and Cu nanoparticles via smaller Pt seeds,⁵ have indicated promise for a direction towards synthesizing the iNPs of Cu and Ni with greater stability and size control. Not only is the dependence on precious metals drastically reduced, the resultant NPs can potentially be coated like we have demonstrated in the case of Pt to allow the synthesis of intermetallic compounds of these more cost-effective transition metals.

Ni₃Zn and Ni_xM_y (where M = Ga and Sn) iNPs have been demonstrated as excellent catalysts for the semi-hydrogenation of alkynes.⁶ In the nickel intermetallic compounds of Sn, increasing amounts of Sn lead to greater site isolation of Ni and hence enhanced selectivity in the semi-hydrogenation of acetylene to ethylene. Further, there have been other reports of Ni-In intermetallic compounds synthesized via a layered double hydroxide strategy that have been demonstrated to be excellent catalysts for the selective hydrogenation of α,β -unsaturated aldehydes to their unsaturated alcohols.⁷ Hence, future efforts will be directed towards adapting

the encapsulation strategies covered in this thesis to non-precious metals based iNPs, keeping in mind the challenges posed in their synthesis in comparison to the precious metals.

References

- (1) Jana, N.R., L. Gearheart, and C.J. Murphy, *Langmuir*, **2001**, 17, 6782-6786.
- (2) Lu, L., Wang, H., Xi S., Zhang, H., *Journal of Materials Chemistry*, **2002**, 12, 156-158.
- (3) Vu, K. B.; Bukhryakov, K. V.; Anjum, D. H.; Rodionov, V. O., *ACS Catalysis* **2015**, 5, 2529-2533.
- (4) Xiao, C.; Maligal-Ganesh, R. V.; Li, T.; Qi, Z.; Guo, Z.; Brashler, K. T.; Goes, S.; Li, X.; Goh, T. W.; Winans, R. E.; Huang, W., *ChemSusChem* **2013**, 6 (10), 1915-1922.
- (5) Grzelczak, M.; Pérez-Juste, J.; Rodríguez-González, B.; Spasova, M.; Barsukov, I.; Farle, M.; Liz-Marzán, L. M., *Chemistry of Materials* **2008**, 20, 5399-5405.
- (6) Liu, Y.; Liu, X.; Feng, Q.; He, D.; Zhang, L.; Lian, C.; Shen, R.; Zhao, G.; Ji, Y.; Wang, D.; Zhou, G.; Li, Y., *Advanced Materials* **2016**, 28, 4747-4754.
- (7) Li, C.; Chen, Y.; Zhang, S.; Xu, S.; Zhou, J.; Wang, F.; Wei, M.; Evans, D. G.; Duan, X., *Chemistry of Materials* **2013**, 25, 3888-3896.